

**TEMPER  
EMBRITTLEMENT  
OF  
ALLOY STEELS**

**STP 499**



**AMERICAN SOCIETY FOR TESTING AND MATERIALS**

# TEMPER EMBRITTLEMENT OF ALLOY STEELS

A symposium  
presented at the  
Seventy-fourth Annual Meeting  
AMERICAN SOCIETY FOR  
TESTING AND MATERIALS  
Atlantic City, N. J., 27 June-2 July 1971

ASTM SPECIAL TECHNICAL PUBLICATION 499  
D. L. Newhouse, symposium chairman

List price \$10.00  
04-499000-02

AMERICAN SOCIETY FOR TESTING AND MATERIALS  
1916 Race Street, Philadelphia, Pa. 19103

© BY AMERICAN SOCIETY FOR TESTING AND MATERIALS 1972  
Library of Congress Catalog Card Number: 73-185535

**NOTE**

The Society is not responsible, as a body,  
for the statements and opinions  
advanced in this publication.

Printed in Baltimore, Md.  
March 1972

## Foreword

The Symposium on Temper Embrittlement of Alloy Steels was presented at the Seventy-fourth Annual Meeting of ASTM held in Atlantic City, N. J., 27 June-2 July 1971. Committee A-1 on Steel sponsored the symposium. D. L. Newhouse, General Electric Co., presided as symposium chairman.

## **Related ASTM Publications**

**Temper Embrittlement in Steel, STP 407 (1968),  
\$21.00**

**Effects of Residual Elements on Properties of Austenitic Stainless Steels, STP 418 (1967), \$7.25**

**Chemical Composition and Rupture Strengths of Superstrength Alloys, DS 9 E (1970), \$3.50**

# Contents

Introduction	1
Temper Embrittlement Study of Ni-Cr-Mo-V Rotor Steels: Part I—Effects of Residual Elements—A Special Task Group Report	3
Temper Embrittlement Study of Ni-Cr-Mo-V Rotor Steels: Part II—Statistical Design and Analysis—B. K. STEWART	37
Chemical Analytical Results—How Accurate?—J. PENKROT AND F. P. BYRNE	51
Temper Embrittlement of Low Alloy Steels—A. JOSHI AND D. F. STEIN	59
Effect of Solute Elements on Temper Embrittlement of Low Alloy Steels—H. L. MARCUS, L. H. HACKETT, JR., AND P. W. PALMBERG	90
Alloy Effects in Temper Embrittlement—B. J. SCHULZ AND C. J. MCMAHON, JR.	104

# Introduction

---

The problems presented by temper embrittlement in the use of alloy steels in heavy sections are much the same in 1971 as they were at the time of the 1967 ASTM Symposium on Temper Embrittlement. Trends toward thicker sections and higher operating stresses have continued in heavy structural components such as large pressure vessels and turbine generator rotors. These trends in size and severity require steel with higher hardenability to provide for the higher through-section strength and fracture toughness needed in such components.

The 1971 Symposium on Temper Embrittlement was convened to present the results of work which has been done in the field of temper embrittlement since the 1967 symposium, the proceedings of which have been published in *ASTM STP 407, Temper Embrittlement of Steel*.

After the 1967 symposium the ASTM Special Task Force on Large Turbine and Generator Rotors of Subcommittee VI on Forgings of Committee A-1 on Steel undertook a study of the effects of residual elements in temper embrittlement. Other research was undertaken by several investigators on the microstructural and segregation aspects of temper embrittlement.

The papers which appear in this volume present new information about the effects of the residual elements, arsenic, antimony, tin, and phosphorus, in the Ni-Cr-Mo-V steel used for rotor forgings. Several papers describing the statistical plan, analysis, and problems encountered in chemical analyses should be useful to those concerned with design and execution of metallurgical experiments. The application of Auger electron spectroscopy to the analysis of fracture surfaces and scanning electron microscopy for characterizing the mode of fracture shed important new light on the mechanisms of embrittlement, on the magnitude of segregation of both alloying elements and impurity elements at grain boundaries, and on the kinetics of embrittlement produced by various elements.

It seems evident that the control of temper embrittlement in alloy steels used in heavy sections or operating in the embrittlement range will require further investigation of the effects of composition and heat treatment; will require further cooperative work in developing procedures for chemical analysis for residual elements; and will be facilitated by further exploitation of new techniques such as Auger emission spectroscopy.

*D. L. Newhouse*

Manager, Forgings Development,  
General Electric Company, Schenectady, N.Y.  
symposium chairman

# Temper Embrittlement Study of Ni-Cr-Mo-V Rotor Steels: Part I—Effects of Residual Elements

---

**REFERENCE:** "Temper Embrittlement Study of Ni-Cr-Mo-V Rotor Steels: Part I—Effects of Residual Elements," *Temper Embrittlement of Alloy Steels*, ASTM STP 499, American Society for Testing and Materials, 1972, pp. 3–36.

**ABSTRACT:** Variations in temper embrittlement of vacuum carbon deoxidized Ni-Cr-Mo-V rotor steels, produced by step cooling through the temperature range of susceptibility, are related primarily to variations in P and Sn content. The embrittlement produced by isothermal exposure at 750 F (399 C) for 1 year is about double that produced by step cooling. The effects of P, As, and a P-Sn interaction are significant, while the significance of the effect of Sn alone is considerably less. Increased Mo is associated with reduced isothermal embrittlement.

Relationships are found between deembrittled Charpy 50 percent fibrous fracture appearance transition temperature (FATT) and P and Sn content. A P-Sn interaction is also observed. Variations in the Charpy 15-mil lateral expansion transition temperature (LETT) in the deembrittled condition are related to P, Mo, a P-Sb interaction, and a Mo-Sb interaction.

Based on previous investigations, the effect of P on temper embrittlement is about as expected while that of Sn is somewhat greater. Sb displays no significant effect in this study; contrary to definite effects which had been reported previously.

**KEY WORDS:** embrittlement, tempering, cooling, heat treatment, isothermal, impact tests, transition temperature, steels, steam turbines, turbogenerators, arsenic, antimony, molybdenum, phosphorus, tin, statistical analysis, correlation, evaluation

## Nomenclature

- FATT V notch Charpy fracture appearance transition temperature; temperature at which the area of cleavage or intergranular fracture is 50 percent of the original area under the notch, deg F
- LETT V notch Charpy lateral expansion transition temperature; temperature of 15-mil lateral expansion, deg F
- $\Delta$ FATT Temper embrittlement as measured by a shift in FATT, deg F
- $\Delta$ LETT Temper embrittlement as measured by a shift in LETT, deg F

This paper was prepared by the Research Subgroup on Temper Embrittlement, ASTM Special Task Force on Large Turbine and Generator Rotors of Subcommittee VI on Forgings of ASTM Committee A-1 on Steel. The members of the subgroup are D. L. Newhouse, chairman, General Electric Co., Schenectady, N. Y.; D. V. Doane, Climax Molybdenum Co. of Michigan, Ann Arbor, Mich.; H. D. Greenberg, Westinghouse Electric Corp., Pittsburgh, Pa.; G. S. Hartman, Bethlehem Steel Corp., Bethlehem, Pa.; A. LaPorte, National Forge Co., Warren County, Pa.; H. C. Myers, Jr., Midvale Heppenstall Co., Philadelphia, Pa.; J. E. Steiner, U. S. Steel Corp., Pittsburgh, Pa.; and D. G. Yorke, International Nickel Co., New York, N. Y.

- WQ Deembrittled by heating specimen blanks 1 h at 1100 F (593 C) and water quenching
- SC Embrittled by heating to 1100 F (593 C), holding 1 h, and step cooling through the range of temper embrittlement as described under tempering
- AG Isothermally embrittled by aging 1 year at 750 F (399 C)

Temper embrittlement is a matter of concern in the production and application of rotor forgings for large steam turbines and generators for two reasons. Variable amounts of embrittlement occurring upon slow cooling from the final tempering or stress relief annealing treatment can cause uncertainty as to whether a forging will meet Charpy 50 percent fibrous fracture appearance transition temperature (FATT) and fracture toughness requirements at low operating and overspeed temperatures. This variability of fracture toughness, caused in part by embrittlement during heat treatment, limits to some degree the effective use of the forgings in applications where larger, more highly stressed rotors with adequate fracture toughness and higher strength are required. For turbine rotors operating at temperatures within the range of embrittlement, 662 to 1067 F (350 to 575 C), long time isothermal embrittlement can cause an increase in notch toughness transition temperature which must be considered in the selection of material and in design.

Temper embrittlement, as used in this paper, means a shift upward in the brittle to ductile transition temperature, produced by heating within, or cooling slowly through, the temperature range 662 to 1067 F (350 to 575 C). It is reversible and may be removed by subjecting the specimens to a temperature of 1100 F (594 C) or higher for a few minutes.

The ASTM Special Task Force on Large Turbine and Generator Rotors, through its Research Subgroup on Temper Embrittlement, has carried out a cooperative research program to determine whether, and to what degree, normal variations in the content of Mo and in the residual impurity elements—P, As, Sb and Sn—contribute to variations of notch toughness transition temperature of Ni-Cr-Mo-V rotor material during heat treatment or exposure to temperature within the range of embrittlement. This paper presents the results of that program.

### **Background**

The ASTM Special Task Force on Large Turbine and Generator Rotors was appointed at the January 1955 meeting of Subcommittee VI on Forgings of ASTM Committee A-1 on Steel, to study the "Cause of Brittle Fracture in Steel Forgings with the Aim of Establishing a Criterion by Means of Which the Tendency of a Material to Fracture in a Brittle Manner may be Appraised . . . and to Discover the Causes of Brittle Fracture and Its Cure." The history of the special task force has been described by Curran [1].

An early action of the task force was the formation of a research group, with representation from each of the member companies, to establish cooperative research programs and to coordinate the activities of the various company laboratories. Developing stronger and tougher rotor forging materials was the group's objective. Their first program was directed toward delineating the effects of the individual alloying elements on the transformation characteristics, microstructures, and Charpy impact transition temperature of alloy steels. The results of the first program, presented to the task force 18 November 1958, indicated that the following composition showed promise of high yield strength, low transition temperature, and adequate magnetic permeability, the latter of significance primarily for generator rotors.

Recommended Composition, %

	First Program
C (max)	0.23 (0.28 for turbine rotors)
Mn	0.20–0.40
P (max)	0.025
S (max)	0.025
Si	0.15–0.30
Ni	3.50–4.00
Cr	1.50–2.00
Mo	0.40–0.60
V	0.05–0.13

The possibility of temper embrittlement was investigated and it was found that high Mn contents were associated with high susceptibility to temper embrittlement.

A second program was carried out to determine the effects of Mn, Mo, and P content on the temper embrittlement susceptibility of the Ni-Cr-Mo-V alloy recommended in the first report. Observations showed that all three of these elements promoted embrittlement in this base composition, P being the most effective and Mo the least. The following equation was derived for calculating the step cooled embrittlement susceptibility for the recommended ASTM alloy under the conditions and within the composition limits of this study.

$$\Delta FATT(SC-WQ) = -206 + 7319(\%P) + 370(\%Mn) + 217(\%Mo) \quad (1)$$

where %P, %Mn, and %Mo denote percent composition. The data from this program were included in an analysis of temper embrittlement in rotor steels by Newhouse and Holtz [2].

The research group, reporting to the task force on 10 May 1960, suggested that the P content be kept as low as possible and Mn and Mo contents as

low as would be consistent with other requirements. A revised recommendation on composition was offered as follows:

Recommended Composition, %	
Second Program	
C (max)	0.23 (0.28 for turbine rotors)
Mn	0.15–0.35
P	Low as possible
S (max)	0.025
Si	0.15–0.30
Ni	3.50–4.00
Cr	1.50–2.00
Mo	0.30–0.50
V	0.05–0.13

Subsequent studies of temper embrittlement in rotor forgings by member companies of the task force revealed it to be a significant problem, especially in the Ni-Cr-Mo-V alloy used for larger low pressure turbine and generator rotors which operate at high stress levels at temperatures near ambient. This alloy is more susceptible to embrittlement than the Cr-Mo-V alloy used at high temperatures or the Ni-Mo-V alloy used for generator rotors. Analysis of data on production rotors by Boyle et al [3,4] indicated that elements contributing to variability of step cooled temper embrittlement (FATT step cooled from 1100 F (593 C) minus the FATT water quenched from 100 F), in decreasing order of importance for the data analyzed, were P, Sb, Si, Mn, Ni, and Cr.

In 1966, the task force organized the Research Subgroup on Temper Embrittlement to plan a program on temper embrittlement in Ni-Cr-Mo-V rotor steel. In the interim period, melting practice for rotor forgings had been modified to provide for vacuum carbon deoxidation, with a maximum Si content of 0.10 percent. The Ni-Cr-Mo-V alloy had been included in the ASTM Specifications for Vacuum Treated Steel Forgings for Generator Rotors (A 469-65, Class 6), Vacuum Treated Carbon and Alloy Steel Forgings for Turbine Rotors and Shafts (A 470-65, Classes 5, 6, and 7), and Vacuum Treated Steel Forgings for Turbine Disks and Wheels (A 471-65, Classes 1 to 6). The first major action of the subgroup was to organize a symposium on temper embrittlement, held at Philadelphia, 3-4 October 1967, to update knowledge and experience with temper embrittlement, to provide a basis for planning a research program, and to stimulate work by other investigators.

The review by McMahan [5] presented at that symposium concluded that embrittlement occurs only in the presence of specific impurities and increases in severity with the concentration of these impurities; that Sb, P, Sn, and As are the major embrittlors, with Mn and Si apparently active in larger concen-

trations. An analysis of production rotor data by Newhouse and Holtz [2] indicated that all of these, plus Mo and Ni, were associated with the variation in embrittlement in Ni-Cr-Mo-V rotors. However, interrelationships between independent variables, especially As, Sb, and Sn, made it impossible to be certain about their individual or combined effects on temper embrittlement in rotors.

Following the 1967 symposium, the research subgroup undertook a planned statistical experiment to determine the individual and interaction effects of normal variations in P, As, Sb, Sn, and Mo on step cooled and isothermal temper embrittlement.

### Testing Plan

The statistical design of the test program and the statistical analysis of the test results are described in Part II (see pp. 37-50) of this work. The statistical consultant defined the heats to be melted and prescribed that melting, forging, heat treatment, and testing procedure sequences be randomized. All operations in any part of the program were to be performed by the same technician, if possible, to prevent the introduction of operator variables.

The statistical design called for melting 22 heats to one base composition with the aim analysis (in weight percent) of 0.25 C, 0.30 Mn, 0.04 Si, 0.010 S, 3.5 Ni, 1.75 Cr, and 0.12 V. The elements to be varied and the aim level of each variation are as follows:

Element	Aim Composition		
	Low	Center Point	High
Mo, %	0.30	0.45	0.60
P, %	0.005	0.010	0.015
Sb, ppm	8	16	24
Sn, ppm	30	75	120
As, ppm	20	70	120

The low level of each trace element was selected as the practical minimum attainable with the best steelmaking practice available for rotor steels; the high level of each element was selected as the maximum experienced in rotor steels in recent years. Mo variations were included to determine whether they would influence temper embrittlement of the bainitic structure obtained in water quenching large rotors.

In brief, the test plan was a half replicate of a five-factor, two-level plan requiring 16 heats to reveal all main effects and two-factor interaction effects between variables. Six center point heats were added to provide statistically significant information concerning the variability of test results and to provide more information concerning the linearity of any effect shown for any variable element.

## Materials

### *Melting*

Steel for the experimental program was provided from the product of 22 vacuum induction melted 50-lb heats processed at the Applied Research Laboratory of the United States Steel Corporation. A detailed description of the melting procedure and charge materials is given in Appendix 1. The heats were melted sequentially according to a prearranged statistical plan. High purity charge materials were melted in a magnesia crucible under vacuum. Ar was added as required to control bath activity during melting and carbon deoxidation. After the base charge of C, Fe, Ni, and Mo was completely melted, the system was backfilled with Ar to a pressure of 250 torr to minimize loss of volatile elements in subsequent additions. Si, P, and S were added, followed by additions of Mn and V, and then Sb, Sn, and As. Each heat was cast under Ar into a square cast iron mold, 4 by 4 in. at the top,  $3\frac{5}{8}$  by  $3\frac{5}{8}$  in. at the bottom, and  $12\frac{1}{2}$  in. high, having a  $3\frac{1}{4}$ -in.-square by  $2\frac{1}{2}$ -in.-high refractory hot top section.

A specimen for chemical analysis was obtained during the pouring of each heat. The first metal from the furnace was cast into a small Cu chill mold (2 in. diameter by 3 in. high). Results of the cup analyses for the 22-heat program indicated that all materials were suitable for the program.

### *Analysis*

Detailed chemical analyses of the 22 heats were performed on forged bar stock. A 12-in. length cut from the midlength of the forged bar of each ingot was forwarded to Westinghouse Electric Company Research Laboratories for sample preparation and distribution of appropriate specimens to organizations cooperating in the analysis. The majority of the analyses were performed by Westinghouse and Bethlehem Steel Corporation. The Climax Molybdenum Company participated in the analysis of trace elements. The analyses, especially for trace elements, presented many problems. A discussion of these problems and the development of procedures to obtain accurate analyses for all elements are the subject of a paper by Penkrot [7].

The results of the analyses of 22 heats are presented in Table 1. The analytical data are presented in a sequence which conforms to the experimental design. Each group of 4 compositions represents a different portion of the half replicate series. (For example, the first 4 compositions are the low P, low Sn steels). The high level of any element is underlined in the table and indicated by 2 in the first 5 columns; low level is indicated by 0. The last 6 heats are the center-point heats referred to previously and are designated level 1 for all 5 elements. Heat numbers indicate the sequence in which the materials were melted; letter codes indicate the sequence in which they were forged. This letter designation was used in subsequent testing to provide a

TABLE 1—Chemical composition of steels in temper embrittlement program.

Levels <sup>a</sup>			Heat Num-ber	Code	Percent										Al, %		ppm			
P	Sn	Mo			As	Sb	C	Mn	P	S	Si	Ni	Cr	Mo	V	Soluble	Total	Sn	As	Sb
0	0	0	0	0	0	0.24	0.31	0.006	0.008	0.056	3.47	1.72	0.31	0.12	0.010	0.016	15	19	18	21
0	0	0	2	2	510	V	0.25	0.32	0.006	0.044	3.45	1.74	0.30	0.11	0.009	0.013	19	160	27	29
0	0	2	0	2	498	W	0.24	0.32	(0.006) <sup>b</sup>	0.011	0.085	3.46	1.74	(0.61)	0.12	0.003	(17)	(25)	(31)	25
0	0	2	2	0	491	H	0.27	0.31	0.006	0.010	0.048	3.49	1.72	0.60	0.12	0.018	15	160	13	24
0	2	0	0	2	505	J	0.26	0.31	0.003	0.059	3.46	1.72	0.29	0.11	0.004	0.009	91	36	27	22
0	2	0	2	0	494	Y	0.24	0.33	0.007	0.011	0.055	3.48	1.73	0.31	0.12	0.006	128	180	12	28
0	2	2	0	0	500	N	0.25	0.32	0.005	0.008	0.068	3.52	1.73	0.60	0.12	0.006	93	34	10	27
0	2	2	2	2	501	O	0.27	0.31	0.006	0.009	0.062	3.48	1.71	0.59	0.12	0.008	105	140	30	25
2	0	0	0	2	495	Z	0.23	0.31	0.016	0.009	0.058	3.47	1.74	0.30	0.12	0.009	17	28	29	32
2	0	0	2	0	493	R	0.24	0.32	0.018	0.008	0.069	3.38	1.71	0.31	0.12	0.011	38	150	12	26
2	0	2	0	0	492	S	0.24	0.32	0.020	0.011	0.073	3.49	1.74	0.63	0.11	0.001	59	28	12	25
2	0	2	2	2	506	G	0.23	0.30	0.016	0.008	0.057	3.52	1.75	0.60	0.12	0.010	20	150	30	27
2	2	0	0	0	508	X	0.25	0.32	(0.016)	0.011	0.055	3.49	1.73	(0.30)	0.12	0.007	(112)	(32)	(12)	28
2	2	0	2	2	489	C	0.24	0.31	0.019	0.011	0.047	3.57	1.76	0.31	0.12	0.002	137	170	30	31
2	2	2	0	2	509	D	0.26	0.32	0.017	0.008	0.047	3.52	1.76	0.61	0.13	0.015	90	38	25	25
2	2	2	2	0	502	B	0.24	0.31	0.018	0.009	0.053	3.54	1.74	0.61	0.12	0.002	98	150	10	30
1	1	1	1	1	504	A	0.24	0.30	(0.011)	0.008	0.078	3.41	1.72	(0.45)	0.12	0.002	(75)	(91)	(19)	20
1	1	1	1	1	497	E	0.19	0.32	0.013	0.010	0.061	3.49	1.77	0.47	0.12	0.003	58	83	13	27
1	1	1	1	1	499	K	0.27	0.33	0.012	0.008	0.073	3.47	1.71	0.46	0.12	0.002	55	99	17	26
1	1	1	1	1	507	L	0.28	0.32	0.011	0.008	0.059	3.47	1.73	0.45	0.12	0.009	73	100	23	31
1	1	1	1	1	503	M	0.25	0.31	0.011	0.008	0.049	3.50	1.72	0.45	0.12	0.006	64	94	19	26
1	1	1	1	1	490	T	0.23	0.32	0.011	0.012	0.059	3.48	1.73	0.46	0.12	0.004	96	90	17	29
16 heats—base, averages					0.25	0.32		0.009	0.058	3.49	1.74		0.12	0.008	0.011					27
8 low level							0.006					0.30								30
8 high level							0.018					0.61								158
6 center heats					0.24	0.32	0.012	0.009	0.063	3.47	1.73	0.46	0.12	0.004	0.008	0.008	70	93	18	26

<sup>a</sup> NOTE—0 = low level; 1 = center point; 2 = high level.

<sup>b</sup> Parentheses enclose data not included in group averages in Table 7 because of abnormally high transition temperatures.

simple identification for test specimens. All processing sequences were part of the statistical design of the experiment.

The results of the chemical analysis indicated the variation from aim composition achieved in the melting campaign and also the range of Al and N contents inherent in the melting procedure used. All the alloying elements added fell within a narrow range. However, the C range was wider than anticipated. Trace element ranges were wide in the case of Sn and As, but not in the case of Sb.

Parentheses enclose values for P, Mo, Sn, As, and Sb for A, W, and X which were not included in group averages due to their abnormally high transition temperatures.

## Processing

### *Forging*

Ingot were forged to  $1\frac{1}{16}$ -in.-square bars at the Bethlehem Steel Corporation plant. Postforging heat treatment followed the practice for Ni-Cr-Mo-V rotors with the exception of holding time at temperature. The details of forging and preliminary heat treatment are given in Appendix 2. The forged bars were cut into 28 to 30-in. lengths (except for the 12-in. chemical analysis section taken from the center of the forged bar) designated by their position, relative to the bottom of the ingot.

## Heat Treatment

Following the preliminary heat treatment in the forge shop, sections for the testing program (the two 28-in.-long bars immediately on either side of the chemical analysis section) were forwarded to the Climax Molybdenum Company for austenitizing and program cooling.

### *Austenitizing*

From each heat, 3 pieces, 7 in. long were cut to provide blanks for impact specimens and 2 pieces,  $7\frac{5}{8}$  in. long were cut to provide blanks for tension specimens and tempering coupons. In addition, 2 extra tension test blanks were cut from each of 3 heats, one at each level of Mo content, to assist in the final definition of the tempering treatment needed to achieve 100,000 psi yield strength in all materials.

The heat treatment was performed in a Homocarb furnace, which utilizes a fan to circulate air through the charge to provide uniform temperature throughout the charge. A dummy load of C steel bars of equivalent size and total weight was subjected to the proposed heat treatment. It was found that the furnace would follow the prescribed cooling curve equivalent to the center of a water quenched, 54-in.-diameter rotor (Fig. 1). The cooling curve was supplied by General Electric Company. All bars for the program were heat treated in one furnace load and spaced to permit uniform circulation of air

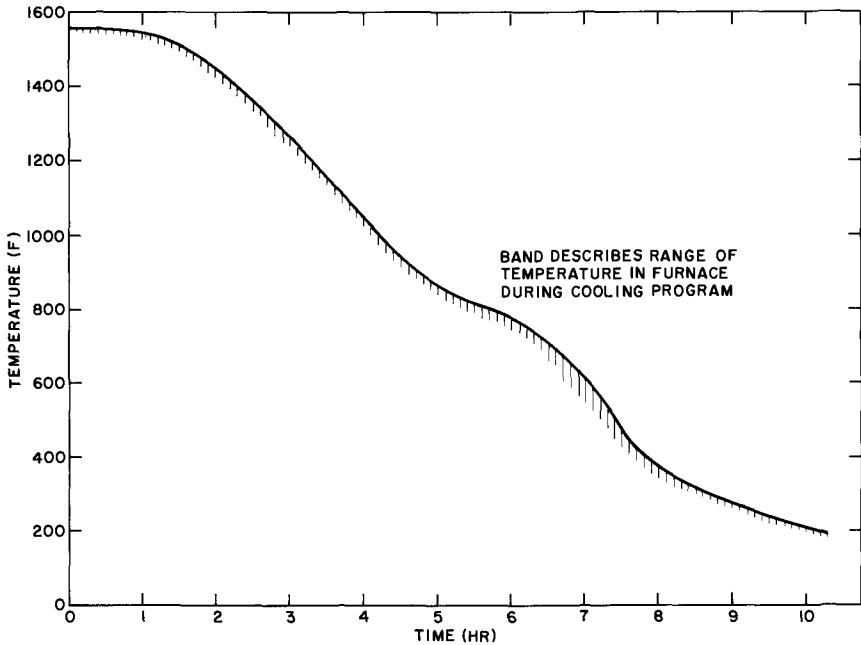


FIG. 1—Program cooling cycle simulating the cooling rate at the center of a water quenched 54-in.-diameter Ni-Cr-Mo-V rotor forging.

throughout the charge. The final austenitizing heat treatment is described below:

1. Heat to 1200 F (649 C) at full power
2. Heat 1200 F (649 C) to 1550 F (843 C) at 50 deg F/h (28 deg C/h) maximum
3. Hold 38 hours at 1550 F (843 C)
4. Cool to room temperature following curve for center of 54-in.-diameter water quenched rotor

The thermocouple records for specimens at the bottom, center, and top of the charge indicated that the entire charge followed the prescribed cooling curve from the austenitizing temperature. The range of temperatures existing in the charge at any given time is shown by the band in Fig. 1. Decarburization, measured on a selected bar after program cooling, extended 0.020 in. This depth represents the total experienced during forging, pretreatment, and final austenitizing and program cooling.

### *Tempering*

Preliminary tempering studies and tempering heat treatment of all test bar blanks were performed by the General Electric Company. The objective of the tempering treatment was to achieve the same 0.02 percent offset yield strength (approximately 100,000 psi) in all bars, using tempering times and

temperatures typical of those used for large rotors. Experience with this steel indicated that a hardness value of HRC 25 was associated with the desired yield strength. Tempering studies were performed on  $\frac{3}{8}$ -in.-thick wafers cut from the austenitized and program cooled bars. A series of double-tempering cycles of 48 h at temperature  $T$  followed by 48 h at  $T - 25$  was designed to develop tempering curves in which hardness could be plotted versus  $P$ , where  $P = (T + 460)(20 + \log \text{time})$ .  $T$  values from 1175 to 1050 F were used.

Based on the tempering studies, selected bars of three Mo contents were tempered and tested in tension. Results indicated the need to modify the tempering treatments to achieve the desired 100,000-psi yield strength in all bars. Final tempering treatments for each alloy in the series are given in Table 2. The steels with higher Mo contents required higher tempering temperatures.

The test bar blanks were subjected to double-tempering treatments in which blanks were heated 48 h at the first tempering temperature given in Table 2, air cooled, heated 48 h at the second tempering temperature, and air cooled.

TABLE 2—*Tempering treatments to achieve uniform tempered yield strength of 100,000 psi (all bars heated 48 h at each tempering temperature and air cooled).*

Steel		Tempering Temperatures, deg F	
Code	% Mo	First Temper	Second Temper
Y	0.28	1100	1090
R	0.29	1110	1090
V	0.30	1110	1090
X	0.30	1110	1090
Z	0.29	1110	1090
A	0.44	1120	1090
E	0.46	1120	1090
J	0.29	1120	1090
P	0.29	1120	1090
C	0.30	1120	1100
H	0.61	1120	1100
N	0.59	1120	1100
T	0.44	1120	1100
W	0.59	1120	1110
L	0.44	1130	1100
M	0.44	1130	1100
B	0.59	1130	1110
D	0.60	1130	1110
G	0.59	1130	1110
K	0.46	1130	1110
O	0.59	1130	1110
S	0.60	1130	1120

A final treatment was designed to prepare the blanks for the temper embrittlement study. Test bar blanks from all steels were heated 1 h at 1100 F (593 C) and then either water quenched (WQ) or step cooled (SC) according to the following schedule:

1. Charge into furnace at 1100 F (593 C), hold 1 h
2. Furnace cool to 1000 F (538 C), hold 15 h
3. Furnace cool to 975 F (524 C), hold 24 h
4. Furnace cool to 925 F (496 C), hold 48 h
5. Furnace cool to 875 F (468 C), hold 72 h
6. Furnace cool below 600 F (316 C), remove from furnace and air cool

### *Isothermal Aging*

Bars from all steels which had been water quenched after being heated 1 h at 1100 F (593 C) were aged 1 year (AG) at 750 F (399 C) in specially designed furnaces at the General Electric Company. Tests were conducted to determine the hardness uniformity after aging. On the basis of the relatively uniform hardness tests, it was decided that only one bar, M, would be subjected to tension tests after aging.

### *Machining*

Tension and impact test specimens were machined from tempered, or tempered and aged test bar blanks. Standard ASTM tension specimens were prepared. One tension bar was prepared from each steel which had been tempered and water quenched, another was prepared from aged material (code M). National Forge Company machined the tension specimens.

Impact test specimens were prepared to ASTM Standard for Notched Bar Impact Testing of Metallic Materials (E 23-66), Type A (Charpy V notch) by Climax Molybdenum Company. Twelve impact specimens were prepared for each steel in each of the 3 conditions (WQ, SC, and AG), a total of 892 specimens. Each 7-in. blank,  $1\frac{1}{16}$  by  $1\frac{1}{16}$  in., was first cut into 3 pieces of equal length. A band saw was used to quarter each piece on the longitudinal axis. Standard impact specimens were prepared by shaping and grinding. All were notched with a single-point, carbide-tipped fly cutter on a horizontal milling machine. All notches were cut on adjacent interior or saw-cut surfaces of each blank.

### **Test Procedures**

Extensive tension testing was conducted on specimens water quenched after tempering, but these same bars were not subjected to hardness tests. After the 750 F (399 C) 1-year aging treatment, complete Brinell hardness tests were conducted. Tension testing was limited to one material.

### *Hardness Testing*

General Electric Company determined Brinell hardness values on each test bar blank after the aging treatment, prior to shipping the blanks for machining. Specimens for the hardness tests were cut from those blanks which had been forged with an additional length for this purpose. Cut faces were surface ground and polished on a rotating wheel with 280-grit paper. The Brinell impressions were made midway between the center and the edge of the specimen, in accordance with ASTM Standard Method of Test for Brinell Hardness of Metallic Materials (E 10-66).

### *Tension Testing*

The Midvale-Heppenstall Company conducted tension tests in accordance with ASTM Standard Method of Tension Testing of Metallic Materials (E 8-69). Testing was conducted at  $\sim 80$  F (27 C) and the crosshead speed was about 0.030 in./min.

### *Impact Testing*

The International Nickel Company performed impact tests in accordance with ASTM Standard Test Method E 23-66. The twelve impact test specimens supplied for each steel in each heat treatment condition were tested over a range of test temperatures to define absorbed energy as a function of test temperature. Broken specimens were examined and evaluated to define percent shear fracture and lateral expansion as a function of test temperature. The details of testing and temperature control to achieve test temperatures are given in Appendix 3.

After broken specimens were examined and evaluated by one operator at the International Nickel Company laboratory, they were forwarded to Bethlehem Steel Company laboratory for an independent examination and evaluation of percent shear fracture and lateral expansion. Again all work was performed by one experienced operator.

## **Test Results**

### *Hardness*

Brinell hardness test values of all steels after austenitizing, program cooling, tempering, and aging 1 year at 750 F (399 C) are presented in Table 3. The hardness ranged from HB 253 to 265, indicating a tensile strength range of 119,000 to 126,000 psi.

### *Tensile Properties*

The tensile properties of all steels after austenitizing and tempering (water quenched after tempering) are summarized in Table 4. Yield strengths (0.02 percent offset) ranged from 96,500 psi (for code S material) to 106,000

TABLE 3—Brinell hardness test values of 22 experimental heats (after heat treatment to simulate large rotors, and aging 1 year at 750 F).

Bar Code	HB	Bar Code	HB
A4	263	N4	262
B4	257	O4	257
C4	254	P2	254
D2	255	R4	256
E4	256	S4	255
G2	253	T2	261
H4	255	V4	259
J2	254	W4	255
K4	255	X4	259
L2	256	Y2	265
M4	253	Z4	259

TABLE 4—Tensile properties of 22 experimental heats.

Code	Tensile Strength, psi	0.02% Offset Yield Strength, psi	Elongation, %	Reduction in Area, %	0.2% Offset Yield Strength, psi
<i>After austenitizing at 1550 F; program cooling, and tempering</i>					
A4	122 000	103 000	21.0	66.4	111 000
B4	122 500	103 000	22.2	62.3	114 000
C4	119 000	101 000	24.0	68.5	108 000
D4	122 000	101 000	23.0	69.5	111 000
E4	120 000	98 500	22.0	70.3	107 000
G2	124 500	99 000	23.0	68.8	107 000
H4	120 500	101 000	23.0	70.1	109 000
J2	124 000	100 000	23.0	70.7	110 000
K4	121 500	101 000	20.7	69.3	110 500
L2	120 000	100 000	22.5	70.5	108 000
M4	121 500	102 000	24.0	67.9	112 000
N4	121 000	101 500	22.5	70.1	113 000
O4	121 000	101 000	24.0	67.7	111 000
P2	119 500	103 000	22.2	71.1	112 000
R4	117 000	104 000	22.2	70.5	113 500
S4	120 000	96 500	22.2	64.7	105 500
T2	121 000	103 500	22.0	69.9	111 000
V4	122 500	103 000	23.2	69.3	112 500
W4	121 500	104 500	22.2	65.9	114 000
X4	120 000	103 000	20.5	62.8	113 000
Y2	121 500	98 500	22.5	70.3	106 500
Z4	121 000	106 000	23.0	70.3	114 000
Avg	121 100	102 000	22.5	68.5	111 000
<i>After aging one year at 750 F (399 C)</i>					
M4	121 000	100 000	23.7	69.9	103 000

psi (for code Z material). The aim was 100,000 psi; the average attained was 102,000 psi.

The single bar tested (code M material) after aging 1 year at 750 F (399 C) exhibited tensile properties very close to the average values obtained on specimens before aging, and very close to the values reported for the same heat before aging (except for the 0.2 percent offset yield strength).

### Impact Properties

Impact test data were plotted by the two laboratories involved in obtaining and evaluating the data. Absorbed impact energy, percent shear, and lateral expansion data were plotted versus temperature and curves fitted to the data points by inspection. Until the end of the program, when the aged data were being obtained, all data were manually plotted. Another technique has been recently developed by Atherton [8], a mathematician at the International Nickel Company Research Laboratory, whereby the raw data are plotted and analyzed by computer. The entire plot is prepared and printed by computer (see Figs. 2-4). The curves are fitted to the data by suitable programming. The intersections of the curves, with preselected criteria, provide best approximations according to the computer program.

A review of all impact data obtained in the program indicated that the most significant parameters for analysis of the effect of the varied elements on temper embrittlement were the following:

1. 50 percent shear FATT
2. Temperature of 15-mil lateral expansion, LETT
3. Energy at 100 percent shear.

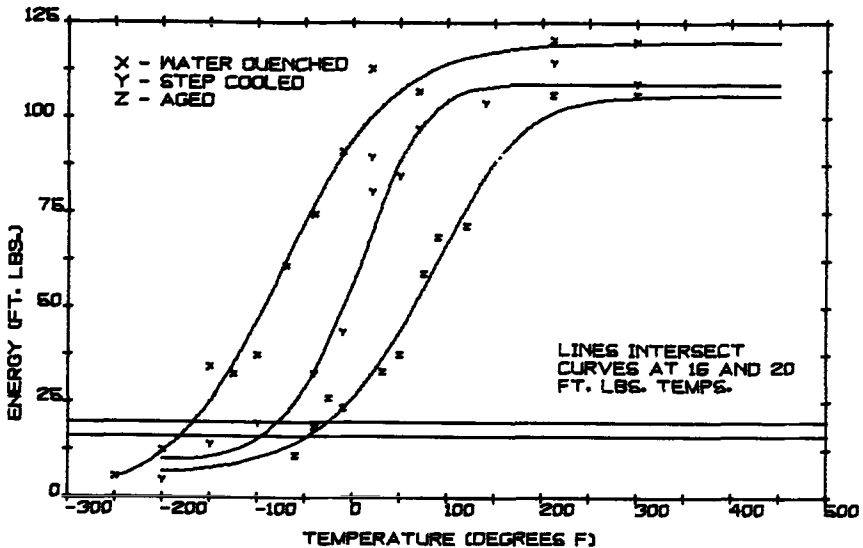


FIG. 2—Steel M—energy transition curves for different embrittling conditions.

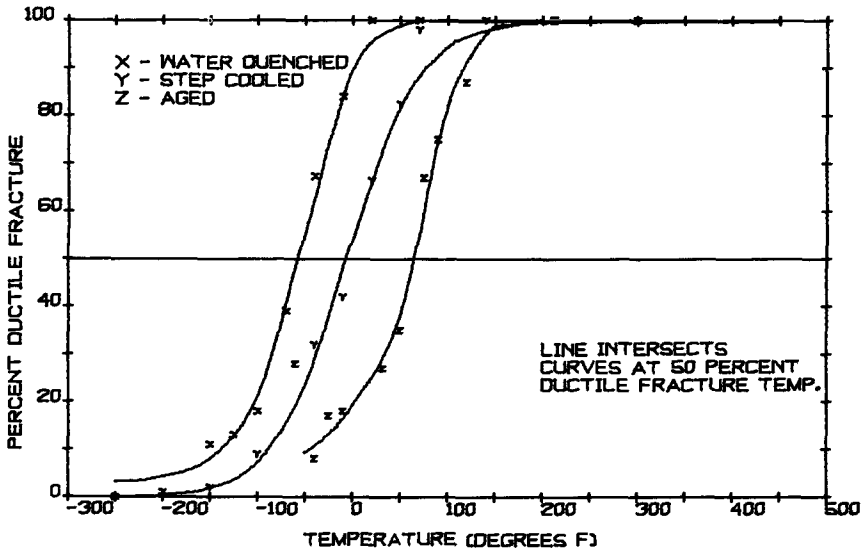


FIG. 3—Steel M—percent ductile fracture transition curves for different embrittling conditions.

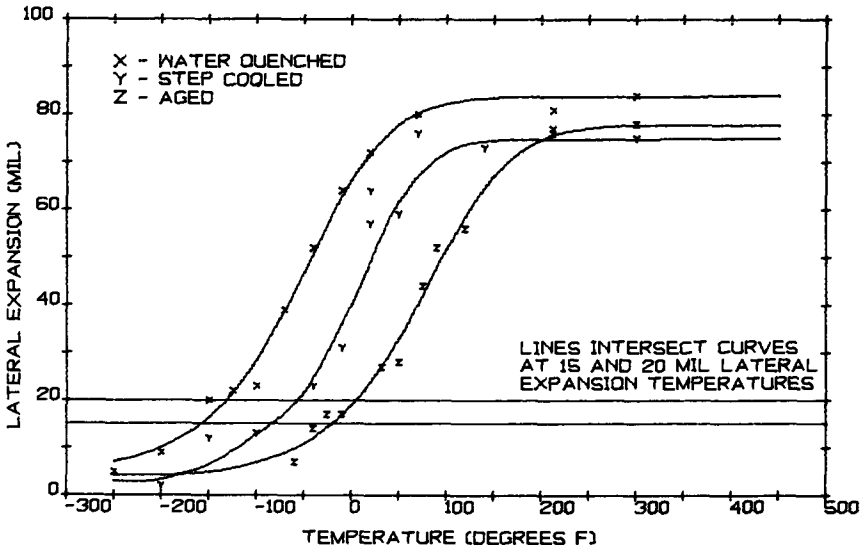


FIG. 4—Steel M—lateral expansion transition curves for different embrittling conditions.

A summary of values for the above parameters obtained on all steels, in all three heat treatment conditions (WQ, SC, and AG), is presented in Table 5. The data are grouped in accordance with the testing plan to aid in evaluating results. Values for 50 percent shear FATT temperatures were obtained from plots of percent shear versus test temperature and were reported to the

TABLE 5—Summary of impact data on 22 experimental heats.

Level	50% Shear FATT, deg F				Temperature of 15 mil lateral expansion, deg F				Energy at 100% shear ft·lb						
	P	Sn	Mo	As	Sb	Code	WQ	SC	AG	(SC-WQ) <sup>Δ</sup>	(AG-WQ) <sup>Δ</sup>	WQ	SC	AG	
0	0	0	0	0	0	P	-50	-30	10	20	60	-130	-125	-75	55
0	0	0	2	2	0	V	-60	-30	65	30	125	-150	-115	0	35
0	0	2	0	2	0	W	(-10)	(-5)	(30)	5	40	(-90)	(-75)	(35)	15
0	0	2	2	0	0	H	-65	-45	15	20	80	-110	-70	-45	40
0	2	0	0	2	2	J	-80	-25	50	55	130	-150	-105	-40	45
0	2	0	2	0	0	Y	-60	55	125	115	185	-130	-5	60	125
0	2	2	0	0	0	N	-80	-5	65	75	145	-110	-45	5	65
0	2	2	2	2	0	O	-75	15	80	90	155	-145	-35	30	110
2	0	0	0	2	2	Z	-50	40	170	90	220	-125	0	95	125
2	0	0	2	0	0	R	-55	55	205	110	260	-145	5	115	150
2	0	2	0	0	0	S	-50	40	145	90	195	-95	15	60	110
2	0	2	2	2	0	G	-55	15	135	70	190	-135	-55	60	80
2	2	0	0	0	0	X	(110)	(225)	(315)	115	205	(35)	(170)	(250)	135
2	2	0	2	2	2	C	-40	105	200	145	240	-110	45	125	155
2	2	2	0	2	0	D	-30	110	150	140	180	-90	60	90	150
2	2	2	2	2	0	B	-35	95	190	130	225	-100	50	125	150
1	1	1	1	1	1	A	(0)	(40)	(100)	40	100	(-45)	(10)	(55)	55
1	1	1	1	1	1	E	-50	10	90	60	140	-130	-55	30	75
1	1	1	1	1	1	K	-75	-10	70	65	145	-125	-45	15	80
1	1	1	1	1	1	L	-65	10	75	75	140	-140	-65	25	75
1	1	1	1	1	1	M	-65	-10	55	55	120	-135	-65	0	70
1	1	1	1	1	1	T	-60	15	85	75	145	-125	-25	10	100
Corrected						W <sup>a</sup>	-55	-50	-15	5	40	-125	-110	-70	15
Corrected						X <sup>a</sup>	-55	60	150	115	205	-125	10	90	135

<sup>a</sup> Transition temperature for W, X, and A in parentheses were too high because of microstructural differences. FATT WQ and LETT WQ were corrected for W and X by substituting the respective means for the other 14 heats of the first 16. Corrected values for the SC and AG conditions were obtained by adding the observed values of Δ(SC-WQ) and Δ(AG-WQ), which were apparently not affected, to the respective transition temperature in the WQ condition.

nearest 5 deg F, after comparing evaluations made by the two laboratories. Temperatures at which 15-mil lateral expansion occurred were obtained from plots of lateral expansion versus test temperature and were reported to the nearest 5 deg F; data from one laboratory were favored because of its use of a more precise measuring device. Energy values at 100 percent shear represent the lowest energy absorbed by those specimens which exhibited 100 percent shear fracture.

A statistical analysis of the data is included in Part II. The analysis is primarily concerned with the change in properties—transition temperatures, to be exact—since it is apparent that impact shelf energy and room temperature tensile properties do not change as a result of step cooling from the tempering temperature nor as a result of aging 1 year at 750 F (399 C). Both the specific temperatures of transition and their shift due to embrittlement, as affected by heat treatment, level of trace elements, and level of Mo addition, are considered in this paper.

A few observations can be made from the data presented in Table 5. With one exception (code X material), the energy at 100 percent shear is relatively unaffected by composition or heat treatment; all data range between 88 and 113 ft·lb. With the exception of codes A, W, and X, the temperatures for 50 percent shear after water quenching from the tempering temperature fall within the range  $-30$  to  $-80$  F ( $-34$  to  $-62$  C).

Examination of the temperature of 15-mil lateral expansion reveals that codes A and X exhibit unusually high values after water quenching from the tempering temperature but that code W is not significantly different from several other materials. With the exception of codes A and X, temperatures of 15-mil lateral expansion after water quenching from the tempering temperature range from  $-90$  to  $-145$  F ( $-68$  to  $-98$  C).

#### *Investigation of A, W, and X*

The irregularly high transition temperatures of specimens XWQ and XSC, and the consequent poor fit of the data from these specimens in the statistical analysis prompted a metallurgical investigation of this irregularity.

For this investigation, the steels were separated into the following five classes: high P-high Mo, high P-low Mo, low P-high Mo, low P-low Mo, and center point heats. Specimens for examination were selected on the basis of the extent to which their transition temperatures in the water quenched condition deviated from those of other specimens within the same class. For example, five of the center point heats exhibited an average FATT of  $-65$  F ( $-54$  C), while the FATT of heat A was  $+5$  F ( $-15$  C). Accordingly, specimen AWQ was examined from this class, specimens XWQ and WWQ were selected from their respective classes, and control specimens from unaffected heats in each class were also selected. The investigation included optical metallography ( $\times 1000$ , picral and selective etchants), electron metallography with

carbon extraction replicas, energy dispersion X-ray spectroscopy utilizing the scanning electron microscope, and structural determination of extracted carbides by X-ray diffraction.

Similar studies were performed on additional material from A, W, and X and normal heats K, O, and Z after a heat treatment similar to the original simulated rotor water quench. Also, material water quenched directly from the austenitizing temperature, without tempering, was studied to see if the high transition temperatures and unusual structures of A, X, and W were peculiar to the first heat treatment or to the cooling rate or were characteristic of these heats. Tension tests and Charpy impact tests were also performed on these materials after tempering to HRC 25–26, water quenching, and step cooling from 1100 F (593 C).

Metallographic examination revealed the presence of clusters of carbides widely dispersed at random locations in the tempered bainitic microstructure of specimens XWQ, WWQ, and AWQ, somewhat more massive in these heats than in others. In these affected areas, the carbides partially outlined prior grain boundaries and were present somewhat in proportion to the variation in FATT WQ. The carbides delineated in the optical microscope were successfully extracted. Their structure was identified as that of the  $M_{23}C_6$  carbide with the composition of the M constituents being principally Fe with lesser amounts of Cr, Mo, and V. An examination of the melting and processing records of the heats revealed no irregularities that would suggest a cause for the formation of the carbides. Similar carbides were observed in the material with a simulated rotor water quench and in the material with a direct water quench without tempering.

While the occurrence of clusters of carbides in heats X, W, and A seemed to be associated with their higher transition temperature, there was no indication that their presence affected the embrittlement produced by step cooling or long time exposure at 750 F. Accordingly, temper embrittlement data from these heats were retained in the analysis. The occurrence of this irregularity in the present experimental program may be of interest to producers and users of heavy forgings, insofar as the presence of such carbide clusters may, in part, explain variations in the unembrittled transition temperature of production rotors of the Ni-Cr-Mo-V steel.

In a separate investigation, white etching areas having the appearance of ferrite when etched with nital, which did not appear in other heats, were observed in heats A and X. However, microhardness tests in these white areas showed that the hardness was about the same as that of the surrounding matrix. Repolishing and etching with sodium metabisulfite produced much smaller white etching areas. By repolishing again and etching with nital, white areas of the original size were reproduced. It was concluded that these white etching areas were not ferrite, but were due to an etching effect probably unrelated to the observed difference in properties.

*Analysis of Results*

Selected data are presented in Table 6 to illustrate some of the principal effects of composition variations. The data for center point heat materials containing all elements at approximately the middle of the extremes investigated are presented in the first group of data in Table 6. Average values are presented with and without A, a material in question. These average values provide the basis for an examination of low- and high-side variations of the testing plan.

TABLE 6—Selected impact data illustrating the effect of composition variations.

Code	50% Shear FATT, deg F					Temperature of 15-mil Lateral Expansion, deg F				
	WQ	SC	AG	$\Delta$ (SC-WQ)	$\Delta$ (AG-WQ)	WQ	SC	AG	$\Delta$ (SC-WQ)	$\Delta$ (AG-WQ)
<i>Center Point Heats</i>										
A	0	40	100	40	100	-45	10	55	55	100
E	-50	10	90	60	140	-130	-55	30	75	160
K	-75	-10	70	65	145	-125	-45	15	80	140
L	-65	10	75	75	140	-140	-65	25	75	165
M	-65	-10	55	55	120	-135	-65	0	70	135
T	-60	15	85	75	145	-125	-25	10	100	135
Avg	-53	9	79	62	132	-117	-41	23	76	140
Avg (-A)	-63	3	75	66	138	-131	-51	16	80	147
<i>All Elements on Low Side</i>										
P	-50	-30	10	20	60	-130	-125	-75	5	55
<i>Trace Elements on High Side</i>										
C	-40	105	200	145	240	-110	45	125	155	235
<i>High Mo, Low P, Low Sn</i>										
H	-65	-45	15	20	80	-110	-70	-45	40	65
<i>High Mo, High P, High Sn</i>										
B	-35	95	190	130	225	-100	50	125	150	225
D	-30	110	150	140	180	-90	60	90	150	180
Avg	-33	103	170	135	203	-95	55	108	150	203

P is the one material in which all varied elements were low. All transition temperatures for this material were significantly lower than the average values for the center point heats after sensitizing heat treatments. This indicates that by lowering one or more of the varied elements, the sensitivity to embrittlement is reduced.

C is the one material in which all varied elements were high except Mo. There was no material in the half replicate testing program in which all varied elements were high. Transition temperatures for the code C material were significantly higher than the average values for the center point heats after

sensitizing heat treatments, indicating that one or more of the varied residual elements contributed to the increase in sensitivity to embrittlement.

Further examination of the data revealed that P and Sn were most detrimental to impact transition temperatures after sensitizing heat treatments. There was some question whether higher Mo contents would lower transition temperatures, or at least reduce the detrimental effects of P and Sn.

H is high in Mo and low in P and Sn. The data for code H material are not significantly different from those of heat P in which all varied elements are low.

B and D are materials high in Mo, P, and Sn. Comparing the results of these materials with the results of C, in which Mo was low but all trace elements were high, indicates that high Mo reduces the detrimental effect of P and Sn on transition temperature after aging 1 year at 750 F (399 C).

To confirm the observations based on selected materials, it was possible to take advantage of the statistical design of the experiment and analyze the results on all materials, establishing the significant influence on each element varied on the level of transition temperatures. Such analysis would expose more subtle effects and interactions that simple inspection of the data would not permit. The fact that W and X of the factorial heats had excessively high transition temperatures, due to microstructural differences, required that they be deleted or corrected before analysis.

A correction of W and X was made by substituting the mean of FATT WQ and LETT WQ for the other 14 factorial heats for W and X. The values of  $\Delta(\text{SC-WQ})$  and  $\Delta(\text{AG-WQ})$  were assumed to be unaffected and were added to the FATT WQ and LETT WQ to obtain FATT SC, FATT AG, LETT SC, and LETT AG. The corrected values thus obtained are listed at the bottom of Table 5. A formal analysis of variance was then made, but inspection of the various group means made it apparent that these corrections were distorting the results. Table 7 presents group averages for transition temperatures without W and X for the various conditions, for high and low concentrations of each significant controlled element, and for the two-factor interactions which seemed significant. These are also plotted in part in Figs. 5 and 6.

Multiple regression analyses were also run using 19 of the 22 heats (omitting A, W, and X) with results summarized in Table 8 as Eqs 2-7. The first five variables in Table 8 are linear terms and the final ten are interaction terms formed by multiplying various two-factor combinations of the first five variables. The methods used in regression analyses were similar to those described by Stewart [6]. Initial correlations were made with the independent variables standardized by subtracting the mean value of each variable for the 19 heats from each individual value:

$$\begin{aligned} \text{FATT WQ} = & b_0 + b_1(\text{P} - \bar{\text{P}}) + b_2(\text{Sn} - \bar{\text{Sn}}) + \dots \\ & + b_{12}(\text{P} - \bar{\text{P}})(\text{Sn} - \bar{\text{Sn}}) + \dots \end{aligned}$$

TABLE 7—Group averages for transition temperatures showing significant main effects and two-factor interaction effects of P, As, Sb, and Sn, with code W and X materials deleted.

Dependent Variable	First Element	Level	Mean Content, ppm or %	Second Element	Level	Mean Content, ppm or %	Number of Observations	Mean of Dependent Variable
FATT WQ	P	0	0.006				7	-67
		2	0.018				7	-45
		0	0.006	Sn	0	16	3	-58
		0	0.005	Sn	2	104	4	-74
		2	0.018	Sn	0	34	4	-52
		2	0.018	Sn	2	108	3	-35
FATT SC	P	0	0.006				7	-9
		2	0.018				7	66
	Sn	0	26				7	6
		2	106				7	50
FATT AG	P	0	0.006				7	59
		2	0.018				7	171
	Sn	0	26				7	106
		2	106				7	123
	As	0	30				6	98
		2	158				8	127
	P	0	0.006	Sn	0	16	3	30
		0	0.005	Sn	2	104	4	80
		2	0.018	Sn	0	34	4	164
		2	0.018	Sn	2	108	3	180
LETT WQ	P	0	0.006				7	-132
		2	0.018				7	-114
	Mo	0	0.30				7	-134
		2	0.61				7	-112
	P	0	0.006	Sn	0	16	3	-130
		0	0.005	Sn	2	104	4	-134
		2	0.018	Sn	0	34	4	-125
		2	0.018	Sn	2	108	3	-100
LETT SC	P	0	0.006				7	-71
		2	0.018				7	17
LETT AG	P	0	0.016				7	-9
		2	0.018				7	96
	Sn	0	26				7	30
		2	106				7	56
	As	0	30				6	22
		2	158				8	59

The equation chosen included all linear terms and all cross product terms for which the F test for deletion of the term from the equation had a significance in excess of about 0.95. To these were added linear terms not significant in themselves but involved in cross product terms in the equation. A second correlation was then made in each case using the actual data, unstandardized, to derive equations with the same linear and cross product terms. This should

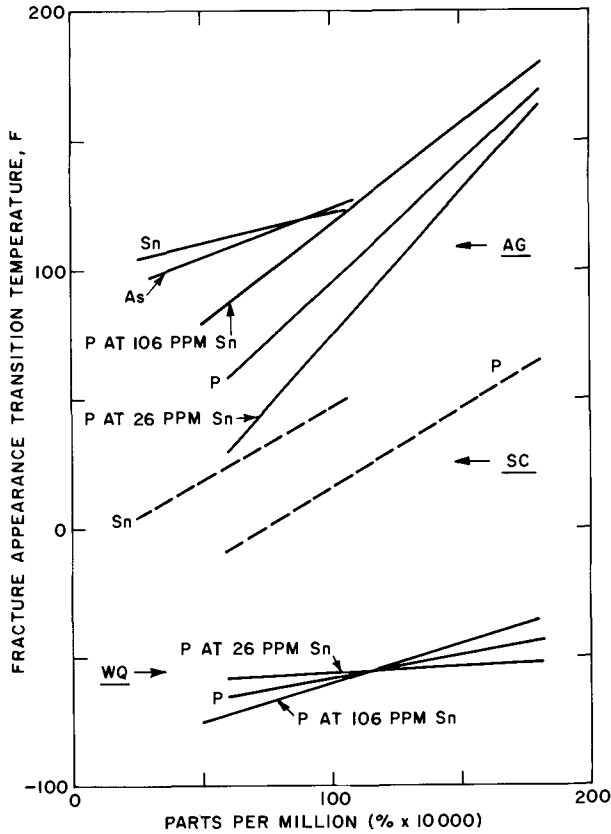


FIG. 5—Significant main effects and two-factor interaction effects of elements on FATT for water quenched, step cooled, and aged conditions.

be equivalent to the original equation but easier to present and use. The equations in Table 8 were those obtained by this method using the actual data, unstandardized, in the following form:

$$\text{FATT WQ} = b_0 + b_1(P) + b_2(\text{Sn}) + \dots + b_{12}(P)(\text{Sn}) + \dots$$

For convenient reference in subsequent discussions, the 4 equations developed by Stewart [6], Eqs 8(22) to 11(22), for step cooled and isothermal temper embrittlement, using all 22 heats, are listed in Table 9 in the unstandardized form described before. Four similar equations were obtained by regression analysis using the same 19 heats that were used in Table 8. These are included in Table 9 as Eqs 8(19) to 11(19) for comparison with the equivalent equations for 22 heats.

The equations in Tables 8 and 9 may be written in the following form:

$$\text{FATT} = -60 + 164(\% P) - 0.273(\text{ppm Sn}) + 23.92(\% P)(\text{ppm Sn}) \quad (2)$$

TABLE 8 — Regression equations for fracture appearance and 15-mil lateral expansion transition temperatures, in the WQ, SC, and AG conditions using 19 heats (W, X, and A deleted).

Equation Number	2	3	4	5	6	7
Dependent Variable	FATT WQ, deg F	FATT SC, deg F	FATT AG, deg F	LETT WQ, deg F	LETT SC, deg F	LETT AG, deg F
Constant	-60	-91	-28	-182	-163	-84
Coefficients for:						
P, %	164	6143	9057	-1343	7369	12 501
Sn,ppm	-0.273 <sup>a</sup>	0.613	0.400		0.661	-0.0109
Mo, %	...	...	...	180.4	...	-206.5 <sup>a</sup>
As,ppm	...	...	...	...	...	0.345
Sb,ppm	...	...	...	...	...	...
(P, %) × (Sn,ppm)	23.92	...	...	0.574 <sup>a</sup>	...	...
(P, %) × (Mo, %)	...	...	...	...	...	...
(P, %) × (As,ppm)	...	...	...	...	...	...
(P, %) × Sb,ppm)	...	...	...	132.4	...	...
(Sn,ppm) × (Mo, %)	...	...	...	...	...	...
(Sn,ppm) × (As,ppm)	...	...	...	...	...	...
(Sn,ppm) × (Sb,ppm)	...	...	...	...	...	2.479
(Mo, %) × (As,ppm)	...	...	...	...	...	...
(Mo, %) × (Sb,ppm)	...	...	...	-5.862	...	...
(As,ppm) × (Sb,ppm)	...	...	...	...	...	...
Mean	-58	22	104	-125	-33	36
Initial Variation(S <sup>2</sup> )	201	2117	3590	332	2908	3318
Variation Removed(R <sup>2</sup> )	0.67	0.83	0.77	0.75	0.81	0.91

<sup>a</sup> Linear terms not significant in correlations using standardized variables ( $X - \bar{X}$ ) but included because they are involved in significant interactions.

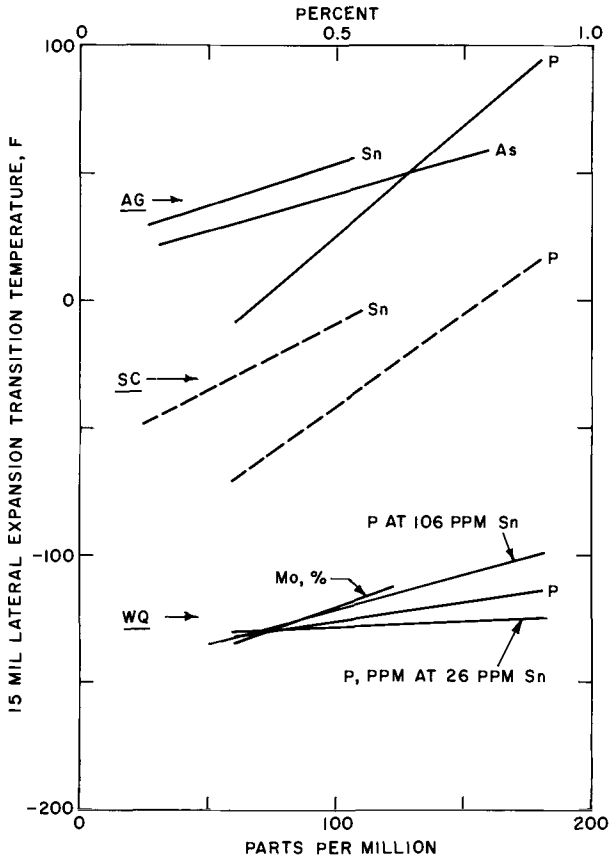


FIG. 6—Significant effects of elements on the 15-mil LETT for water quenched, step cooled, and aged condition.

*Transition Temperature, Deembrittled, WQ*

From Fig. 5 and Eq 2, it appears that FATT WQ is directly affected by P content and that this effect is greater when higher Sn is present. With 15-mil lateral expansion (LETT WQ) as a criterion, the effect of P and its interaction with Sn are still evident. Mo tends to increase LETT WQ. Equation 5 shows significant linear effects for P and Mo and interactions between P and Sb and between Mo and Sb, not plotted in Fig. 6.

*Step Cooled Transition Temperature, SC*

Only P and Sn significantly affect step cooled FATT and LETT, and both the plots of Figs. 5 and 6 and the coefficients of Eqs 3 and 6 show their effects to be similar on the basis of percent by weight or parts per million (multiply the coefficient of Sn by 10,000 to convert to percent). The average FATT and

TABLE 9—Regression equations for step cooled and isothermal embrittlement as determined by shift in fracture appearance and 15-mil lateral expansion transition temperatures, from Stewart [6] for 22 heats versus 19 heats, with A, W, and X deleted.

Equation Number	8(22)	8(19)	9(22)	9(19)	10(22)	10(19)	11(22)	11(19)
Dependent Variable	$\Delta FATT$ (SC-WQ)	$\Delta FATT$ (SC-WQ)	$\Delta FATT$ (AG-WQ)	$\Delta FATT$ (SC-WQ)	$\Delta FATT$ (SC-WQ)	$\Delta FATT$ (SC-WQ)	$\Delta FATT$ (AG-WQ)	$\Delta FATT$ (AG-WQ)
Number of Heats	22	19	22	19	22	19	22	19
Constant	-16	-11	0	1	-17	-83	15	0.81
Coefficients for:								
P, %	4394	4254	13 544	13 397	5888	5784	12 728	13 477
Sn,ppm	0.6175	0.6145	1.295	1.299	0.5669	0.5593	1.146 <sup>a</sup>	1.278 <sup>a</sup>
Mo, %	...	...	-93.06	-85.7	...	...	-116.1	-111.0
As,ppm	...	...	0.2132	0.2148	...	0.6204 <sup>a</sup>	0.3096	0.361
Sb,ppm	...	...	...	...	...	3.0556 <sup>a</sup>	...	...
(P, %) × (Sn,ppm)	...	...	-81.32	-82.3	...	...	-73.52	-86.13
(As,ppm) × (Sb,ppm)	...	...	...	...	...	-0.02614	...	...
Mean	76	79	156	162	89	92	156	161
Initial Variation(S <sup>2</sup> )	1552	1361	3267	2718	2079	1931	3328	2919
Variation Removed(R <sup>2</sup> )	0.82	0.84	0.85	0.86	0.79	0.87	0.83	0.86

<sup>a</sup> Linear terms not significant in correlations using standardized variables ( $X - \bar{X}$ ) but included because they are involved in significant interactions.

LETT are 81 F and 93 F (45 C and 52 C) higher than for the WQ condition. The coefficient for P is also much higher.

#### *Transition Temperature after Aging, AG*

The mean FATT and LETT after 1 year of aging at 750 F (399 C) are 160 F and 162 F (89 C and 90 C) higher than for the water quenched condition, reflecting a shift in transition temperature on the order of twice as much as that produced by step cooling (Eqs 4 and 7). The effect of P is considerably greater and that of Sn less than those for the step cooled conditions. In the case of LETT AG, for the first time positive effects were observed for As and interactions involving P-Sn and Sn-Mo were found to be significant.

#### **Discussion**

Perhaps the most noteworthy results of this program were the strong effects of P and Sn on transition temperature and on step cooled and isothermal embrittlement. Also important was the complete lack of effect observed for Sb, previously identified as a strong contributor to temper embrittlement. Difficulties experienced in obtaining consistent and reproducible analyses for both residual elements and common alloying elements as described by Penkrot [7] revealed problems in this area at least partly unexpected, especially where well standardized analytical procedures for common elements were involved.

Previous analyses of transition temperature and step cooled temper embrittlement have consistently shown high coefficients for P, on the order of 5000 to 7000 F/percent in linear equations. Newhouse and Holtz [2] reported coefficients ranging from 1.68 to 4.4/ppm for Sb and 0.21 in one case for Sn. However, they observed that As, Sb, and Sn were highly correlated and so could not be sure that at least some of the effect attributed to Sb might not have been due to As or Sn. Results of this factorial experiment showed this to be the case to the extent that the effect of Sb on embrittlement seemed the least significant of that of any of the five variables under the conditions and within the limits of this experiment. The effects observed for Sn were conclusive because they rested on a foundation of reliable chemical analysis. It should be recognized that effects of any of the elements may be different in another base composition, in a Si deoxidized steel, or with variations in tensile strength, grain size, or other factors.

The assumption was made earlier that the shifts in transition temperature by step cooling and aging were not affected by the microstructural features associated with the higher values for FATT WQ and LETT WQ in heats A, W, and X, because they were consistent with similar heats in the experiment. However, Newhouse and Holtz [2] observed a correlation between  $\Delta$ FATT SC and FATT WQ in their equations. An increase in FATT WQ was associated with reduced  $\Delta$ FATT SC, and, if this was due to similar differences in structure, there may have been minor effects on embrittlement in the

experiment described in the current work. A comparison of the regression equations for temper embrittlement of Stewart [6] using 22 heats, with those using 19 heats in Table 9 shows little difference in the significant terms included or in their coefficients except for Eqs 10(22) and 10(19). The latter had similar coefficients for P and Sn, but Eq 10(19) also included an As-Sb interaction, significant for  $\Delta\text{LETT SC}$ , at a much lower level of significance than P and Sn. It was concluded that the assumption that shifts in transition temperature of A, W, and X were not affected by whatever caused their higher deembrittled transition temperatures and that equations for FATT and LETT in Table 8 for which only 19 heats were used are valid.

Comon et al [9] replaced  $\Delta T$  with a logarithmic function of  $\Delta T$  ( $\log \Delta T + 27$ ) to permit an analysis of interesting effects with simple linear terms for the independent variables and drew conclusions about the effects of a number of compositional and heat treatment variables. This model was examined but the results offered no advantage in the analysis of the results of this experiment.

The identification of Sn and As as contributors to embrittlement in the vacuum carbon deoxidized rotor steel emphasizes a need for improved methods of analysis, and for accumulation of data on the occurrence of these residual elements in rotors and on possibilities for their control. The difficulties in obtaining consistent chemical analyses in carrying out this program, even for some common elements, illustrate the difficulties to be expected and the caution required in trying to analyze data on production forgings from a number of sources.

Of the 4 residual elements, only P can be reduced appreciably by refining operations during steelmaking. The others can thus far only be controlled by using raw materials which contain very low levels. The results for Mo show that increasing the level of this element tends to reduce isothermal embrittlement, contrary to previous reports by several investigators [2,9]. This tends to counteract its tendency to increase the unembrittled LETT so that there is no apparent effect of Mo content on transition temperature after step cooling or isothermal aging.

Recent work has been done which shows the continued importance of temper embrittlement in relation to the design and application of heavy section components, particularly those operating at high stresses and at temperatures within the range of embrittlement. For example, Viswanathan [10] describes results of exposing Ni-Cr-Mo-V steel at 95 and 145-ksi yield strength to a temperature of 850 F (454 C) for 35,000 h. The fracture appearance transition temperature after exposure was 270 F (132 C) for the steel with lower yield strength and 955 F (513 C) for the other. Control of isothermal embrittlement is clearly a serious problem for high strength parts operating at elevated temperatures. Sticha [11] has reported up to 60 F (33 C) increase in Charpy transition temperature in quenched and tempered  $2\frac{1}{4}\text{Cr-1Mo}$  steel after aging 10,000 h at 800 F (427 C). Up to 100 F (56 C) embrittlement has been produced in ASTM A 542 by step cooling [12].

## Summary and Conclusions

The results of this program confirm the previously noted effects of P and in addition show that Sn contributes to embrittlement in this steel to an equivalent degree. Sb did not have an effect but amounts were low in this program, typical of current practice in the United States. Vacuum carbon deoxidation may also have contributed to the absence of effect of Sb. Interactions were also observed between the effects of Sn and P. As had a significant effect only for isothermal embrittlement. Several other interactions were found. Mo within the range studied was shown to increase the unembrittled LETT but, contrary to previous reports, was observed to decrease isothermal embrittlement. Under the conditions of this experiment, step cooled embrittlement can be used to provide an estimate of embrittlement produced by 1 year of exposure at 750 F (399 C), as shown by Stewart [6].

Three heats of the 22 of the series had unusually high transition temperatures, but the shift produced by step cooling or isothermal exposure at 750 F seemed consistent with those of the other steels. The same heats exhibited unusual grain boundary carbides identified as  $M_{23}C_6$ , which may have contributed to the unusual properties of these heats.

## APPENDIX 1

### Melting and Casting

Steel for the experimental program was provided from the product of 22 vacuum induction melted 50-lb. heats that were melted and cast at the Applied Research Laboratory of the United States Steel Corporation. The heats were melted in a Stokes vacuum induction melting furnace, Model 436-504. The crucible used was a Lava Crucible Refractories Company 50-M magnesia crucible, which is basically 90 percent electrically fused magnesia with a magnesium silicate bond. In this furnace system, all additions are preweighed and placed in charging hopper chambers within the vacuum system prior to evacuation, and means are provided for adding the various materials to the melt as required during the progress of the heat. The heats were melted sequentially according to a prearranged statistically random plan in one campaign using one crucible that was new at the beginning of the campaign. No other melting was done in the crucible or in the system during the course of the six days required for the completion of the campaign. The heats were cast into a square cast iron mold 4 by 4 in. at the top, 3  $\frac{5}{8}$  by 3  $\frac{5}{8}$  in. at the bottom, and 12  $\frac{1}{2}$  in. high, having a 3  $\frac{1}{4}$  by 3  $\frac{1}{4}$ -in.-square by 2  $\frac{1}{2}$ -in.-high refractory hot top section.

The raw materials and melting stock used for these heats were largely those used by the U.S. Steel Applied Research Laboratory in the routine preparation of a large variety of special experimental heats where close composition control is necessary. Table 10 gives the trade name, supplier, physical form, purity, and some information on residuals for each of the elemental additions used in this program.

TABLE 10—Information on melting stock.

Element	Physical Form	Trade Name	Supplier	Purity, %	Residuals, %				
					Sb	As	Sn	Al	
C	crushed 1/8 by 1/8 in. electrolytic lump	Elmang	Ringsdorff Carbon Corp.	99.9	...	...	...	...	...
Mn	1 in. to powder		Union Carbide Corp.	99.9	...	...	...	...	...
P	1/2 in. diameter stick	Ferrous Sulphide Stick	Duquesne Works, USS	25.0	...	...	...	...	...
S	1 by 1/4 in. squares	QM squares	Allied Chemical Co.	33.0	...	...	...	...	0.004 Total
Si	1 by 1/8 in. crushed briquettes pellets	Elchrome (Vacuum Grade)	Union Carbide Corp.	93.0	...	...	...	...	0.012 0.35 0.52
Ni	1 in. by down 1/8 by 1/8 in. ash	High Speed Grade	Inco Sherritt Co.	99.9	...	...	...	...	...
Cr	powder	Arsenic Metal Purified Code 1390	Union Carbide Corp.	99.87	...	...	...	...	0.01
Mo	stick 3/8 in. diameter electrolytic	Antimony Metal Reagent Code 1361 Analytical Reagent	Climax Molybdenum Company	99.9	...	...	...	...	...
V	stick 3/8 in. diameter electrolytic	Plast Iron A-101-B	Union Carbide Corp.	75.0	...	...	...	...	0.03 Soluble 0.19 Total
As			Allied Chemical Co.	99.8	...	X	...	...	...
Sb			Allied Chemical Co.	99.7 min	X	0.01	0.01	0.01	...
Sn			Mallinckrodt Chem. Works	99.9	0.02	0.0001	X	...	...
Fe			Metals Division, Gidden- Durkee Division, SCM Corp.	99.9	...	...	...	...	0.002

TABLE 11—Cup test analyses of steels<sup>a</sup> for ASTM temper embrittlement program, percent.

Heat Number	C	Mn	P	S	Si	Ni	Cr	Mo	V	Solu-ble Al	Total Al
Z20489	0.26	0.31	0.018	0.011	0.052	3.57	1.76	0.31	0.12	0.002	0.004
Z20490	0.25	0.32	0.010	0.012	0.074	3.48	1.73	0.46	0.12	0.004	0.005
Z20491	0.28	0.31	0.002	0.010	0.051	3.49	1.72	0.60	0.12	0.018	0.020
Z20492	0.27	0.32	0.021	0.011	0.09	3.49	1.74	0.63	0.11	0.001	0.004
Z20493	0.25	0.32	0.015	0.008	0.076	3.38	1.71	0.31	0.12	0.011	0.015
Z20494	0.28	0.33	0.006	0.011	0.08	3.48	1.75	0.31	0.13	0.006	0.007
Z20495	0.25	0.31	0.014	0.009	0.066	3.47	1.74	0.30	0.12	0.009	0.012
Z20496	0.26	0.31	0.002	0.008	0.064	3.47	1.72	0.31	0.12	0.010	0.016
Z20497	0.22	0.32	0.007	0.010	0.086	3.49	1.77	0.47	0.12	0.003	0.008
Z20498	0.26	0.32	0.007	0.011	0.11	3.46	1.74	0.61	0.12	0.003	0.005
Z20499	0.29	0.33	0.007	0.008	0.09	3.47	1.71	0.46	0.12	0.002	0.006
Z20500	0.29	0.32	0.003	0.008	0.09	3.52	1.73	0.60	0.12	0.006	0.012
Z20501	0.27	0.31	0.002	0.009	0.074	3.48	1.71	0.59	0.12	0.008	0.012
Z20502	0.27	0.31	0.019	0.009	0.061	3.54	1.74	0.61	0.12	0.002	0.003
Z20503	0.26	0.31	0.009	0.008	0.064	3.50	1.72	0.45	0.12	0.006	0.012
Z20504	0.26	0.30	0.010	0.008	0.082	3.41	1.72	0.45	0.12	0.002	0.005
Z20505	0.28	0.31	0.002	0.007	0.052	3.46	1.72	0.29	0.11	0.004	0.009
Z20506	0.27	0.30	0.013	0.008	0.064	3.52	1.75	0.60	0.12	0.010	0.012
Z20507	0.29	0.32	0.006	0.008	0.076	3.47	1.73	0.45	0.12	0.009	0.013
Z20508	0.31	0.32	0.021	0.011	0.063	3.49	1.73	0.30	0.12	0.007	0.011
Z20509	0.29	0.32	0.015	0.008	0.060	3.52	1.76	0.61	0.13	0.015	0.017
Z20510	0.28	0.32	0.004	0.011	0.055	3.45	1.74	0.30	0.11	0.009	0.013

<sup>a</sup> United States Steel Corporation Applied Research Laboratory.

The heats were melted and cast in accordance with usual vacuum induction melting practices. A typical heat log was as follows:

Time  
elapsed,  
min

Charging C-Ni-Mo and a portion of the Fe charged into crucible, balance of Fe and other elements charged into remote controlled addition hoppers and system sealed.

0 Power on.

1 System evacuated to 50  $\mu$ m.

10 to 20 After initial charge of about 20 lb was melted, balance of Fe and then Cr was added. Ar used as required in range 10 to 25-torr pressure during this period to control bath activity.

35 Heat melted. Full vacuum (50  $\mu$ m) applied.

40 Held 5 min after all base charge is melted for carbon finish (stabilization of C). Temperature 2840 F (1560 C).

41 Argon added to system until a pressure of 250 torr is reached to minimize loss of volatile elements in subsequent additions.

42 Added Si, P, and S.

43 Added Mn and V.

45 Temperature 2845 F (1563 C).

46 Added Sb, Sn, and As.

48 Tapped (approximately 1 to 2 min after finishing alloy additions).

During the course of the melting of these heats, good mixing and agitation of the bath was obtained by natural induction stirring of the system. Temperatures were obtained by means of remotely controlled Pt, Pt-Rh immersion thermocouples. The ingots were cast in the 250-torr Ar atmosphere by remote control, after which the system was air released to atmospheric pressure and the molds removed.

A specimen for chemical analysis was obtained during the pouring of these heats. At the beginning, as the first liquid steel was being poured, a small copper chill mold was rotated into position under the pouring spout of the furnace and a specimen measuring 2-in. in diameter by 3-in. high and weighing approximately 2 1/2 lb was obtained from the pouring stream. The cup test analyses listed in Table 11 were obtained by either instrumental or wet chemical analytical techniques or both, from a diametrical cross section cut approximately 1 in. from the bottom of these specimens.

## APPENDIX 2

### Forging and Preliminary Heat Treatment

The twenty-two 50-lb. ingots were forged at the Bethlehem Steel plant of the Bethlehem Steel Corporation. The standard practices for forging and preliminary treatment in effect at the time for Ni-Cr-Mo-V vacuum carbon deoxidized turbine rotors were used for these ingots. A maximum furnace temperature of 2200 F (1204 C) with minimum soaking time of 2 h was specified. The minimum forging temperature specified was 1600 F (871 C) with polishing allowed to 1400 F (760 C).

The ingots were forged on a 2000-lb double-framed Erie Steam hammer. Two heating operations were required to forge out the entire body of the ingot to 1 1/16 in. square to the specified lengths. All 22 ingots had at least pieces 1 and 2 forged and cut apart on the first heating operation with several of the ingots having piece 3 final forged on the first operation. (See Fig. 7.) Ingots A, B, C, D, E, K, O, P, and V had, in addition to pieces 4 and 5, a sixth piece forged varying in length from 4 to 11 in. All ingots had the sinkhead cropped with the exception of code Y material which had 3 in. of the 1 1/16-square sinkhead remaining in piece 5.

After the first and second forging operations, the finished pieces were hot stamped and cut apart prior to burying in SIL-O-CEL to slow cool to room temperature. After cooling to room temperature all of the 1 1/16-in.-square material was placed in a Hayes electric furnace rated at 95 kW, box type (8 by 34 by 72 in. in depth), and given the following conditioning cycle:

Heat at 100 F/h (56 deg C/h) maximum to 1850 F (1010 C), hold 4 h

Furnace cool about 2 days to 500 F (260 C), equalize 4 h

Heat at 100 deg F/h (56 deg C/h) maximum to 1700 F (927 C), hold 2 h

Furnace cool (door open below 1200 F (650 C)) about 1.5 days to 500 F (260 C), equalize 4 h

Heat at 100 deg F/h (56 deg C/h) maximum to 1200 F (649 C), hold 4 h

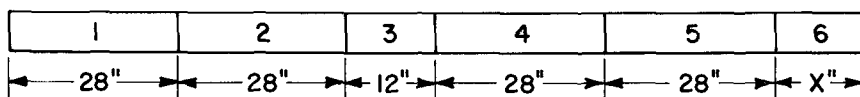


FIG. 7—Orientation and identification of forged bars in relation to the ingot.

TABLE 12—Forging data for 22-heat program.

Order of Forging	U.S. Steel Heat Number	BSCorp Code Number	Time Charged in Furnace	Furnace Temperature at Charge, deg F	Draw Time	Furnace Temperature at Draw, deg F	Start Forge Temperature, deg F	Finish Forge Temperature, deg F	Finish Sizing Temperature, deg F	Re-charge Time	Furnace Temperature at Charge, deg F	Redraw Time	Furnace Temperature, deg F	Start Forge Temperature, deg F	Finish Forge Temperature, deg F	Final Temperature, deg F
1	504	A	12:01A	Cold	8:30A	2100	1990	1640	1550	8:36A	2100	10:00A	2050	1970	1720	1490
2	502	B	12:01A	Cold	8:37A	2100	1970	1600	1500	8:43A	2090	10:10A	2050	1905	1640	1440
3	489	C	12:01A	Cold	8:44A	2120	1950	1630	1450	9:03A	2090	10:20A	2090	1940	1660	1540
4	509	D	12:01A	Cold	9:06A	2130	1980	1620	1460	9:15A	2120	10:30A	2120	1920	1650	1540
5	497	E	12:01A	Cold	9:33A	2150	1980	1650	1450	9:41A	2150	10:39A	2150	1990	1670	1550
6	506	G	12:01A	Cold	9:42A	2150	1980	1620	...	9:50A	2150	10:47A	2150	1950	1600	1510
7	491	H	10:58A	2140	1:08P	2150	1980	1570	1420	1:14P	2130	1:58P	2150	2000	1650	...
8	505	J	10:58A	2140	1:15P	2130	1980	1740	1430	1:24P	2130	2:08P	2170	2070	1670	...
9	499	K	10:58A	2140	1:25P	2130	1970	1740	...	1:35P	2140	2:23P	2140	1920	1730	...
10	507	L	10:58A	2140	1:44P	2130	2000	1660	1400	1:51P	2150	2:30P	2130	1990	1630	...
11	503	M	10:58A	2140	1:52P	2150	2000	1660	1440	1:57P	2160	2:35P	...	1970	1640	1550
12	500	N	12:05P	2120	2:14P	2130	2000	1650	1440	2:22P	2140	2:40P	...	1950	1570	1510
13	501	O	2:08P	2170	4:11P	2140	2020	1770	1450	4:18P	2150	5:50P	2120	2020	1840	1570
14	496	P	2:30P	2130	4:38P	2160	2020	1770	1400	4:49P	2180	5:58P	2180	2040	1870	1500
15	493	R	2:34P	2130	4:50P	2180	2040	...	1400	5:03P	2150	6:07P	2180	2040	...	1620
16	492	S	2:40P	2120	5:04P	2150	2020	1740	1400	5:13P	2120	6:14P	2200	2100	1730	1600
17	490	T	2:47P	2120	5:15P	2120	1990	1720	1410	5:23P	2120	6:21P	2140	2060	1670	1550
18	510	V	2:47P	2120	5:40P	2190	2050	1740	1490	5:48P	2120	6:26P	...	2090	1700	1590
19	498	W	6:05P	2180	8:14P	2150	1970	1750	1480	6:13P	2200	9:25P	2150	2010	1870	1560
20	508	X	6:14P	2200	8:20P	2150	2000	1680	1520	6:19P	2150	9:43P	2140	2020	1870	1560
21	494	Y	6:20P	2140	8:59P	2150	2010	1680	1490	6:25P	2150	9:55P	2160	2010	...	1510
22	495	Z	6:26P	2150	9:05P	2140	2000	1640	1500	6:34P	...	10:10P	...	2010	1880	1550

Furnace cool in  $\frac{3}{4}$  day (door open) to 600 F (316 C)

Air cool to room temperature. (See Table 12.)

Pieces 2 and 4 of each code were sent to Climax Molybdenum for further processing while piece 3 was sent to Westinghouse Electric Corporation for determination of chemical analysis.

## APPENDIX 3

### Impact Test Procedures

The impact tester used in this work was a standard Riehle machine of dual range, that is, 0 to 120 and 0 to 240 ft·lb capacity. Recent calibration using standard CVN impact specimens provided by Watertown Arsenal specifically for this purpose showed the following comparison:

CVN specimen standard reported by Watertown Arsenal	Watertown Arsenal CVN specimen standard tested by Inco
ft·lb at -40 F (-40 C)	ft·lb at -40 F (-40 C)
68	67 65.5
48	47.5 46.5
14	13.5 13.5

The measured time interval between removing the specimen from the thermal bath and contact with the impact striker was 3 to 4.5 s.

Standard practice for heating or cooling Charpy specimens was as follows:

Temperature Range, deg F	Heater or Cooler	Environment	Time and Temperature, Min
above 212	electric furnace	air	30
75 to 212	electric hot plate	water	20
75 to -100	dry ice	methanol	20
-100 to -270	liquid nitrogen	2-methyl butane	20
-320	liquid nitrogen	liquid nitrogen	20

The temperature of the electric furnace was controlled by a Leeds and Northrup controller, and exact temperatures were determined by means of a dummy test specimen, thermocouple, and portable potentiometer. The hot plate was controlled by hand with a built-in rheostat. The temperature of the cooling baths was measured by a Wheelco temperature indicator and was controlled by the careful manual addition of coolant in generous quantities initially and then in gradually decreasing amounts as the test temperature was approached and maintained. Test temperatures were controlled within  $\pm 5$  F (2.8 C). All temperature measuring and indicating instruments were periodically checked with a standardized thermocouple and a highly accurate portable potentiometer.

## References

- [1] Curran, R. M., "The History of the Special ASTM Task Force on Large Turbine and Generator Rotors," Symposium on Improved Properties in Large Rotor Forgings, 68th Annual Meeting, American Society for Testing and Materials, W. Lafayette, Ind., June 1965.
- [2] Newhouse, D. L. and Holtz, H. G. in *Temper Embrittlement in Steel*, ASTM STP 407, American Society for Testing and Materials, Aug. 1968, pp. 106-126.
- [3] Boyle, C. J., Curran, R. M., DeForest, D. R., and Newhouse, D. L., *Proceedings*, American Society for Testing and Materials, ASTEA, 1962, pp. 1156-1175.
- [4] Boyle, C. J., Curran, R. M., DeForest, D. R., and Newhouse, D. L., "Further Progress in the Development of Large Steam Turbine and Generator Rotors," Symposium on Improved Properties in Large Rotor Forgings, 68th Annual Meeting, American Society for Testing and Materials, W. Lafayette, Ind., June 1965.
- [5] McMahon, C. J., Jr. in *Temper Embrittlement in Steel*, ASTM STP 407, American Society for Testing and Materials, Aug. 1968, pp. 127-167.
- [6] Stewart, B. K. in *Temper Embrittlement of Alloy Steels*, ASTM STP 499, American Society for Testing and Materials, 1972, pp. 37-50.
- [7] Penkrot, J. and Byrne, F. in *Temper Embrittlement of Alloy Steels*, ASTM STP 499, American Society for Testing and Materials, 1972, pp. 51-58.
- [8] Atherton, M. J., "An Unbiased Method for Drawing Transition Curves" to be published by the American Society for Testing and Materials.
- [9] Comon, J., Martin, P. F., and Bastien, P. G. in *Temper Embrittlement in Steel*, ASTM STP 407, American Society for Testing and Materials, 1968, pp. 74-89.
- [10] Viswanathan, R., *Metallurgical Transactions*, American Society for Metals, MTGTB, Vol. 2, March 1971, pp. 809-815.
- [11] Sticha, E. A., "Notched Stress Rupture Data for Quenched and Tempered 2 $\frac{1}{4}$  Chrome 1 Moly Steel," ASME Symposium on 2 $\frac{1}{4}$  Chrome-1 Molybdenum Steel for Pressure Vessels and Piping, Denver, Colo., Sept. 1970.
- [12] "Study of the Embrittlement of Heavy Section Pressure Vessel Steels in the High Temperature Range," Quarterly Report No., 2, Thermal and Mechanical Treatments Subcommittee, Fabrication Div., Pressure Vessel Research Committee, Welding Research Council, New York, 30 April 1970.

B. K. Stewart<sup>1</sup>

# Temper Embrittlement Study of Ni-Cr-Mo-V Rotor Steels: Part II—Statistical Design and Analysis

---

**REFERENCE:** Stewart, B. K., “Temper Embrittlement Study of Ni-Cr-Mo-V Rotor Steels: Part II—Statistical Design and Analysis,” *Temper Embrittlement of Alloy Steels, ASTM STP 499*, American Society for Testing and Materials, 1972, pp. 37–50.

**ABSTRACT:** A program was planned to obtain quantitative information on the effects of residual impurity elements on the reversible temper embrittlement susceptibility of Ni-Cr-Mo-V rotor steels. The statistical design of the experiment and statistical analysis of the data are described. The basic design was a supplemented  $1/2$  fraction of a  $2^5$  factorial to study the effects of P, Mo, Sn, As, and Sb, including 2-factor interactions among these elements.

**KEY WORDS:** embrittlement, tempering, transition temperature, design, statistical analysis, statistical distributions, statistical tests, evaluation, mathematical models, steels, arsenic, antimony, phosphorus, molybdenum, tin

Previous work had indicated deleterious effects of P, Sn, As, and Sb on embrittlement but had not provided unambiguous information on the magnitude of these effects. Mo had been determined in some cases to be detrimental and in other cases beneficial. Little work had been done to investigate possible interaction effects among these elements. To study how these 5 elements affect embrittlement, statistical principles were utilized to obtain accurate and pertinent data in an economical manner and to assess whether effects observed in the data could be attributed to the elements under study or were the results of chance variation only. This paper, Part II, describes the statistical design, the statistical analytical procedures used, the results of the statistical analysis, and the general usefulness of a statistically planned program of this type. The background of the program, the experimental and testing procedures, and detailed results of the experiment are discussed in Part I (see pp. 3–36).

## Experimental Design

During the original planning discussion, the following questions were considered to be of major interest:

<sup>1</sup> Senior research statistician, Applied Research Laboratory, U.S. Steel Corp., Monroeville, Pa. 15146.

(1) Does an increase in the amount of a given element in the steel over a specified range cause a change in the amount of embrittlement? If so, in what direction is the change and what is the magnitude of the change?

(2) Is this change the same at all levels of other elements in the steel, or are there interactions such that the magnitude of the change for a given element depends upon the levels of other elements?

Also of interest were answers to the following:

Is the change in embrittlement, corresponding to each element over the range of experimentation, essentially a linear function of the amount of the element, or is there curvature in the embrittlement behavior corresponding to some elements?

These questions can be stated in mathematical terms by postulating a mathematical model and asking which of the terms in the model should be retained and which should be deleted. A model appropriate for studying the above questions is as follows:

$$\begin{aligned} \text{Embrittlement} = & b_0 + b_1(\text{P}) + b_2(\text{Mo}) + b_3(\text{Sn}) + b_4(\text{As}) + b_5(\text{Sb}) \\ & + b_{11}(\text{P})^2 + b_{22}(\text{Mo})^2 + b_{33}(\text{Sn})^2 + b_{44}(\text{As})^2 + b_{55}(\text{Sb})^2 \\ & + b_{12}(\text{P})(\text{Mo}) + b_{13}(\text{P})(\text{Sn}) + b_{14}(\text{P})(\text{As}) + b_{15}(\text{P})(\text{Sb}) \\ & + b_{23}(\text{Mo})(\text{Sn}) + b_{24}(\text{Mo})(\text{As}) + b_{25}(\text{Mo})(\text{Sb}) \\ & + b_{34}(\text{Sn})(\text{As}) + b_{35}(\text{Sn})(\text{Sb}) + b_{45}(\text{As})(\text{Sb}) + \text{error} \quad (1) \end{aligned}$$

where the coefficients in the first line ( $b_i$ ) represent linear effects, those in the second line ( $b_{ii}$ ) represent quadratic effects, and the remaining ( $b_{ij}$ ) represent interactions between linear effects of 2 elements. The error represents the variability in embrittlement not accounted for by the terms in the model. The magnitude of this residual variability is measured by the residual standard deviation and provides a measure of experimental error assuming the correctness of the model.

### *Composite Design*

One of the more economical and efficient statistical designs that can be used to obtain information on the above model is known as a composite design. As the name implies, it is a "composite" of 2 simpler designs. The basic design is a  $\frac{1}{2}$  fraction of a  $2^5$  factorial. A  $2^5$  factorial is one in which each of 5 factors (or variables) is controlled at 2 levels only and experimentation is conducted at all combinations of these 2 levels (32 experimental points). It provides separate estimates of linear effects of the controlled factors and all interactions among these linear effects. A  $\frac{1}{2}$  fraction of this  $2^5$  factorial (16 specified experimental points) cuts in half the amount of experimentation and still provides separate estimates of all linear effects and all 2-factor linear interactions, which are the only interactions present in the model. The compositions of the 16 heats required by this fractional factorial design are shown in Table 1.

TABLE 1—*Composition of experimental heats required by a composite design.*

	P, %	Mo, %	Sn, ppm	As, ppm	Sb, ppm
Fractional factorial heats	0.005	0.30	30	20	8
	0.005	0.30	30	120	24
	0.005	0.30	120	20	24
	0.005	0.30	120	120	8
	0.005	0.60	30	20	24
	0.005	0.60	30	120	8
	0.005	0.60	120	20	8
	0.005	0.60	120	120	24
	0.015	0.30	30	20	24
	0.015	0.30	30	120	8
	0.015	0.30	120	20	8
	0.015	0.30	120	120	24
	0.015	0.60	30	20	8
	0.015	0.60	30	120	24
	0.015	0.60	120	20	24
	0.015	0.60	120	120	8
Star heats <sup>a</sup>	LAP <sup>b</sup>	0.45	75	70	16
	0.020	0.45	75	70	16
	0.010	0.15	75	70	16
	0.010	0.75	75	70	16
	0.010	0.45	LAP	70	16
	0.010	0.45	165	70	16
	0.010	0.45	75	LAP	16
	0.010	0.45	75	170	16
	0.010	0.45	75	70	LAP
	0.010	0.45	75	70	32
Center heats	0.010	0.45	75	70	16
	0.010	0.45	75	70	16
	0.010	0.45	75	70	16
	0.010	0.45	75	70	16
	0.010	0.45	75	70	16
	0.010	0.45	75	70	16

<sup>a</sup> These heats were not melted in the first phase of the program.

<sup>b</sup> Low as possible.

The other part of the composite design is made up of factor combinations called “star points” and “center points.” The center points represent repeat runs in which each factor is controlled at a level midway between its 2 factorial levels. In each star point all but one of the factors are controlled at their center levels and the remaining factor is set at a level beyond the range of its factorial levels. This part of the design makes it possible to estimate the quadratic effects in the model. The variation among the repeat center points also provides an estimate of experimental error. The compositions of the 16 heats required by this part of the design are also shown in Table 1. The fact that the composite design can be built up in stages makes it useful for

sequential experimentation. (More details concerning this experimental design are discussed by Cochran and Cox.<sup>2</sup>)

Because of the complexity and time involved in melting, processing, and testing the experimental material, it was desirable, initially, to limit the number of heats to about 20. Recall that the 2 questions of major interest in this program were concerned with linear effects only and that the factorial part of the composite design provides estimates of these effects. The more important information could be obtained from these 16 fractional factorial heats and only these would be melted initially. To obtain an estimate of experimental error against which terms in the model could be tested, the 6 center heats were also to be melted in this first phase. The star heats were to be held in abeyance until test data from the first phase had been analyzed. If as a result of this analysis it was decided to investigate quadratic effects, the star heats would be melted in a second phase, together with additional center heats to check on the consistency of the results for the 2 phases. This paper discusses the results of the first phase only.

The model postulated for the first phase of the program, was one that did not include quadratic terms:

$$\begin{aligned} \text{Embrittlement} = & b_0 + b_1(\text{P}) + b_2(\text{Mo}) + b_3(\text{Sn}) + b_4(\text{As}) + b_5(\text{Sb}) \\ & + b_{12}(\text{P})(\text{Mo}) + b_{13}(\text{P})(\text{Sn}) + b_{14}(\text{P})(\text{As}) + b_{15}(\text{P})(\text{Sb}) \\ & + b_{23}(\text{Mo})(\text{Sn}) + b_{24}(\text{Mo})(\text{As}) + b_{25}(\text{Mo})(\text{Sb}) \\ & + b_{34}(\text{Sn})(\text{As}) + b_{35}(\text{Sn})(\text{Sb}) + b_{45}(\text{As})(\text{Sb}) + \text{error} \quad (2) \end{aligned}$$

The coefficients in the model were to be estimated and decisions were to be made as to which terms in the model should be retained and which should be deleted. These decisions were to be based on the judgment and experience of the experimenters with the help of statistical tests of significance. A test of significance for each coefficient would denote whether the magnitude of its estimate was sufficiently large to be indicative of more than chance variation. The resulting equation, after all coefficients were tested, would contain terms for only those factors or combinations of factors that were judged to significantly affect embrittlement.

The reduced equation should be a good representation of the embrittlement behavior of Ni-Cr-Mo-V rotor steels with compositions within the ranges investigated. A possible exception is that the postulated model, Eq 2, fails to contain some higher order terms which should have been included, such as those shown in Eq 1. This situation is referred to as "lack of fit" of the model. If a statistical test of this lack of fit were to suggest that higher order terms should have been included, further experimentation should be carried out to investigate them. The addition to the program of star heats, for example, would reveal which quadratic terms, if any, the equation should

<sup>2</sup> Cochran, W. G. and Cox, G. M., *Experimental Designs*, 2nd ed., Wiley, New York, 1957.

contain. If the presence of higher order interactions were suspected, they could be studied by adding the other half fraction of the  $2^5$  factorial.

The entire program—melting, processing, testing—was carried out with careful control and with randomization employed whenever feasible. Each step in the program was handled by only one of the cooperating laboratories to ensure that variation in experimental procedures among the laboratories did not become confounded with variation due to changes in composition.

### Statistical Analysis

A number of properties were measured in specimens from each of the experimental heats, and 3 were chosen as the most meaningful for evaluation of temper embrittlement: 50 percent shear fracture appearance transition temperature (FATT); temperature of 15 mil lateral expansion (LETT); and energy at 100 percent shear.

Specimens were tested under three conditions:

- (1) Water quenched from tempering temperature;
- (2) Step cooled from tempering temperature; and
- (3) Aged for 1 year at 750 F after tempering and water quenching.

Step cooled embrittlement was defined to be the change in the property from the water quenched condition to the step cooled condition. Isothermal embrittlement was defined to be the change in the property from the water quenched condition to the aged condition.

Embrittlement data for the 3 properties and coded design composition levels for the 22 heats are shown in Table 2. It can be seen from Table 2 that the variation in embrittlement evaluated on the basis of change in energy at 100 percent shear was quite small. This property is not a good measure of embrittlement, and therefore the data were not analyzed.

Actual compositions of the 22 heats are shown in Table 3. These differed slightly from the design compositions in Table 1. Reasonably small variations from the design compositions should not, however, invalidate most of the advantages of the planned program, especially since the technique used to analyze the data (regression analysis) was based on the actual rather than the design compositions.

### *Method of Analysis*

The data were analyzed by the technique of multiple regression. This is a well known analytical method, the details of which can be found in many books on statistics.<sup>3</sup> As used in this program, it is a technique that estimates the effects in the model and tests whether these estimates are large enough that the effects can be considered to be significantly greater than zero.

<sup>3</sup> Draper, N. R. and Smith, H., *Applied Regression Analysis*, Wiley, New York, 1966.

TABLE 2—Summary of embrittlement data on experimental heats.<sup>a</sup>

P	Coded Design Composition Level <sup>b</sup>			Heat <sup>c</sup> Code	50 percent shear FATT, deg F		15 mil LETT, deg F		Energy at 100 percent shear, ft. lb.		
	Sn	Mo	As		Sb	$\Delta(\text{SC-WQ})^d$	$\Delta(\text{AG-WQ})^e$	$\Delta(\text{SC-WQ})$	$\Delta(\text{AG-WQ})$	$\Delta(\text{SC-WQ})$	$\Delta(\text{AG-WQ})$
0	0	0	0	0	0	20	60	5	55	-3	-4
0	0	0	2	2	0	30	125	35	150	-2	-3
0	0	2	0	2	0	5	40	15	55	4	4
0	0	2	2	0	0	20	80	40	65	-5	1
0	2	0	0	2	0	55	130	45	110	-2	-4
0	2	0	2	0	0	115	185	125	190	9	6
0	2	2	0	0	0	75	145	65	115	-3	1
0	2	2	2	2	0	90	155	110	175	-3	-12
2	0	0	0	2	2	90	220	125	220	6	-1
2	0	0	2	0	0	110	260	150	260	-2	6
2	0	2	0	0	0	90	195	110	155	-5	-4
2	0	2	2	2	0	70	190	80	195	-2	-11
2	2	0	0	0	0	115	205	135	215	5	21
2	2	0	2	2	0	145	240	155	235	-1	7
2	2	2	0	2	0	140	180	150	180	-2	7
2	2	2	2	0	0	130	225	150	225	-1	2
1	1	1	1	1	1	40	100	55	100	-4	-1
1	1	1	1	1	1	60	140	75	160	-7	-4
1	1	1	1	1	1	65	145	80	140	-11	-5
1	1	1	1	1	1	75	140	75	165	0	-8
1	1	1	1	1	1	55	120	70	135	-9	-7
1	1	1	1	1	1	75	145	100	135	-10	-6

<sup>a</sup> The heats are ordered according to the elements having larger effects on embrittlement.<sup>b</sup> 0 = Low level, 1 = Center level, 2 = High Level.<sup>c</sup> The heat code is included for cross reference with tables in Part I, pp. 3-36.<sup>d</sup>  $\Delta(\text{SC-WQ})$  = Change in property from water quenched condition to step cooled condition.<sup>e</sup>  $\Delta(\text{AG-WQ})$  = Change in property from water quenched condition to aged condition.

TABLE 3--Chemical composition of experimental heats melted.

Coded Design Composition Levels <sup>a</sup>				Actual Composition Level, percent											Al, percent			ppm		
P	Sn	Mo	As	Code	C	Mn	P	S	Si	Ni	Cr	Mo	V	Soluble	Total	Sn	As	Sb	N	
0	0	0	0	0	P	0.24	0.31	0.006	0.008	0.056	3.47	1.72	0.31	0.12	0.010	0.016	15	19	18	21
0	0	0	2	2	V	0.25	0.32	0.006	0.011	0.044	3.45	1.74	0.30	0.11	0.009	0.013	19	160	27	29
0	0	2	0	2	W	0.24	0.32	0.006	0.011	0.085	3.46	1.74	0.61	0.12	0.003	0.005	17	25	31	25
0	0	2	2	0	H	0.27	0.31	0.006	0.010	0.048	3.49	1.72	0.60	0.12	0.018	0.020	15	160	13	24
0	2	0	0	2	J	0.26	0.31	0.003	0.007	0.059	3.46	1.72	0.29	0.11	0.004	0.009	91	36	27	22
0	2	0	2	0	Y	0.24	0.33	0.007	0.011	0.055	3.48	1.75	0.31	0.13	0.006	0.007	128	180	12	28
0	2	2	0	0	N	0.25	0.32	0.005	0.008	0.068	3.52	1.73	0.60	0.12	0.006	0.012	93	34	10	27
0	2	2	2	2	O	0.27	0.31	0.006	0.009	0.062	3.48	1.71	0.59	0.12	0.008	0.012	105	140	30	25
2	0	0	0	2	Z	0.23	0.31	0.016	0.009	0.058	3.47	1.74	0.30	0.12	0.009	0.012	17	28	29	32
2	0	0	2	0	R	0.24	0.32	0.018	0.008	0.069	3.38	1.71	0.31	0.12	0.011	0.017	38	150	12	26
2	0	2	0	0	S	0.24	0.32	0.020	0.011	0.073	3.49	1.74	0.63	0.11	0.001	0.004	59	28	12	25
2	0	2	2	2	G	0.23	0.30	0.016	0.008	0.057	3.52	1.75	0.60	0.12	0.010	0.012	20	150	30	27
2	2	0	0	0	X	0.25	0.32	0.016	0.011	0.055	3.49	1.73	0.30	0.12	0.007	0.011	112	32	12	28
2	2	0	2	2	C	0.24	0.31	0.019	0.011	0.047	3.57	1.76	0.31	0.12	0.002	0.004	137	170	30	31
2	2	2	0	2	D	0.26	0.32	0.017	0.008	0.047	3.52	1.76	0.61	0.13	0.015	0.018	90	38	25	25
2	2	2	2	2	B	0.24	0.31	0.018	0.009	0.053	3.54	1.74	0.61	0.12	0.002	0.003	98	150	10	30
1	1	1	1	1	A	0.24	0.30	0.011	0.008	0.078	3.41	1.72	0.45	0.12	0.002	0.005	75	91	19	20
1	1	1	1	1	E	0.19	0.32	0.013	0.010	0.061	3.49	1.77	0.47	0.12	0.003	0.008	58	83	13	27
1	1	1	1	1	K	0.27	0.33	0.012	0.008	0.073	3.47	1.71	0.46	0.12	0.002	0.006	55	99	17	26
1	1	1	1	1	L	0.28	0.32	0.011	0.008	0.059	3.47	1.73	0.45	0.12	0.009	0.013	73	100	23	31
1	1	1	1	1	M	0.25	0.31	0.011	0.008	0.049	3.50	1.72	0.45	0.12	0.006	0.012	64	94	19	26
1	1	1	1	1	T	0.23	0.32	0.011	0.012	0.059	3.48	1.73	0.46	0.12	0.004	0.005	96	90	17	29

<sup>a</sup> 0 = Low level, 1 = Center level, 2 = High level.

Had the compositions designated by the design been achieved exactly, the results of the regression analysis would have been identical with results from a technique referred to as an analysis of variance. Because estimation of the effects and tests of their significance are more understandable from an analysis-of-variance approach than from a regression approach, and because the differences between design compositions and actual compositions were small, explanations of estimation and testing procedures will be in terms of the analysis of variance. Discussion of results, however, will be based on the regression analysis.

In the analysis of variance, each linear effect in the model ( $b_i$ ) is estimated by the difference between the average embrittlement at the high level of the element and the average embrittlement at the low level of the element. For example, the linear effect of P on FATT isothermal embrittlement is estimated by subtracting the average of the first 8 heats in Table 2 (115 F) from the average of the second 8 heats (214 F). This difference (99 F) represents the average estimated increase in embrittlement when P is increased from 0.005 to 0.015 percent. It also may be regarded as the estimated linear effect of P over this range when the other 4 elements are set at their center level. Each interaction effect in the model ( $b_{ij}$ ) is estimated by the difference between the linear effect of a particular element at the high level of another element and its linear effect at the low level of the other element. For example, the interaction effect on FATT isothermal embrittlement between P and Sn is estimated as follows: the linear effect of P at low Sn is measured by subtracting the average of the first group of 4 heats in Table 2 (76 F) from the average of the third group of 4 heats (216 F); the linear effect of P at high Sn is measured by subtracting the average of the second group of 4 heats (154 F) from the average of the fourth group of 4 heats (212 F); the difference between these two effects (58 F — 140 F = —82 F) is an estimate of the interaction effect. If this interaction effect is significant, it indicates that P has a different effect on FATT isothermal embrittlement at the two levels of Sn.

After the effects in the model were estimated, the estimates were tested to determine whether they were sufficiently large to be indicative of more than chance variation. The statistic used in these tests is the  $t$  statistic or  $F$  statistic. (These two tests are equivalent when individual effects in the model are being tested.) Stated briefly, the  $t$  statistic is the ratio of the estimate of the effect to the standard error of the estimate. The standard error of the estimate is a measure of how much the estimate may vary in repeated experimentation; it is based upon the variation in embrittlement among heats melted to the same composition, referred to as experimental error and estimated from the center heats in the present design. The test consists of hypothesizing that there is no effect and comparing the  $t$  value calculated from the data with a theoretical value of  $t$ . If the test is made at a 5 percent level of significance, then under the hypothesis of no effect, the probability of the calculated  $t$  exceeding the theoretical value of  $t$  is 5 percent. Thus if the theoretical value

is in fact exceeded, it can be concluded that the estimated effect is unlikely to be the result of chance variation and that there is a significant effect. An example of a  $t$ -test is given in the following section. All  $t$ -tests in this program were made at the 5 percent level of significance.

The program was designed to furnish information on higher order terms possibly missing from the model, referred to as "lack of fit" of the model. The existence of such terms is evaluated by comparing the average embrittlement of the fractional factorial heats with the average embrittlement of the center heats. Such a comparison makes sense because if Eq 2 were correct, the average embrittlement for the 16 fractional factorial heats should, except for random variations, equal the average embrittlement for the 6 center heats. The  $t$  statistic can be used to test this lack of fit. For example, under the hypothesis that there is no lack of fit in the FATT isothermal embrittlement model, there should be no difference between the 2 averages except that brought about by chance variation. The difference observed in the data is 33 F (165 F average for the fractional factorial heats and 132 F average for the center heats). The estimated experimental error in FATT isothermal embrittlement (calculated from the variation among the center heats) is 18.1 F, and the corresponding standard error of the observed difference is 8.67 F. The value of the  $t$  statistic for this difference is  $33/8.67 = 3.81$ . Since this exceeds the theoretical  $t$  value of 2.57 it is unlikely that the difference observed is the result of chance variation, and a statistically significant lack of fit for the postulated model is indicated.

## Discussion of Results

### 50 Percent Shear FATT

The equations resulting from regression analyses of embrittlement based on the change in 50 percent shear FATT are the following:

Step cooled

$$\text{embrittlement} = -16.22 + 4394 (P, \%) + 0.6175 (\text{Sn, ppm}) \quad (3)$$

Isothermal

$$\begin{aligned} \text{embrittlement} = & 62.95 + 8092 (P, \%) - 93.06 (\text{Mo, } \%) \\ & + 0.3563 (\text{Sn, ppm}) + 0.2132 (\text{As, ppm}) \\ & - 81.32 (P - 0.0115, \%) (\text{Sn} - 67.0, \text{ppm}) \end{aligned} \quad (4)$$

These equations explain, respectively, 82 and 85 percent of the total variation in embrittlement in the 22 heats. This percent of total variation is referred to as the coefficient of determination and is symbolized by  $R^2$ . It measures the proportion of the total variation about the mean that is explained by the regression.

It may be noted that Eq 4 differs slightly in form from the model equation, in that the elements in the interaction term have been coded by subtraction of a constant value. This constant is the mean value of the given element within the 22 heats; it was subtracted in order that the coefficients of the linear terms for P and Sn might represent the effects of the elements near the center of the composition range studied. To illustrate, the estimated linear coefficient for P (8092) indicates that for material containing 67 ppm Sn, an 0.01 percent increase in P results in an increase in embrittlement of 81 F; note that when Sn is set equal to 67 ppm the interaction term in the equation drops out, giving the above result. Were the equation in the form of the model, the interaction term would drop out when Sn was set equal to 0; hence, the coefficient of the linear term for P would represent the effect of P when no Sn was present in the material, a composition which may not be of concern since it is outside the composition range under investigation.

It is also of interest to note that in the coded form (Eq 4) the linear coefficients represent an effect analogous to that represented in the analysis-of-variance calculations.

In this program the sole purpose of the coding was to achieve greater clarity. If the constants had not been subtracted, the final results would have been the same.

Equation 3 indicates that FATT step cooled embrittlement was affected significantly only by P and Sn. The effects of these 2 elements are shown graphically in Fig. 1 in terms of predicted embrittlement over the composition ranges studied. These elements caused about the same amount of change in embrittlement, 44 F increase when P was increased from 0.005 to 0.015 percent, and 55 F increase when Sn was increased from 30 to 120 ppm.

Equation 4 indicates that FATT isothermal embrittlement was affected by all the elements except Sb. P and Sn had the strongest effects, as shown in Fig. 1.<sup>4</sup> P caused an average increase of 75 F and Sn caused an average increase of 43 F. An interaction between these 2 elements is shown by a difference in the slopes. With P at 0.005 percent, Sn caused a large increase in embrittlement of 80 F, whereas with P at 0.015 percent, Sn caused only a slight increase of 7 F. (Note that the slopes for the step cooled embrittlement are the same, reflecting no interaction between these elements in the step cooled condition.)

The effects of Mo and As are also shown graphically in Fig. 1. Mo decreased the embrittlement by 28 F as it was increased from 0.3 to 0.6 percent. As caused a 28 F increase as it was changed from 30 to 160 ppm. (The slope of 0 shown in these figures for the step cooled embrittlement indicates no effect.)

<sup>4</sup> In all cases, elements included in the equation but not in the figure were set at the following levels: 0.010 percent P, 75 ppm Sn, 0.45 percent Mo, and 95 ppm As.

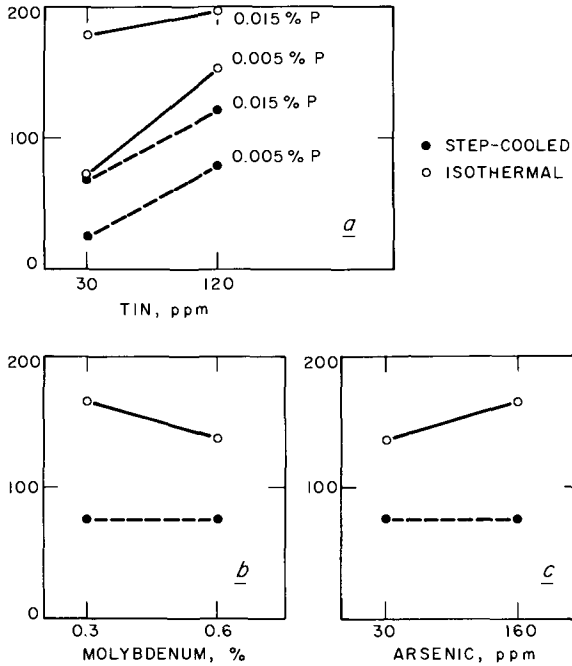


FIG. 1—Predicted effects of composition on embrittlement based on the increase in 50 percent shear FATT.

Temperature of 15 mil LETT

Embrittlement evaluated on the basis of change in temperature of 15 mil LETT exhibited patterns very similar to those evaluated on the basis of change in FATT. Again, P and Sn were the only 2 elements that strongly affected either the step cooled embrittlement or the isothermal embrittlement.

The following equation for predicting step cooled embrittlement explains 79 percent of the total variation

$$\begin{aligned} &\text{Step cooled} \\ &\text{embrittlement} = -17.35 + 5888 (P, \%) + 0.5669 (Sn, \text{ppm}) \end{aligned} \quad (5)$$

The effects of these elements are shown in Fig. 2. P caused a 59 F increase in embrittlement as it was changed from 0.005 to 0.015 percent, and Sn caused a 51 F increase as it was changed from 30 to 120 ppm.

The following equation for predicting isothermal embrittlement explains 83 percent of the total variation

$$\begin{aligned} &\text{Isothermal} \\ &\text{embrittlement} = 72.05 + 7799 (P, \%) + 0.2967 (Sn, \text{ppm}) \\ &\quad - 116.1 (Mo, \%) + 0.3096 (As, \text{ppm}) \\ &\quad - 73.52 (P - 0.0115, \%) (Sn - 67.0, \text{ppm}) \end{aligned} \quad (6)$$

48 TEMPER EMBRITTLEMENT OF ALLOY STEELS

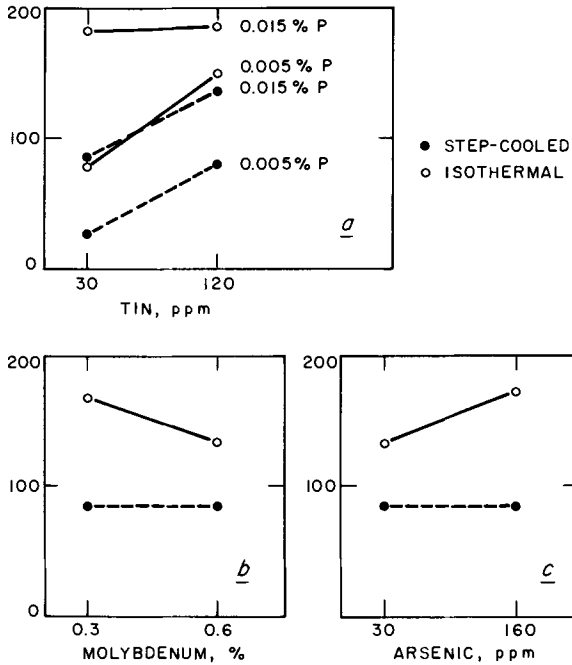


FIG. 2—Predicted effects of composition on embrittlement based on the increase in temperature of 15 mil LETT.

P caused an average increase in embrittlement of 72 F as it was increased from 0.005 to 0.015 percent, and Sn caused an average increase of 37 F as it was increased from 30 to 120 ppm. An interaction between P and Sn, similar to that for FATT and graphed in Fig. 2, indicated considerable increase in embrittlement due to Sn when P was at 0.005 percent (70 F) and almost no increase when P was at 0.015 percent (4 F). Mo appeared to decrease the embrittlement by 35 F as it was changed from 0.3 to 0.6 percent, and As appeared to increase the embrittlement by 40 F as it was changed from 30 to 160 ppm.

*Lack of Fit of the Models*

Set forth in Table 4 are the calculated *t* values used in the statistical tests to evaluate whether, for each of the embrittlement criteria, the postulated model, Eq 2, fails to contain some higher order terms which should have been included. The tests were based on the residual variability among the center heats from the regression analysis. The *t* values for all criteria except LETT isothermal embrittlement exceed the theoretical value of *t*, indicating a statistically significant lack of fit. Since only one interaction term (between P and Sn) appears in any of the reduced equations, it is probable that the terms which should have been included are quadratic terms rather than higher order interaction terms.

TABLE 4—Tests for lack of fit.

Embrittlement Criteria	Calculated, $t^a$
50% shear FATT $\Delta$ (SC-WQ)	3.78
50% shear FATT $\Delta$ (AG-WQ)	4.79
15 mil LETT $\Delta$ (SC-WQ)	4.01
15 mil LETT $\Delta$ (AG-WQ)	2.10

<sup>a</sup> Theoretical  $t$  value corresponding to a 5 percent level of probability = 2.57.

### Residual Variability

Two residual standard deviations for each of the embrittlement criteria are listed in Table 5. These measure the variability in embrittlement not accounted for by the effects judged to be significant. The first standard deviation includes the variability due to lack of fit; the second does not. While the coefficients of determination ( $R^2$ ) reported with the reduced equations are based on the residual standard deviation that includes the variability due to lack of fit, it should be noted that the same reduced equations result regardless of which residual standard deviation is used as an aid in deriving the equations.

TABLE 5—Residual variability.

Embrittlement Criteria	Residual Standard Deviation <sup>a</sup>	Residual Standard Deviation <sup>b</sup>
50% shear FATT $\Delta$ (SC-WQ)	17.6	14.4
50% shear FATT $\Delta$ (AG-WQ)	25.6	17.0
15 mil LETT $\Delta$ (SC-WQ)	21.8	20.2
15 mil LETT $\Delta$ (AG-WQ)	27.0	23.7

<sup>a</sup> Includes lack of fit variability.

<sup>b</sup> Excludes lack of fit variability.

### Recommendations

If future experimentation is undertaken to further study the effects of these elements on the embrittlement susceptibility of Ni-Cr-Mo-V rotor steels, the lack of fit of the models postulated in the present program need be considered.

It is also recommended that statistical design principles be utilized in future experimentation. A large number of statistical designs are available to assist planners of programs in obtaining accurate and pertinent data in the most economical manner. In the present program the following beneficial uses of these design principles were deemed important.

(1) Effects observed in the data can be attributed with a minimum of ambiguity to specific sources.

(2) The number of experiments and tests required to attain the objectives of the program can generally be reduced.

(3) Estimation of effects is achieved by a maximum use of the data. (In the present program, data from essentially all the heats were used to estimate each coefficient in the model.)

(4) Interaction terms can be included in the model and their effects can be estimated.

(5) An estimate of experimental error is provided against which observed effects can be tested.

(6) Experimentation can be performed sequentially, if desirable, with information from earlier phases being used to plan later phases in a manner that permits analysis of the data *in toto*.

The list of advantages could be extended, but perhaps the most important in any program, is that the statistical design approach usually brings about a more complete definition and development of objectives. Precise formulation in the planning stage of experimentation leads to more useful and meaningful results.

#### *Acknowledgments*

I thank F. A. Sorensen, Applied Research Laboratory, U.S. Steel Corp., for his many helpful comments.

## Chemical Analytical Results—How Accurate?

---

**REFERENCE:** Penkrot, J. and Byrne, F. P., “**Chemical Analytical Results—How Accurate?**” *Temper Embrittlement of Alloy Steels, ASTM STP 499*, American Society for Testing and Materials, 1972, pp. 51–58.

**ABSTRACT:** Twenty-two heats of low alloy steel were made to definite chemical compositions in order to study the effects of certain elements on temper embrittlement. It was necessary to confirm the composition of these heats by chemical or spectrochemical analysis by at least two different laboratories. This paper describes the chemical analytical procedures used for the analysis, the problems encountered in obtaining accurate and consistent results, and the solutions found for these problems.

**KEY WORDS:** chemical analysis, temper (metallurgy), embrittlement, alloy steels, carbon, silicon, phosphorus, aluminum, arsenic, antimony, molybdenum, tin.

To study the effects of Mo, P, As, Sn, and Sb on the temper embrittlement of steel, 22 heats of low alloy steel were made to definite compositions. The impurities were added at the two levels of greatest interest encountered in the commercial production of a low alloy steel of the composition, in weight percent, 0.25 C, 0.3 Mn, 0.01 S, 0.06 Si, 3.5 Ni, 1.7 Cr and 0.12 V. These elemental levels were Mo at 0.3 and 0.6 percent, P at 0.006 and 0.018 percent, As at 0.003 and 0.016 percent, Sb at 0.0012 and 0.0030 percent, and Sn at 0.0025 and 0.011 percent. The heats were analyzed in part spectrographically and in part chemically.

Since the Mn, Ni, Cr, Mo, and V were within specified limits, close to the charged composition, and because any slight variation in composition of these elements would have had little or no effect on the experiment, these results were accepted as correct. C, S, P, Si, Sb, Sn, and As, on the other hand, varied from the charged composition and could have had considerable effect on the experiment; thus they were also analyzed by another laboratory. In addition, the Al content of the alloys was analyzed by another laboratory: although the starting materials were identical for all heats, the Al concentration, despite the fact that it was not charged, fluctuated from 0.003 to 0.020 percent.

<sup>1</sup> Supervisor, Analytical Chemistry Dept., Westinghouse Electric Corp., Pittsburgh, Pa. 15235.

<sup>2</sup> Manager, Analytical Chemistry Dept., Westinghouse Electric Corp., Pittsburgh, Pa. 15235.

Table 1 shows the methods used in the analysis of the 22 heats and the expected reproducibility between laboratories. Reproducibility is a quantitative measure of the variability associated with different analysts and equipment in different laboratories. It is defined as the greatest difference between a result obtained in one laboratory and one obtained in another laboratory that is to be expected due to random errors on the bias of the 95 percent confidence level.

TABLE 1—*Methods used and their reproducibility.*

Element	Percentage Range	Method	Reproducibility
Mo	0.3 to 0.6	spectrographic	0.06
P	0.005 to 0.012	colorimetric, moly blue color	0.006
Sb	0.0010 to 0.0035	colorimetric, brilliant green color	0.0003
Sn	0.0010 to 0.014	colorimetric, quercetin color	0.0010
As	0.0020 to 0.020	colorimetric, moly blue color	0.0010
C	0.2 to 0.3	combustion	0.01
Mn	0.2 to 0.4	spectrographic	0.03
S	0.005 to 0.020	combustion	0.007
Si	0.02 to 0.10	perchloric acid dehydration	0.012
Ni	3.4 to 3.6	spectrographic	0.21
Cr	1.6 to 1.8	spectrographic	0.15
V	0.10 to 0.15	spectrographic	0.13
Soluble Al	0.002 to 0.020	spectrographic	0.003
Total Al	0.002 to 0.020	spectrographic	0.003
Soluble Al	0.002 to 0.020	colorimetric, aluminon	0.003
Total Al	0.002 to 0.020	colorimetric, aluminon	0.003
N	0.001 to 0.004	colorimetric, Nessler reaction	0.0013

### Results of Interlaboratory Analyses

The variations in chemical analyses between the cooperating laboratories for such common elements as C, P, Si, Al, and Sn were so far beyond acceptable limits that the study of the effects of these elements on temper embrittlement became impossible. Table 2 shows some of the check results between the cooperating laboratories. With such results, it was impossible to statistically correlate the metallurgical and chemical data to determine the effects of these elements at the various elemental concentrations.

### Variations in Elemental Determination

C is one of the most frequent elements requested in the analysis of steels due to its pronounced effect on metallurgical properties. Its concentration is considered to be one of the least difficult to accurately determine because several excellent methods are available. With this in mind, one would wonder how errors as high as 50 percent of the amount of C present could occur in such an easy analysis. Although excellent methods are available, the techniques for a particular method are not standardized in all the laboratories.

TABLE 2—*Typical first check results between cooperating laboratories.*

C	P	Elements in Percent				
		Si	Al		Sn	
0.22, 0.27	0.002, 0.007	0.08, 0.054	0.020,	0.013	0.0074, 0.0109	
0.23, 0.28	0.002, 0.006	0.09, 0.072	0.007,	0.017	0.0100, 0.0145	
0.24, 0.29	0.007, 0.012	0.09, 0.068	0.006,	<0.001	0.0140, 0.0196	
0.22, 0.27	0.002, 0.007	0.076, 0.059	0.011,	<0.001	0.0090, 0.0143	
0.20, 0.29	0.004, 0.008	0.060, 0.047	0.020,	0.010	0.0060, 0.0105	
0.22, 0.29	0.002, 0.007	0.064, 0.048	...		0.0010, 0.0051	

NOTE—The results in a line across the table do not necessarily refer to the same specimen.

For example, a simple step such as the removal of contaminating oil with a solvent is not practiced by all laboratories. In some cases it is assumed that the specimens are clean and they are, therefore, analyzed as received along with any oil or grease that may be present. A request to repeat the C analyses still produced unsatisfactory results. The task force felt that  $\pm 0.01$  percent was the maximum spread that could be tolerated. The results of the recheck are shown in Table 3.

TABLE 3—*Carbon recheck results.*

Specimen	Lab 1	Lab 2	Lab 3
1	0.28	0.24	...
2	0.31	0.27	0.27
3	0.29	0.26	0.28
4	0.28	0.24	0.28
5	0.22	0.19	...
6	0.29	0.24	0.27

In order to resolve this spread of results, three National Bureau of Standards certified specimens and two previously analyzed specimens were supplied with the quantity of each being just enough for a single determination. One of the standards was supplied in duplicate and one of the analyzed specimens in triplicate. The specimens were coded so that the true identity was unknown to the analysts. Each laboratory was requested to make certain that its apparatus was in excellent operating condition and that all specimens were cleaned with acetone. The results, shown in Table 4, indicated the necessary agreement required by the task force. The 22 heats were reanalyzed by two of the laboratories and the results agreed within  $\pm 0.01$  percent.

P also showed a wide variation in check results; for example, determinations on the same specimen ranged from 0.002 to 0.012 percent. This meant that there was no way in which to correlate the various levels of P to the formation of temper embrittlement. The specimens were resubmitted for P analysis with the understanding that greater care should be taken and a

larger specimen used. Typical check analyses are shown in Table 5: the results were in good agreement and acceptable.

TABLE 4—Carbon rechecks of standards and specimens.

Identification	Certified Value	Range of			
		Certified Values	Lab 1	Lab 2	Lab 3
NBS 10g	0.240	0.235 to 0.245	0.258	0.224	0.24
NBS 11g	0.191	0.185 to 0.195	0.203	0.204	0.18
NBS 72b	0.321	0.316 to 0.329	0.328	0.316	0.31
NBS 72b	0.321	0.316 to 0.329	0.333	0.304	0.34
Specimen 1	Lab 1, 0.27	...	0.26	0.24	0.24
	Lab 2, 0.27	...			
	Lab 3, 0.31	...			
Specimen 2	Lab 1, 0.28	...	0.27	0.28	0.27
	Lab 2, 0.20	...			
	Lab 3, 0.26	...			

TABLE 5—Typical phosphorus rechecks.

Specimen	Lab 1	Lab 2	Lab 3
1	0.011	0.010	0.011
2	0.006	0.009	0.008
3	0.006	0.007	0.005
4	0.006	0.005	0.005
5	0.011	0.012	0.010
6	0.002	0.004	0.003
7	0.018	0.019	0.018

The original Si concentrations were obtained by a spectrographic procedure. Since the values were higher than expected, four specimens were analyzed chemically. The results between the two methods were in poor agreement, as is shown in Table 6. The disagreement between the spectrographic and chemical Si analyses led to a request that another laboratory analyze the same specimens chemically. These results are shown in Table 7.

TABLE 6—First comparison of silicon results.

Specimen	Lab 1, spectrographic	Lab 2, chemical
1	0.08	0.055
2	0.09	0.072
3	0.09	0.068
4	0.07	0.044

TABLE 7—*First comparison of silicon results.*

Specimen	Lab 2	Lab 3
1	0.055	0.02
2	0.072	0.04
3	0.068	0.03
4	0.044	0.02

During the investigation of the methods used for the Si determination, it was found that Lab 3 used a small specimen weight which could not produce the desired accuracy required for a low Si determination. In gravimetric analysis, normally a four-place balance is used to weigh the precipitate of silica ( $\text{SiO}_2$ ). The weight of  $\text{SiO}_2$  can be read to  $\pm 0.1$  mg. In the determination of Si in steel, four weighings are involved; two for the blank and two for the specimen. Statistically, the weighing error will be  $\sqrt{4(0.1)^2}$ , or 0.2 mg. If the error is to be limited to 5 percent of the  $\text{SiO}_2$  weighed, then the weight of the  $\text{SiO}_2$  must be 4.0 mg. Since a Si concentration of 0.05 percent will produce 1.0 mg of  $\text{SiO}_2$ , at least a 4-g specimen must be used. Normally at this Si level, a 5-g specimen is used. In addition, to recover small amounts of silica from a dissolved specimen, it is necessary to dehydrate the solution twice with perchloric acid with an intervening filtration.

The specimens were reanalyzed by Lab 3 using an appropriate specimen weight and a double dehydration step. Table 8 shows the effect on precision when known techniques were applied. The spectrographic results of Lab 1 were discarded because the specimens had a different metallurgical history than the standards. Past experience has shown that specimens for Si determination must be metallurgically identical for satisfactory results.

TABLE 8—*Silicon rechecks using known techniques.*

Specimen	Lab 2	Lab 3
1	0.055	0.056
2	0.072	0.073
3	0.068	0.067
4	0.044	0.047

Although the 22 heats were made from the same starting materials and Al was not added intentionally, spectrographic analysis showed a variation of 0.003 to 0.020 percent Al. Therefore, it was necessary to have another laboratory check some of the specimens. Table 9 shows some of the checks between two laboratories. Since the spectrographic and chemical results were not in agreement, a third laboratory volunteered to analyze the 5 specimens. These results, along with those in Table 9, are shown in Table 10.

TABLE 9—Comparison of spectrographic and chemical results.

Specimen	Lab 1, Spectrographic	Lab 2, Chemical
1	0.020	0.013
2	0.007	0.017
3	0.006	<0.001
4	0.011	<0.001
5	0.020	0.010

TABLE 10—Original and recheck aluminum results.

Specimen	Lab 1, Spectrographic	Lab 2, Chemical	Lab 3, Chemical
1	0.020	0.013	0.0192
2	0.007	0.017	0.0065
3	0.006	<0.001	0.0058
4	0.011	<0.001	0.0104
5	0.020	0.010	0.0195

Lab 2 pushed the gravimetric procedure beyond its limits for accurate Al results. The method is not satisfactory for amounts less than 0.05 percent. To obtain the necessary accuracy, Lab 3 used a photometric procedure which is satisfactory in the range of 0.0005 to 0.10 percent Al.

As and Sb presented no analytical problems. However, there was a significant difference in Sn results as shown in Table 11.

TABLE 11—Typical tin check results.

Specimen	Lab 1	Lab 2	Lab 2, rechecks
1	0.0074	0.0109	0.0079
2	0.0100	0.0145	0.0097
3	0.0140	0.0196	0.0135
4	0.0090	0.0143	0.0090
5	0.0060	0.0105	0.0057
6	0.0010	0.0051	0.0018
7	0.0100	0.0136	0.0105

There appeared to be a bias of approximately 0.0040 percent Sn between the two laboratories. Lab 2 volunteered to repeat their analyses. The check analyses agreed with the results of Lab 1. It appeared that one of the reagents used in the determination was contaminated with iron, which produces high results.

## Summary

In the few examples shown, considerable expense and time could have been saved if standard methods of analysis were properly used.

## APPENDIX

Chemical analysis is an art requiring care and patience. One can become a reliable analyst after training and practice, but this does not guarantee that one is also a good analytical chemist. An analyst has good quantitative technique with or without an understanding of the chemical principles involved. Difficulties may be encountered by an analyst skilled in a certain type of analysis when he must apply an entirely new method. He may push this method beyond its limits. The lower limit of analysis is zero, but the lower limit of any method is set by the detectability of that method. The essential feature of any method is not the determination of a specific element alone but the determination of that element in the presence of other elements that may seriously affect a reaction involving the specific element. Analysts are usually careless in reporting analytical results with respect to not only their probable accuracy and precision but also the faith that should be put in them. For example, if a method is only accurate to  $\pm 0.2$  percent at the 20 percent level, many analysts will report 2 decimal places, which will thus give a false limit to the precision of the method.

### Definition of Terms

The terms "accuracy" and "precision" are sometimes used interchangeably, therefore, it is essential to define these terms as they are used in this paper. "Accuracy" refers to the degree with which experimental results agree with certified values or values which are assumed to be correct. "Precision" refers to the degree with which replicates agree with each other regardless of the deviation from the certified value or from the value that is assumed to be correct. Therefore, it is possible to have highly precise, yet inaccurate results.

### Choosing the Correct Method

An analytical chemist must know the limitation of the methods that he uses and why certain methods give more satisfactory results than others. He must have an understanding of the fundamental theory and be acquainted with the various sources of errors in the methods.

The choice of the correct analytical method depends on the principle that a unit change in concentration produces a definite change in signal output. This change, defined by an *S*-shaped curve, may be a change in absorbance in a photometric procedure, a change in weight in a gravimetric procedure, a sharp change in an electrical impulse in a potentiometric procedure, or a color change in a visual titrimetric procedure.

In the lower and upper portions of the *S* curve, sensitivity is lost because any increase in concentration produces a small change in signal. Therefore, it is necessary to select that portion of the curve that produces a maximum change in signal for a unit change in concentration. (This portion of the curve is indicated within the two horizontal dashed lines of Fig. 1.)

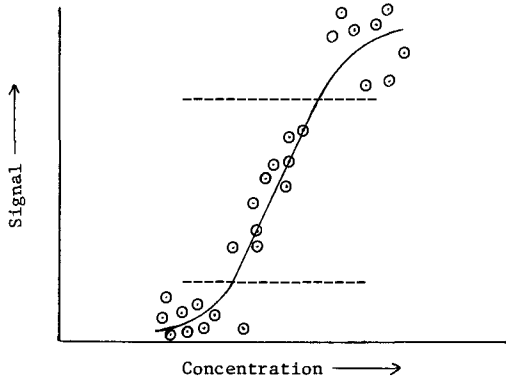


FIG. 1—Signal output versus concentration change.

## Temper Embrittlement of Low Alloy Steels

---

**REFERENCE:** Joshi, A. and Stein, D. F., "Temper Embrittlement of Low Alloy Steels," *Temper Embrittlement of Alloy Steels, ASTM STP 499*, American Society for Testing and Materials, 1972, pp. 59-89.

**ABSTRACT:** In an effort to understand the role various elements play on the temper embrittlement of low alloy steels, chemical analyses of fracture surfaces of nonembrittled and embrittled steels are conducted using Auger electron spectroscopy. The alloying elements, nickel and chromium, and trace elements antimony and tin segregated to grain boundaries during the embrittling treatment. No segregation was detected in nonembrittled steels. An attempt is made to relate the segregation of various elements and the observed embrittlement. The nature and extent of segregation is determined by ion sputtering experiments followed by Auger spectroscopic analysis. The segregation of impurity and alloying elements is examined considering both the Gibbsian and nonequilibrium models for segregation. A model is proposed to explain the observed concentration profiles. The effect of solute segregation on the grain boundary embrittlement is discussed in terms of true surface energy and plastic strain energy criteria.

**KEY WORDS:** spectroscopy, Auger electrons, grain boundaries, fracture surfaces, embrittlement, separation, sputtering, alloy steels, iron, tin, nickel, antimony, phosphorus, chromium, arsenic, carbon

The phenomenon of temper brittleness has attracted many reviewers and workers in recent years and was the topic of an ASTM special technical session in 1968. The work carried out in the past five years has contributed greatly to the understanding of the mechanisms of the problem and has brought about the creation of tentative models. Capus [1] and McMahan [2] summarized the status of the problem up to 1968. Steven, Balajiva, and co-workers [3,4] were the first to identify the association of embrittlement with impurities. Subsequently, Low et al [5] demonstrated the influence of specific impurity elements such as Sb, P, Sn, and As and of alloying elements Ni and Cr. Many techniques used to identify the grain boundary precipitation or segregation that may be associated with embrittlement were unsuccessful

<sup>1</sup> Formerly, research associate, Dept. of Mechanical Engineering, University of Minnesota; now, visiting assistant research professor, Dept. of Metallurgical Engineering, Michigan Technological University, Houghton, Mich. 49931.

<sup>2</sup> Formerly, professor, Dept. of Mechanical Engineering, University of Minnesota; now, professor and head, Dept. of Metallurgical Engineering, Michigan Technological University, Houghton, Mich. 49931.

[5–7], including autoradiographic [5,7–9] techniques. Electron microscopic examination of grain boundary fracture facets did not reveal any noticeable difference in the precipitate (carbide) morphology between the embrittled and nonembrittled steels [5,10]. Positive evidence of segregation in embrittled steels was obtained from the work of Plateau et al [11], who observed striations on intergranular fracture surfaces, and from microhardness measurements by Low et al [5].

The only direct evidence of segregation, prior to 1968, was provided by Arkharov et al [12] who showed segregation of P in an embrittled steel and by Inman and Tipler [13] who demonstrated segregation of P in Fe. While it is known that a combination of alloying elements enhances embrittlement, the role of the alloying elements is not certain. Several proposals have been made to explain their role, including the following: 1. modification of diffusion kinetics of impurities by alloying elements [5]; 2. alloying elements segregate to boundaries during austenitizing and chemically attract and interact with the impurity elements during embrittling treatment, resulting in double segregation [1]; and 3. the effect of alloying elements on the strength of the carbide matrix interface [5]. Little is understood of the actual segregation mechanisms due to the lack of experimental tools to detect the minute quantities of solute segregation involved.

Recent developments in the technique of Auger electron emission spectroscopy have contributed to a better understanding of the surfaces [14,15]. Chemical analysis of extremely thin surface layers ( $\sim 5$  to  $10 \text{ \AA}$ ) has been made possible by this technique. The usefulness of the technique has already been demonstrated in the study of surfaces of semiconductors [16,17] and metals [18,19].

The objective of the investigation is to understand and clarify the following:

1. The role of the trace impurities Sb, As, and Sn. These elements are known as active embrittlers in low alloy steels [5]. Whether they all segregate to grain boundaries is not known. If they do, at what stage and how potent is the segregation in causing embrittlement?

2. Role of carbon. Low alloy steels with little or no C exhibit temper embrittlement [5]. C accentuates the embrittlement, which may in part be attributed to carbides present in the grain boundaries. Segregation of impurity elements to the interphase boundaries between carbides and ferrite grain is said to provide a path of easy fracture and thus intensify the embrittlement [2,10,20]. This proposal will be examined.

3. Role of alloying elements Cr and Ni. Temper embrittlement is not prominent in plain Fe-C steels containing the trace impurities Sb, As, Sn, and P. Alloying and multiple alloying causes a rapid enhancement of embrittlement. The role of these elements and their segregation to grain boundaries requires careful analysis.

## Experimental Techniques

In order to minimize contamination of fracture surfaces by the atmosphere prior to and during analysis, the specimens are fractured and the fresh surfaces analyzed in an ultrahigh vacuum. The high vacuum is achieved by use of an all metal vacuum system provided by Varian Associates and consists of an ion pump supplemented by a titanium sublimator. Rough pumping is obtained by use of vacsorb pumps.

The technique of Auger electron spectroscopy [14-19,21,22] is used to analyze the fracture surfaces of steels. Primary electrons with an energy of 3 keV are used and the secondary emitted electrons analyzed. The characteristic Auger electrons of the emission current are of extremely low energy (usually less than 1 keV) and represent only the atoms present in the first 5 to 15 Å deep layer from the surface.

Specimen cooling is often necessary to obtain a brittle fracture. The cooling is achieved by heat conduction through a copper block (Fig. 1) situated underneath the specimen holder which is cooled by circulated liquid nitrogen. The temperature attained by the specimens is directly measured by a thermocouple. Prior to analysis, the specimens are fractured by means of a hammer arm attached to the end of a rotary feed through.

In addition the equipment has provision for ion sputtering. The sputtering gun ionizes cleaned xenon gas maintained at a pressure of  $1 \mu\text{m}$  and accelerates the ions onto the target. A typical ion energy of 400 eV and current

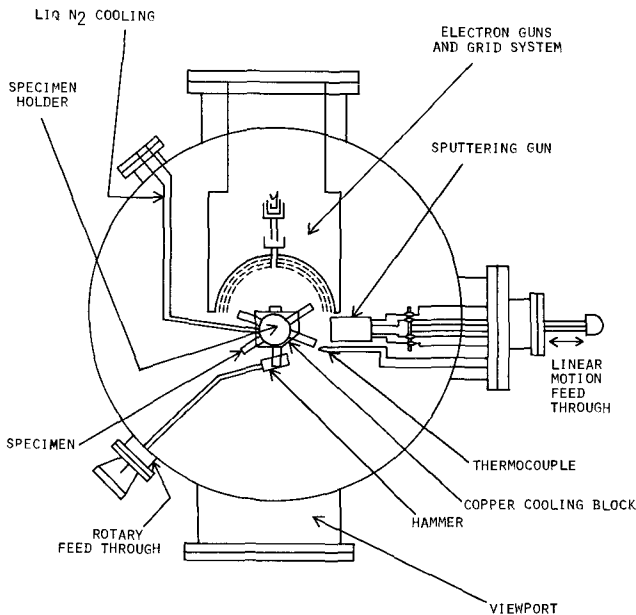


FIG. 1—Layout of the equipment in the vacuum system.

density of  $200 \mu\text{A}/\text{cm}^2$  are used during the investigation. This technique provides a method of removing a small number of atoms from the surface and is particularly useful in removing layers from the fracture surface. An Auger analysis followed by small steps of sputtering gives the chemical analysis as a function of distance from the original fracture surface. The amount of the material to be removed from the fracture surface can be calculated by knowing the yield behavior. Such information for most materials is readily obtainable from the published data of Wehner [23].

Identification of the elements corresponding to the various Auger peaks is accomplished with the help of known electron binding energies. However, not all transitions are equally probable. (For Fe, the prominent emissions correspond to energies of 28, 48, 550, 590, 600, 610, 651, 702, and 712 eV approximately.) At this time Auger transitions are not well enough understood to predict which of the transitions will occur; therefore, it is usually necessary to run spectra on pure elements for materials with known compositions to determine the exact spectra for each element. Several researchers [19,24] have determined the Auger spectra for many pure elements. In general, the procedure followed is to place the specimens in the vacuum system, pump to a vacuum of  $10^{-9}$  torr or better, and, after baking the entire system at 180 C for 2 days, fracture the specimens by impact with the hammer. The severely embrittled specimens are fractured at room temperature while others are cooled before fracturing. While it cleans the system and reduces the contamination of the fracture surface baking does not alter the specimen properties.

### Materials and Heat Treatment

All of the steels used in this investigation were vacuum melted and cast at the G.E. Research and Development Laboratories. The preparation of these materials has been described in detail by Low et al [5]. Table 1 indicates the compositions of the various steels. Figure 2 shows the measured transition temperatures of all the steels tested.

TABLE 1—Analysis of steels used in the investigation. (All values shown are by weight.)

Heat Number	Percentage					Parts per Million				Percentage
	C	Ni	Cr	Mn	Si	Sb	As	P	Sn	Other
31-100	0.39	3.5	1.6	0.003	...	620	6	50	10	S = 0.004
814-30	0.38	4.0	1.6	0.005	...	90	...	20	...	S = 0.005
2407	0.24	4.4	1.7	...	...	400	...	...	...	Re = 0.26
3710	0.40	3.5	...	...	...	650	...	...	...	...
2433	0.40	...	...	...	...	800	...	...	...	...
3022	0.30	3.7	1.7	...	...	...	530	...	...	...
3023	0.31	3.7	...	...	...	...	520	...	...	...
3024	0.31	3.7	...	...	...	...	...	...	480	...
3239	0.45	3.50	1.74	0.92	0.25	...	...	...	...	Be = 0.01
3240	0.43	3.45	1.71	0.90	0.27	Not Analyzed				Be = 0.06
3241	0.38	3.48	1.74	0.03	0.03	Not Analyzed				Be = 0.01
3242	0.43	3.46	1.69	0.03	...	Not Analyzed				Be = 0.09

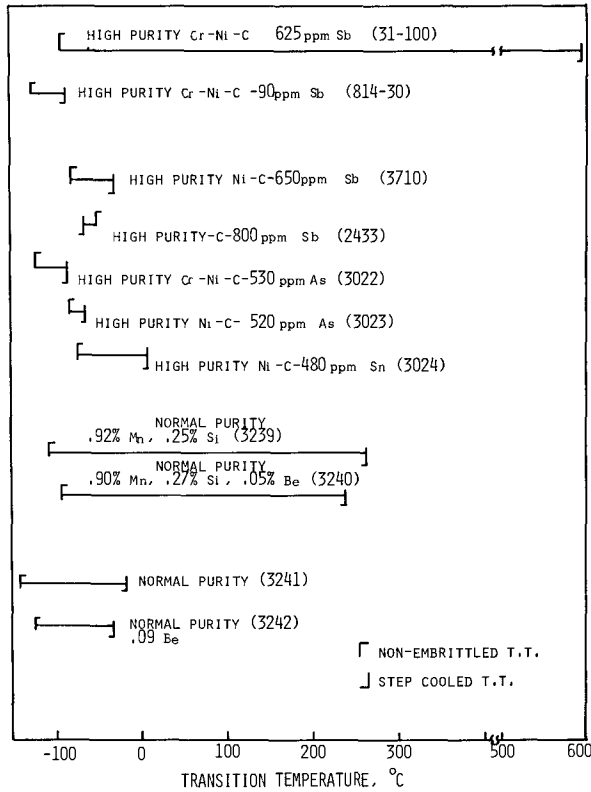


FIG. 2—Changes in transition temperature as a result of step cooling for steels used in the investigation.

All steels are tested for embrittlement in the tempered martensitic condition. A treatment of 1 h at 870 C, water quench, liquid nitrogen quench, temper 1 h at 625 C, and water quench is given to all the steels. Steels in this condition are designated as nonembrittled. The following step cooling cycle is used to produce embrittled specimens: temper 1 h at 593 C; furnace cool to 538 C, hold 15 h; cool to 524 C, hold 24 h; cool to 496 C, hold 48 h; cool to 468 C, hold 72 h; cool to 315 C; and air cool to room temperature. Powers [6] has shown that this treatment results in substantial embrittlement and is equivalent to a 1000-h treatment at 480 C. Most steels are tested in both the embrittled and nonembrittled states.

In order to evaluate the interaction between alloying elements (Ni and Cr) and impurities (Sb, Sn, As, and P) and to understand the kinetics of the step cooling process, specimens were analyzed after water quenching from various steps in the step cooling process. The 31-100 heat of steel was used for this study.



of the element present [17]. Thus, the amount of segregation has been estimated as the ratio:

$$\frac{\text{height of Ni peak}}{\text{height of Fe peak}} \Big|_{\text{emb}} \div \frac{\text{height of Ni peak}}{\text{height of Fe peak}} \Big|_{\text{sputt}}$$

This factor gives a segregation ratio in the fracture surface of embrittled steel from which the Ni/Fe content in the boundary can be evaluated by multiplying it by the bulk Ni/Fe ratio. The 850 eV Ni line and the 530 eV Cr line are used and normalized by dividing the height of the peaks at these voltages by the height of 650 eV Fe peak. The assumption made previously [25] is that, in the nonembrittled state, no segregation of Ni and Cr occurs to the grain boundaries. Deep sputtering by ion bombardment did not appreciably alter the peak heights in the nonembrittled steel, thereby ensuring the validity of the assumption. The result of such a calculation (Table 2) shows that there is about 9.5 percent Ni in the grain boundaries of embrittled 31-100 heat steel.

TABLE 2—Change in transition temperature with solute segregation.

Embrittled Steel Heat Number	Shift ΔTT, deg C	Grain Boundary Composition, atomic percent, Averaged over three to four Atomic Monolayers			C/Fe Peak Height Ratio
		Ni	Cr	Sb, Sn, or As	
31-100	695	10.0	5.0	3.6 Sb	0.19
2407	296	10.6	4.5	2.4 Sb	0.22
3710	50	5.7	...	1.8 Sb	0.6
814-30	39	4.0	1.6	Sb not detected (0.60 or less)	0.2
3022	41	3.7	1.7	As not detected	0.19
3023	22	3.7	...	As not detected	0.28
3024	84	4.5	...	1.0 Sn (estimate for Sn made assuming same Auger yield as Sb)	0.26

Sb concentration (Table 2) in the grain boundaries is estimated by using the results of Auger analysis of Fe-2.2 Sb alloys made by Palmberg and Marcus [27].

Since strong segregation of Sb as well as of Ni and Cr is observed, it is of interest to examine whether Ni and Cr segregate to grain boundaries during the embrittling treatment in the absence of Sb in the alloy. In the complete absence of Sb, grain boundary fractures could not be obtained. Hence, steels with varying contents of Sb were examined. The results of this study are shown in Figs. 4 to 6. Figure 6 clearly demonstrates that Ni and Cr do not segregate to the grain boundaries when Sb is low or absent; therefore, it is not possible to completely isolate the role of alloying elements.

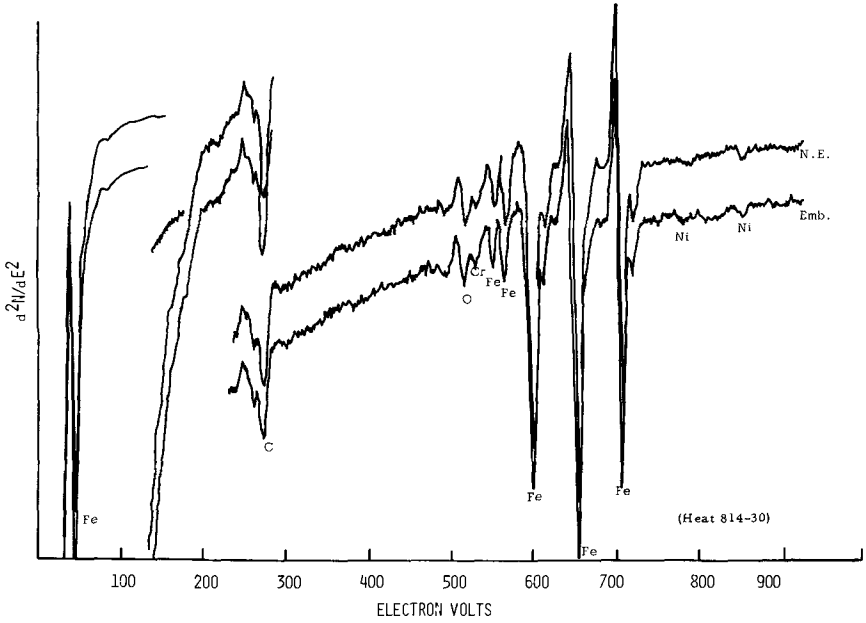


FIG. 4—Auger spectra of nonembrittled and embrittled Ni-Cr-C-90 ppm Sb steel (heat 814-30).

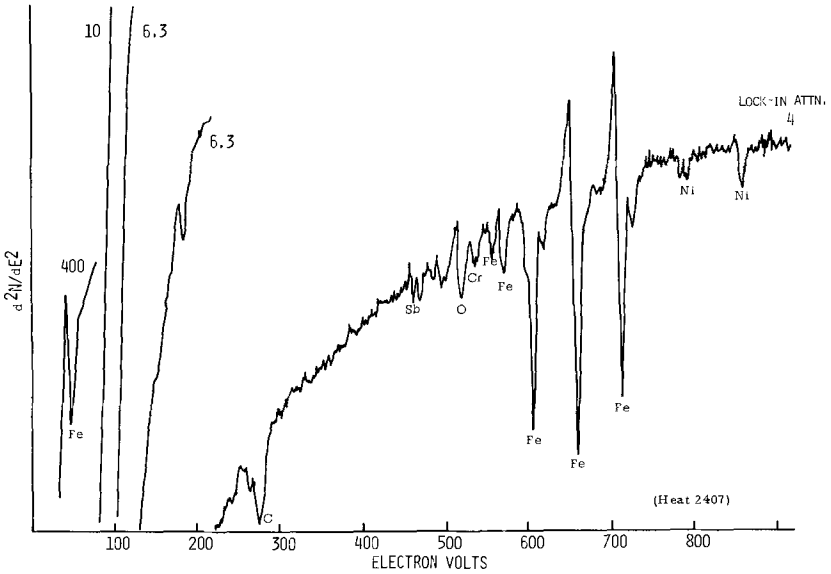


FIG. 5—Auger spectra of embrittled Ni-Cr-C-400 ppm Sb steel (heat 2407).

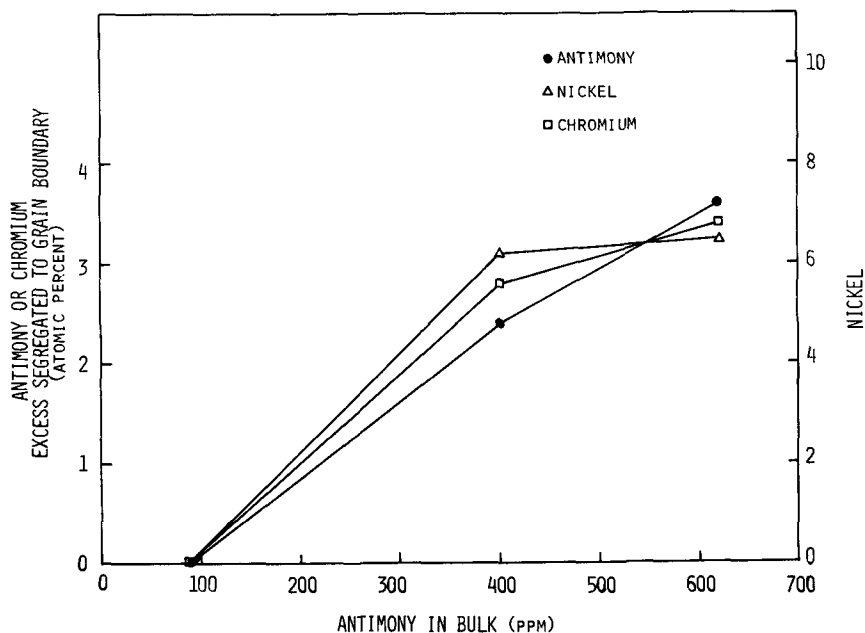


FIG. 6—Segregation of Ni, Cr, and Sb to grain boundaries in Ni-Cr-C steels versus Sb bulk concentration.

In an effort to examine how segregated Cr and Ni influence the shift in transition temperature ( $\Delta T_T$ ) a heat of steel was prepared without Cr (heat 3710) containing Ni and 650 ppm Sb. Steels containing only Sn or As were also prepared to determine the role of those elements during embrittlement. The Auger spectra of the fracture surfaces of these steels are presented in Figs. 7 to 10. No segregation of As is detected in the grain boundaries, while small amounts of Sn are. The estimated quantities of individual segregants (Ni, Cr, and Sb) are plotted against  $\Delta T_T$  in Fig. 11.

An attempt is made to estimate the extent (depth) of segregation of the various elements from the grain boundary. The variations in the Cr peak height could not be evaluated accurately because of the overlap from the oxygen peak. The peaks of Ni, Sb, and Sn were followed with the progression of sputtering and the results are shown in Figs. 12 to 15. Figures 13 and 14 show the results on the concentration profiles of Sb and Ni in the steel (31-100 heat) step equilibrated and water quenched from various temperatures in the step cooling process. The 524 deg C curve represents a specimen which was oil quenched from 825 C, quenched to liquid nitrogen; tempered 1 h at 625 C, water quenched; and given the step cooling treatment of 593 C for 1 h, furnace cool to 538 C, hold 15 h, cool to 524 C, hold 24 h, and water quench. A dip and hump in the concentration profiles is clear in most specimens and it is interesting to note the hump moving closer to the boundary with the progression of the step cooling process.

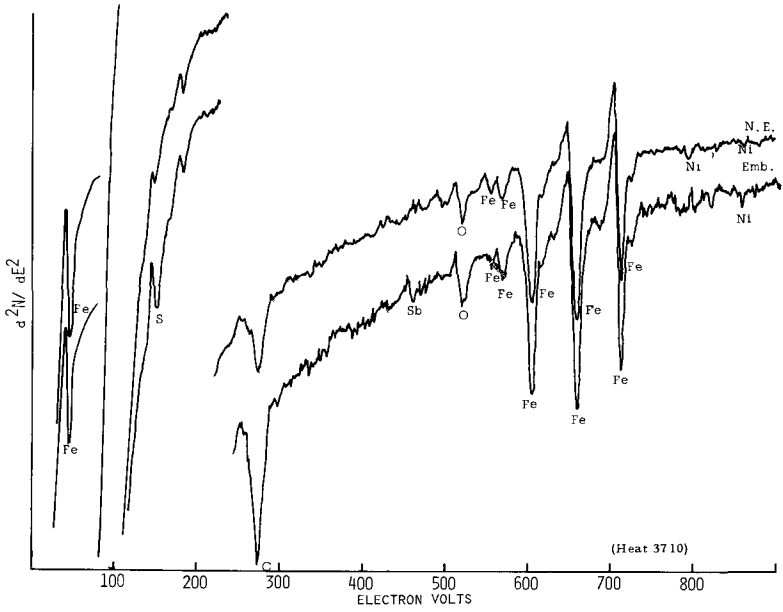


FIG. 7—Auger spectra of nonembrittled and embrittled Ni-C-650 ppm Sb steel (heat 3710).

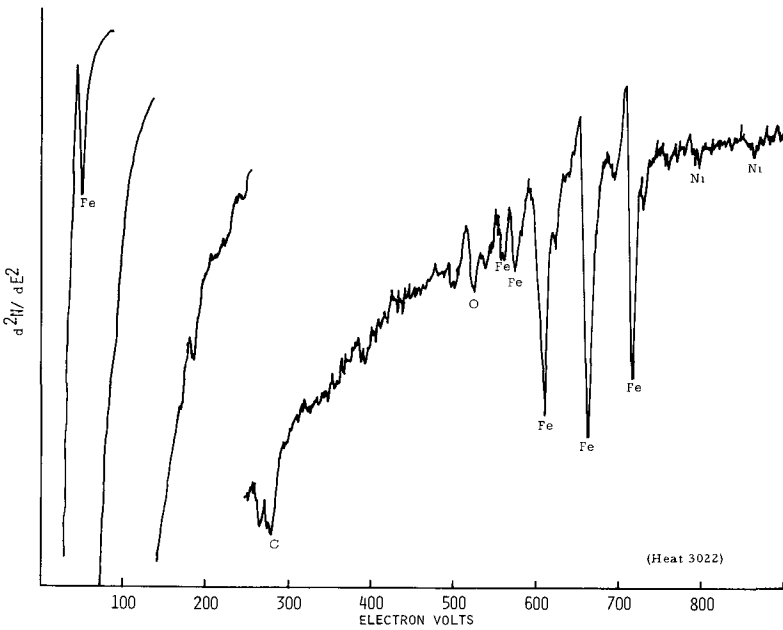


FIG. 8—Auger spectra of embrittled Ni-Cr-C-530 ppm As steel (heat 3022).

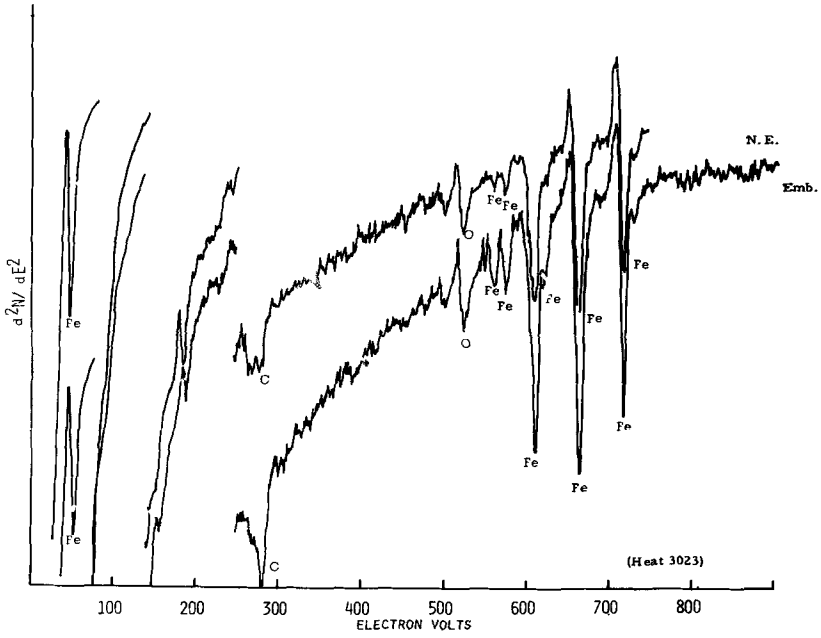


FIG. 9—Auger spectra of nonembrittled and embrittled Ni-C-520 ppm As steel (heat 3023).

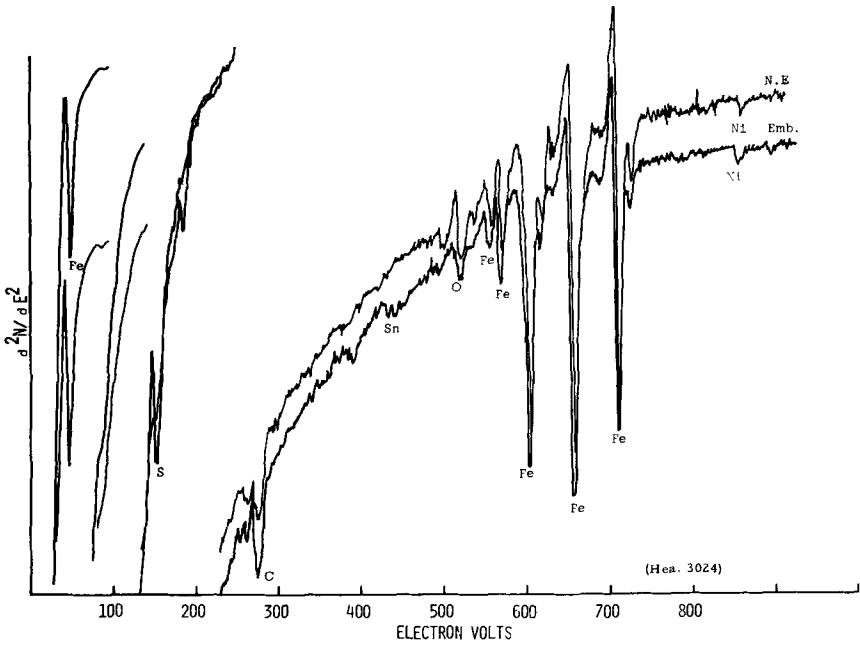


FIG. 10—Auger spectra of nonembrittled and embrittled Ni-C-480 ppm Sn steel (heat 3024).

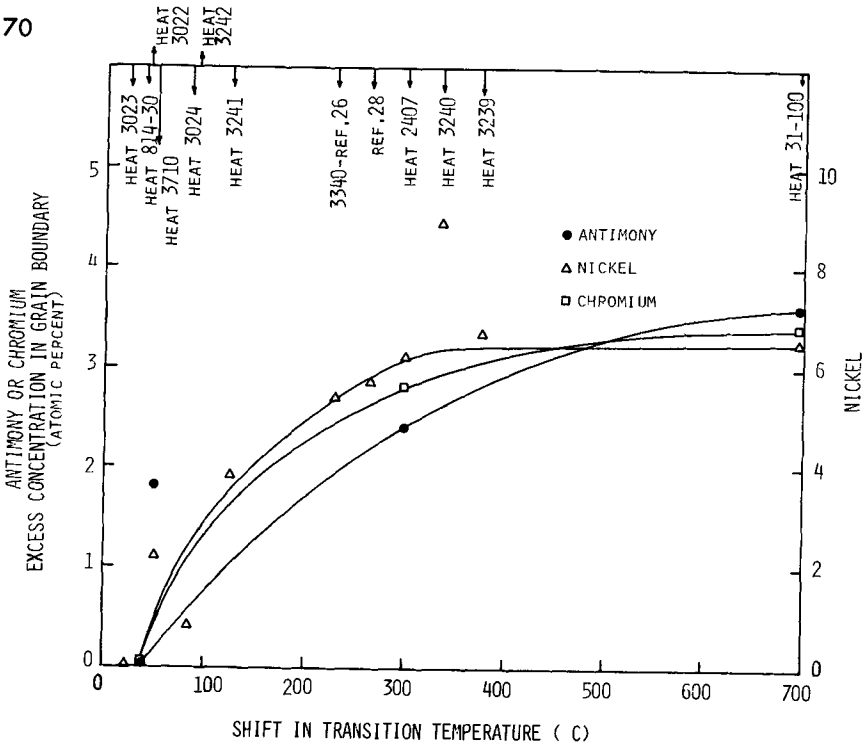


FIG. 11—Shift in transition temperature related to segregation.

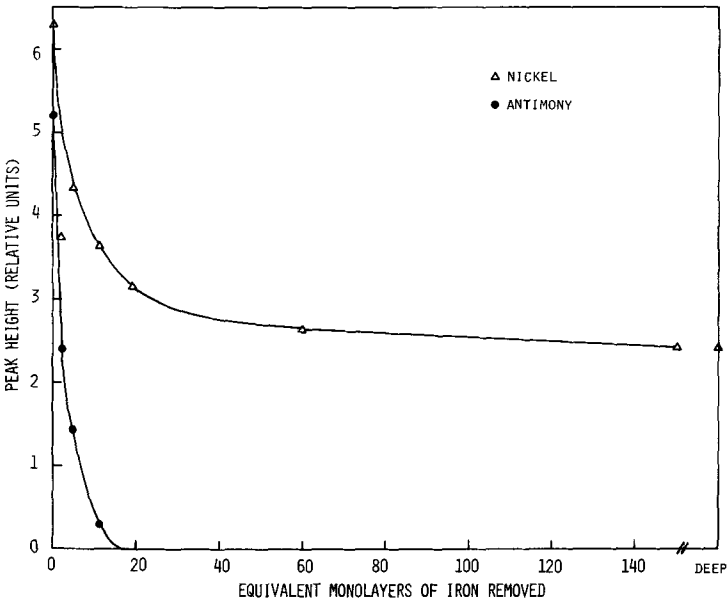


FIG. 12—Variations in Ni and Sb concentrations with distance from intergranular fracture surface of embrittled Ni-Cr-C400 ppm Sb steel (heat 2407). (Level at DEEP indicates the bulk concentration.)

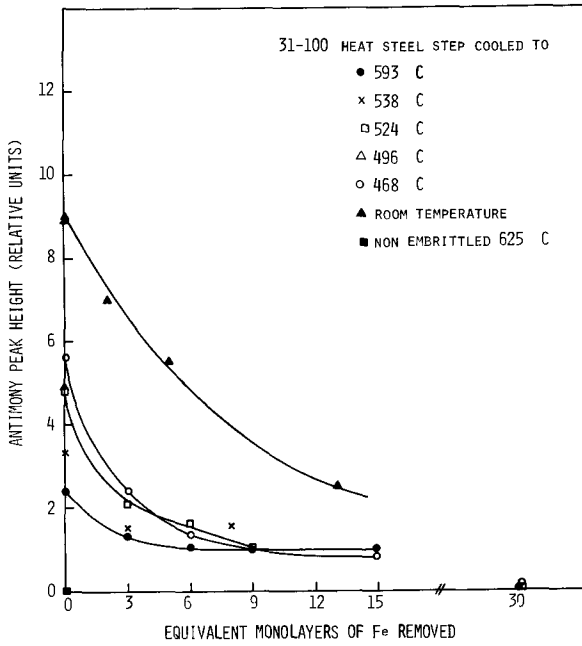


FIG. 13—Variation in Sb concentration as a function of distance from intergranular fracture surface of steel (31-100 heat) specimens quenched from various steps in the step cooling process.

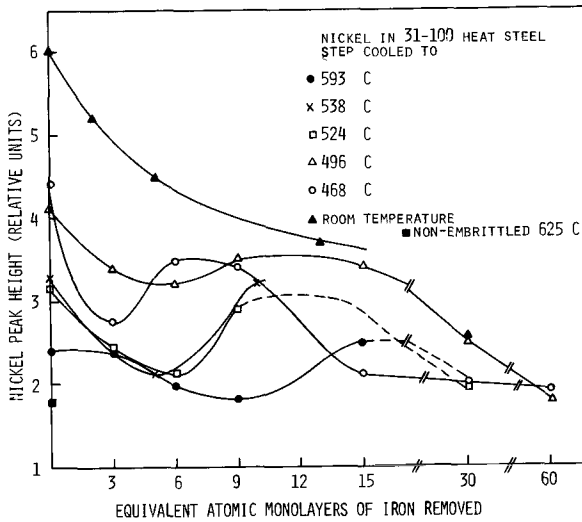


FIG. 14—Variation in Ni concentration as a function of distance from intergranular fracture surface of steel (31-100 heat) specimens quenched from various steps in the step cooling process.

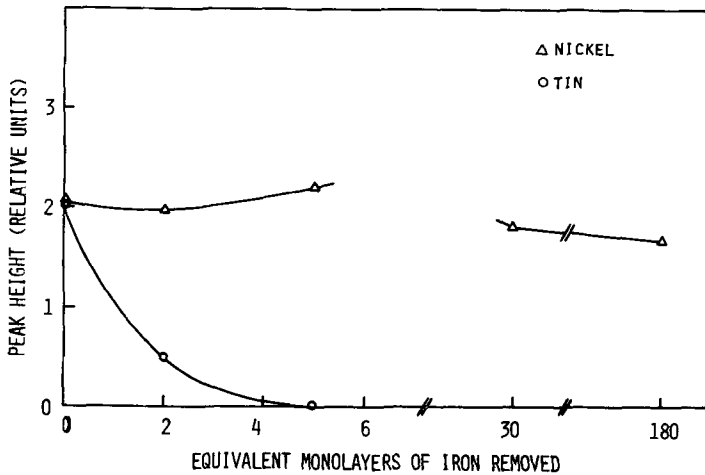


FIG. 15—Variation in Sn concentration with sputtering in a Ni-C-480 ppm Sn steel (heat 3024).

### Brief Summary of Results

1. Sb, Ni, and Cr segregate to grain boundaries upon step cooling of a steel containing Cr, Ni, Sb, and C.

2. Segregation of Sb, Ni, and Cr and the associated shift in transition temperature upon step cooling increased with increasing Sb content of the alloy steel.

3. Significant amounts of Sn and Ni segregated in a Ni-C-Sn steel upon step cooling.

4. Ni and Cr segregated in most steels upon step cooling. No such segregation occurs in nonembrittled steels.

5. Segregation is not observed in steels containing As, Ni, Cr, and C. These steels show only a very small shift in transition temperature upon step cooling.

6. Segregation of C is observed in many steels after step cooling, particularly in those not containing Cr.

7. Segregation of Sb and Sn appears to be concurrent with that of alloying elements Ni and Cr. No segregation of Sb occurs in the absence of Ni or Cr and vice versa.

8. Segregation of Sb, even in the most embrittled case, is limited to about 15 to 20 atomic layers from the grain boundary. Segregation of Sn is not observed beyond 5 atomic layers. In contrast, the segregation of Ni and less obviously of Cr is observed beyond 100 atomic monolayers.

9. The segregation of Sb and Ni and Cr occur almost simultaneously during the entire step cooling process. The Ni concentration profile (Fig. 14) exhibits a hump in the close vicinity of the grain boundary. It is apparent that the hump moves closer to the grain boundary as the step cooling process progresses.

## Discussion

An attempt is made in Fig. 11 to relate the quantity of each element segregated to the shift in transition temperature. The lines are drawn through the data points corresponding to Ni-Cr-Sb-containing steels. From this (and Table 2) it appears that the quantity of each element segregated to grain boundaries influences the transition temperature in a direct way. The available data for Ni segregation from other steels are also plotted on the same graph. Even though embrittlement is associated with each case of segregation, a good correlation between the Ni segregation and  $\Delta T_T$  does not exist. This suggests the probability that segregated Ni alone is not embrittling by nature. It segregates along with other impurity elements such as Sb and P [28] which are known to cause embrittlement in Fe.

An important conclusion from Figs. 7 and 11 is that Ni and Cr segregate to grain boundaries during the embrittling treatment and only in the presence of impurities such as Sb, Sn, or P. This might appear to contradict the results reported earlier in commercial purity steels [25] (heats 3240 and 3241) in which segregation of Ni and Cr was observed but no segregation of Sb, P, or Sn was reported. It was suspected, however, that Mn or Si had segregated in these steels but could not be identified by the Auger technique. Similarly, Viswanathan [28] observed considerable segregation of Ni in embrittled Ni-Cr-C steel. However, he also observed some P segregation. This result is again in agreement with the earlier conclusion. The experiments of Viswanathan and Sherlock [29] also confirm that increased segregation of any of the elements P, Sn, Ni, and Cr is accompanied by increased segregation of the others. All these observations suggest interaction between the elements Ni and Cr and the metalloids. In view of the results obtained, segregation appears to be the major controlling factor during embrittlement. The various models used to explain embrittlement, based upon segregation, are discussed below.

### *Double Segregation Model*

Capus [1] has proposed that grain boundary enrichment with alloying elements such as Mn, Cr, and Mo during austenitizing can lead to enhanced segregation of embrittling elements such as P, As, Sb, or Sn by chemical interaction. Only the latter elements cause the shifts in transition temperature and the change over from cleavage to intergranular brittle fracture.

According to this model, the presence of Cr would be expected at the prior austenite boundaries in high concentrations, even in the nonembrittled state. However, it is observed that segregation of Ni and Cr as well as of Sb, Sn, etc., proceeds only during embrittling treatment. Hence, a model based upon double segregation does not explain the present observations.

*Two Dimensional Phase Transformation*

This theory attributes embrittlement to a continuous intercrystalline film of a second phase which is itself brittle or which produces a weak interface with the adjoining matrix grains. The argument in this case, in view of the electron microscopic investigations, may be made that the second phase film is extremely thin, tending toward that of a two dimensional surface phase [30].

In the present study no correlation is found to exist (Table 3) between the Sb/Ni or Sb/Cr ratios for the various specimens. This indicates the absence of a compound at the grain boundaries. Further, the solute element concentration in grain boundaries varies widely with embrittling temperature, thus contradicting a theory based upon two dimensional phase transformation.

TABLE 3— $\frac{Sb}{Ni}$  and  $\frac{Sb}{Cr}$  peak height ratios in embrittled steels.

Steel	Treatment	$\frac{Sb}{Ni}$	$\frac{Sb}{Cr}$	
31-100	Step cooled	1.5	1.6	
		1.7	2.0	
	Quenched from	524 C	1.6	1.4
		468 C	1.3	1.6
		538 C	1.0	1.0
2407	Step Cooled	593 C	1.0	0.8
		0.8	1.3	
3710		1.5	...	
3340 (Ref 26)		2.6	3.8	

*Equilibrium Segregation*

A distinction may be made between two kinds of segregation: a. equilibrium segregation, favored by thermodynamic considerations, for example, the decrease in the free energy of the entire system due to segregation to grain boundaries; and b. nonequilibrium segregation due to other reasons, for example, interaction of solutes with vacancies.

For the case of grain boundary adsorption, whereby the solute elements segregate and reduce  $\gamma_b$  (grain boundary energy per unit area), Cahn and Hilliard [31] have made calculations to estimate the segregation at the grain boundary. Their calculations, limited to a binary system, estimate the upper limit as

$$\Gamma_{2(1)}^0 < (\gamma_b/kT)[1 + \ln(X_e/X)]^{-1} \quad (1)$$

for the range  $0 \leq X_0 \leq X_e$  where  $X_0$  is the atomic fraction of component 2 (solute) and  $X_e$  the solid solubility limit of component 2 in 1.  $\Gamma_{2(1)}$  for a two component system is defined by

$$\Gamma_{2(1)} = \Gamma_2 - [X/(1 - X)]\Gamma_1$$

$\Gamma_{2(1)}^0$  is the measured value of  $\Gamma_{2(1)}$  at an atomic fraction of solute  $X_0$ . The excess component  $\Gamma_i$  per unit area of the boundary is defined as the difference between the actual amount of the component in the system and that which would have been present in the same volume if the phases were homogeneous right up to an imaginary dividing surface. Thus, if the number of solute atoms experimentally measured is plotted against the perpendicular distance to the grain boundary in atomic monolayers (schematic in Fig. 16), the area under the curve hatched between  $AA'$  is  $\Gamma_{2(1)}$ . There is no theoretical limitation put upon the distance  $A$  or  $A'$  from the grain boundary. In the case of Sb, the Auger analysis indicates excess concentration only in the first 10 to 15 atomic layers approximately. (See Appendix.) Since the limit of detectability of Sb by the Auger technique [27] is only 0.6 atom percent, while the bulk level is 650 ppm even in the steel with highest Sb, the segregation is expected well beyond the actually observed 10 to 15 monolayers. If the total amount of segregated Sb in the approximate 15 layers is estimated, it represents a portion of the overall Sb segregation.

In a binary system of the Fe-Sb type, the theoretical estimation of Sb segregation according to Gibbs adsorption may be made using Eq 1. However, the presence of other elements, such as Ni, Cr, and C in steel, complicates the processes involved in several ways. First, they may affect the value  $X_e$  of Sb in Fe. Schulz and McMahon [32] have recently reported that solubility of Sb in Fe is reduced rapidly by addition of 1 or 2 percent Ni. This, in effect, reduces the  $X_e$  or increases the theoretical estimate  $\Gamma_{Sb(Fe)}^0$  of Eq 1. For an accurate estimate, the influence of other elements such as Cr and C should also be taken into account. In view of this, comparison of theoretical estimates of  $\Gamma_{Sb(Fe)}^0$  to measured  $\Gamma_{Sb(steel)}$  is not justified.

Second, partial reduction of the boundary energy  $\gamma_b$  may occur as a result of segregation of the alloying elements. If the reduction in  $\gamma_b$  is the driving

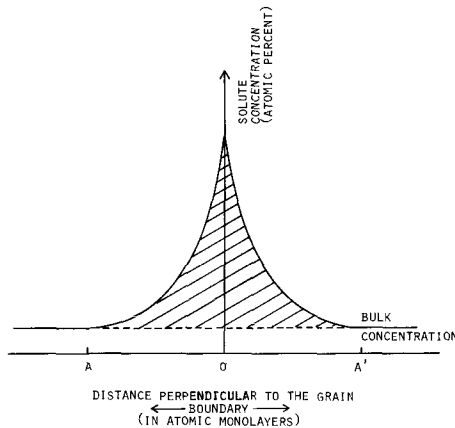


FIG. 16—Segregation at a grain boundary.

force for the segregation of Sb as well as Ni and Cr, then the cumulative rather than individual effect of segregation on  $\gamma_b$  should be considered.

The influence of Sb additions on the equilibrium solubility of Ni in Fe may be examined. The highest Sb content in the most embrittled steel is 620 ppm and the effect on solid solubility of Ni may be assumed to be negligible in such small amounts. If it is also assumed that the effect of 1.6 percent Cr and 0.4 percent C on the equilibrium solubility of Ni is negligible, a theoretical estimate  $\Gamma_{\text{Ni(steel)}}$  can be made. The later value can then be compared to the measured  $\Gamma_{\text{Ni(steel)}}$  value, thus determining if the observed segregation is compatible with equilibrium segregation.

Finally, the elements may be involved in a complicated Sb-X or Sb-X-vacancy interaction. No data are available regarding such interactions in the systems of present interest.

*Comparison to experimental results.* A comparison can now be made of the experimentally observed segregation to the theoretical estimate  $\Gamma_{\text{Sb(Fe)}}$  to get a rough idea of what is happening. As an example, the embrittled steel Ni-Cr-C-400 ppm by weight Sb (heat 2407 SC) will be considered. Following Cahn and Hilliard [31] and using  $\gamma_b$  of austenite, 850 erg/cm<sup>2</sup> [33] ( $\gamma_b$  of ferrite is not known),  $X_0 = 0.00018$ ,  $X_e = 0.028$  [34], and  $T = 750$  K it turns out  $\Gamma_{\text{Sb(Fe)}}^0 = 0.136 \times 10^{16}$  atoms/cm<sup>2</sup>. Using the data obtained on Sb segregation (Fig. 12) in embrittled steel (heat 2407 SC) gives a measured  $\Gamma_{\text{Sb(Fe)}} = 0.30 \times 10^{15}$  atoms/cm<sup>2</sup>. This result, in view of the assumption that Sb segregation is limited to the region AA', is possibly close although an under estimate. Since  $\Gamma_{\text{Sb(Fe)}}^{\text{measured}} < \Gamma_{\text{Sb(Fe)}}^0$  this indicates a consistency with equilibrium segregation. This comparison, however, is not fully justified in view of the effect of alloying elements on  $X_e$  of Sb in Fe.

Data are also available on the second of the effects considered above. The actual amounts of Ni and Cr segregated to the boundaries have been estimated (Fig. 12 for Ni in embrittled steel heat 2407); therefore, the segregation of Ni may be examined to see if it is consistent with equilibrium segregation. Considering the segregation of Ni in Fe and substituting reasonable values for an embrittled steel (heat 2407),  $X_0 = 0.042$ ,  $X_e = 0.005$ , [34],  $T = 750$  K, and  $\gamma_b(\gamma\text{-Fe}) = 850$  erg/cm<sup>2</sup>, into Eq 1 gives  $\Gamma_{\text{Ni(Fe)}}^0 = 0.7 \times 10^{16}$  atoms/cm<sup>2</sup>. Calculating  $\Gamma_{\text{Ni(Fe)}}^{\text{measured}}$  from the concentration profiles gives  $\Gamma_{\text{Ni(Fe)}}^{\text{measured}} = 0.76 \times 10^{16}$  atoms/cm<sup>2</sup>.  $\Gamma_{\text{Ni(Fe)}}^{\text{measured}} > \Gamma_{\text{Ni(Fe)}}^0$  indicates an inconsistency with equilibrium segregation.

This result should be more closely examined in view of the available experimental data on the grain boundary energy measurements and the influence of impurities on them. In case of an Fe-P system it has been reported [35,36] that the  $\gamma_b$  value of  $\delta$ -Fe does not decrease beyond approximately 400 erg/cm<sup>2</sup>. It reached a minimum value of  $\gamma_b/2$  approximately, but did not go any lower in spite of increasing the P content. The indication is that  $\gamma_b$  does not reach anywhere near zero, the limit used in the derivation of Gibbs' adsorption expression [1]. This appears to be true of other systems such as Cu-Bi and

Cu-Sb that have been investigated. Thus the result that  $\gamma_b \rightarrow 0$ , or identically  $\Gamma^{\text{measured (cumulative)}} \rightarrow \Gamma_0$ , tends to give negative support to the equilibrium segregation model. Grain boundary activity measurements of Ni and Cr reported by Hondros [35,36] ( $\Delta\gamma_b/\Delta X = 54$  and  $87$  erg/cm<sup>2</sup>/atom percent  $X$ , respectively, as compared to  $575$  erg/cm<sup>2</sup> for P) do not indicate strong tendency of these elements to segregate in  $\gamma$  Fe by a Gibbs-type mechanism.

In addition to the segregation of Ni and Sb, it was also found that Cr is segregated in these alloys. As discussed earlier a reduction in  $\gamma_b$  alone cannot be the driving force for all the segregation observed and, therefore, the total observed segregation appears to be inconsistent with equilibrium segregation even if the Sb segregation is completely neglected.

The following are the additional points, based upon the present results, which bring into question the equilibrium segregation model.

1. Segregation of Ni or Cr does not occur in the absence of Sb, Sn, or P in the alloy. This is difficult to explain through a simple model based upon Gibbsian adsorption. Complex interactions of the Sb- $X$ -vacancy type, as discussed earlier, may have to be assumed and nonequilibrium segregation suggests itself as the natural choice for explaining it.

2. The concentration profile of Ni exhibits a hump in the vicinity of the grain boundary, which is unexplained by a simple model of the Gibbs type.

In order to explain these and other observations a model based upon non-equilibrium segregation is considered.

### *Nonequilibrium Segregation*

Aust et al [37] have examined the influence of different solutes on the grain boundary hardening of zone-refined Zn, Sn, and Pb. It was observed that a certain class of solute atoms, characterized empirically by distribution coefficient  $K < 1$ , results in excess hardening near the grain boundary after quenching, while another class of solutes with  $K > 1$  gives a region which is softer near the grain boundary than in the grain. The distribution coefficient  $K$  is defined as the ratio of solute concentration in the solid solvent to that in the liquid phase with which it is in equilibrium. It was shown [37] that solutes with  $K < 1$  have negative binding energy with vacancies. According to their solute clustering mechanism, excess quenched-in vacancies tend to disappear at grain boundary sinks. Those systems with a positive solute-vacancy binding energy ( $K < 1$ ) can produce a vacancy-coupled uphill diffusion of solute atoms toward the boundary. If positive thermodynamic deviations are also present, metastable or stable cluster formation can occur near the boundary. Systems with  $K > 1$  or  $a < 1$  ( $a$  is the activity coefficient) will not lead to enrichment of the solute or to clustering near the boundary. The hard grain boundaries are due to solute clusters, while the soft boundaries are due to the absence of solute clusters and secondary defects. It was also shown [37] that the addition of a suitable solute can remove the excess boundary hardening due to another solute.

The occurrence of excess boundary hardening upon embrittlement has been reported [5] in the alloy steels (31-100) and all the solute elements of concern possessed  $K$  values less than unity in their binary solid solutions with Fe. The complexity to multiple solutes is not known. The distribution coefficients of Ni and Cr in Fe appear to be greater than unity [38] and hence these elements would be expected to segregate to boundaries even in the absence of impurities. In the present investigation, however, it appeared that no segregation of these elements occurs in the absence of impurities. This is not in agreement with the theory. However, it may be assumed that the complex interactions between alloying element impurity vacancy alone give rise to cluster stability in the vicinity of the grain boundary. This, then, explains the absence of segregation when alloying elements or impurities alone are present.

When alloying elements are present the characteristics of the near grain boundary regions are changed entirely. The grain boundaries become richer in Ni and Cr as the embrittling treatment progresses. Ni is a  $\gamma$  stabilizer and is completely miscible in  $\gamma$  Fe. Cr, while possessing limited solubility in  $\gamma$  Fe (13 atom percent), acts as a  $\gamma$  stabilizer up to concentrations as high as 7.5 atomic percent. Thus the Ni-Cr rich region, containing C in the solution in the vicinity of the grain boundary, is expected to be a less stable  $\alpha$  phase with respect to  $\gamma$ . At higher temperatures ( $\sim 800$  K) the  $\gamma$  phase may be stable if substantial Cr, Ni, and C segregation has occurred. Such a phase, if present would have reduced solubility for and tend to reject Sb, Sn, and P into the adjacent boundaries. Assuming that initiation problems dominate, the absence of a  $\gamma$  phase film or two phase ( $\alpha + \gamma$ ) region can be imagined. In such an event, it would not be unlikely that this region (Ni-Cr rich  $\alpha$  region<sup>4</sup>) would reject Sb, Sn, and P into the grain boundaries. This explains the rapidly increased segregation of the trace elements due to multiple alloying.

When the extent and the nature of segregation profiles of Ni and Cr are examined, two outstanding features are evident. First, the segregation of Ni and, not so evidently, that of Cr occur over a large range, as suggested by a nonequilibrium segregation model. This would explain the microhardness measurements [5], which indicate segregation occurs in regions far from the boundary. Second, the hump in the Ni concentration observed within the first 10 to 20 atomic monolayers is the kind of Ni profile observed in most temper embrittled specimens examined. The probability of a similar hump exists for Sb but is probably offset by the sharpness of the concentration profile. Such a possibility appears even in the data of Marcus and Palmberg [26] on Sb segregation and on Ni segregation in Viswanathan's [28] experiments. The observation can be interpreted in one of two ways:

1. Assume a segregation of individual atoms, resulting in the observed general profile; or
2. Assume atomic segregation at the boundary layers. However, in the near grain boundary monolayers, atomic segregation is present to a lesser

<sup>4</sup> In  $\alpha$ Fe, addition of Ni is known to reduce the solid solubility of Sb [32].

degree. Some precipitates or, more likely, clusters appear within a narrow range characterized by the hump. Beyond that zone the cluster size diminishes and after a considerable distance the cluster dimensions are so small they may be considered to represent atomic segregation. This segregation extends to a depth of 100 Å or more as depicted by the Ni concentration profile. The distribution of clusters and segregation according to this model is shown in schematic figures. (See Fig. 17a.)

This explanation is supported by the evidence provided by Tarng and Wehner [39] in their experiments on sputter deposition and removal. The Mo deposited on gold forms islands, and when the substrate is sputtered the results obtained are as shown in Fig. 18. (Also, see Appendix.) The apparent increase in solute concentration at a small distance from the grain boundary is thought to be a result of some smearing action during sputtering.

*Combined Model*

The above observations can be explained using a combination of non-equilibrium and equilibrium models of segregation. The nonequilibrium segregation model provides a basis for solute enrichment of the grain boundary produced by vacancy drag [40]. The Sb-X-vacancy complexes move to-

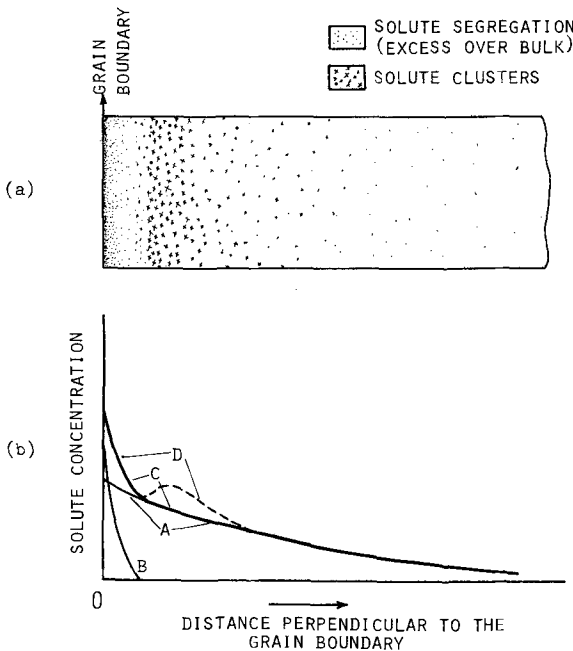


FIG. 17—(a) Schematic showing the distribution of clusters and segregation near the grain boundary. (b) An explanation of the segregation based upon the nonequilibrium equilibrium model: A—from nonequilibrium segregation model; B—Gibbs mechanism; C—combination of A and B (the true solute concentration); D—same as C, but the apparent concentration due to sputtering of clusters.

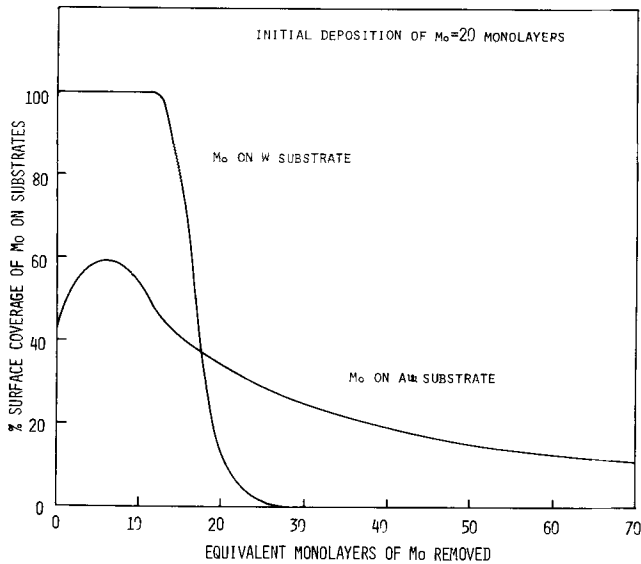


FIG. 18—Sputter deposition and removal studies of Mo on various substrates. (Courtesy of Targ and Wehner [39]).

ward the grain boundary and form stable clusters in the embrittling range of temperatures. Carbon may also be included in the complex if required. The large spatial extent of the solute gradient (Fig. 14) can be explained with this model [41]. Curve *A* in Fig. 17*b* represents the solute concentration (probably present in the form of clusters) according to a simple nonequilibrium segregation model. Segregation at the boundary, which occurs by a simple Gibbsian adsorption, is represented in the schematic curve *B* of Fig. 17*b*.

The influence of each of the models on the other may be examined. The high concentration in the vicinity of the grain boundary provided by a nonequilibrium model will have a pronounced effect (increase) on the strain energy of the lattice. Also, the high concentration, as felt by the boundary, will be equivalent to the increased solute concentration  $X_0$  in Eq 1. These two factors will contribute to increased  $\gamma_b$  and  $X_0$  values in Eq 1 and will result in enhanced segregation to the boundary. This segregation can occur by a continuous depletion of solute atoms from atomic layers only a short distance from the boundary. Since the segregation and associated depletion occur continuously during the embrittling process, no clusters will form in the atomic layers characterized by the depletion distance. In essence, the concentration profile that results is that shown as schematic curve *C* in Fig. 17*b*. Figure 17*a* shows the distribution of clusters. The chemical composition as determined by Auger spectroscopy is given by curve *D*. The hump observed in curve *D* is taken as evidence for clusters. Auger spectroscopy measures an excess of solute concentration due to smearing action which occurs during the sputtering of clusters.

Figure 14 also indicates that the hump in the concentration profile moves closer to the grain boundary with a decrease in the step cooling temperature. This behavior could be predicted by imagining what might happen to the two models of segregation with a decrease in temperature. Figure 19 shows the expected variations in curves *A*, *B*, and *D* with temperature. The segregation due to the nonequilibrium model, curve *A*, increases with temperature. It passes through a peak and becomes small again at high temperatures (550 C) because then the high thermal energy equals the vacancy-solute binding energy. The decrease might also be a consequence of the instability of clusters at high temperatures. The segregation due to Gibbsian adsorption, curve *B*, is expected to steadily decrease with temperature. The combination of the two is plotted as curve *D*. The illustration is made to clarify how segregation and the observed hump might vary with the embrittling temperature. This also explains why the hump is not prominent in fully cooled 31-100 heat steel.

## Embrittlement

### *C Curve Behavior*

The embrittlement behavior (embrittling temperature versus embrittling time) exhibits a C curve behavior with the knee at approximately 525 C [42-44]. This can be explained by a nonequilibrium segregation model [45]. At 625 C (normal tempering temperature) or above, the thermal energy  $kT$  is large compared to the solute-vacancy binding energy. The magnitude of the mobilities of various atomic species dominates the mobility due to vacancy drag. This results in little or no segregation at boundaries. Also, at these temperatures it is presumed that the vacancy population in the matrix is in equilibrium. When the temperature is lowered, there is an excess vacancy concentration in the matrix attempting to attain equilibrium by maintaining an influx towards the grain boundary. With a decrease in temperature, the vacancy-solute interaction energy predominates over the thermal energy, resulting in uphill diffusion towards the grain boundary. This process continues below 500 C, below that temperature range the segregation tends to be controlled by the prevailing (low) mobility of vacancy-solute complexes. Thus, at low temperatures, such as 350 C, large embrittlement is observed after a long period of time. This kind of an explanation is supported by grain boundary hardness measurements made in Pb-Sn alloys [46] as a function of quenching temperature.

### Embrittlement Phenomena

While embrittlement has been shown to be associated with segregation, it is not clear why some segregants embrittle grain boundaries while others do not. A discussion of the problem of intergranular embrittlement appears in a

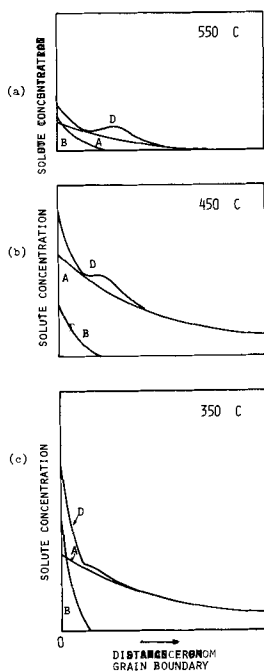


FIG. 19—Schematic showing variation of solute concentration with distance from grain boundary at three different temperatures: A—from nonequilibrium segregation model; B—equilibrium model; D—combination of A and B, the apparent concentration due to sputtering of clusters.

recent article by Low [35]. A general and qualitative approach to the problem can be made using the Griffith equation:

$$\sigma_b = [2E\gamma'/\pi c]^{1/2} \quad (2)$$

where  $\sigma_b$  is the breaking stress,  $E$  is Young's modulus,  $\gamma'$  is the total energy required per unit increase in area of crack, comprising the true surface energy and the plastic work done by the stress concentration at the moving crack tip, and  $c$  is the crack length.

Replacing  $\gamma'$  by the true surface energy, plus the plastic work term  $\gamma_p$ , results in the following expression:

$$\sigma_b = [2E(\gamma + \gamma_p)/\pi c]^{1/2} \quad (3)$$

The plastic work term  $\gamma_p$  is often a large part ( $\sim 10^5$  erg/cm<sup>2</sup>) of  $\gamma'$  as compared to the true surface energy  $\gamma$  ( $\sim 10^3$  erg/cm<sup>2</sup>). Thus  $\gamma$  has only a minor or negligible influence on  $\sigma_b$  or the decohesion that occurs in the case of a normal fracture. In the case of grain boundary decohesion, the segregated solute might be expected to cause solution hardening in the near grain boundary atomic layers, thereby decreasing the plastic deformation required at the

tip of the moving crack. In the case of embrittled steels the solute clusters present in the close vicinity of the boundary (if so assumed), or the concentration gradients, would enhance the resistance to dislocation motion. Thus, in the case of temper embrittlement of low alloy steels, the lowering of  $\sigma_b$  due to lowered  $\gamma_p$  appears to be a plausible embrittling mechanism. In fact, if reduction in  $\gamma$  alone is the cause, several of the known phenomena in steels would be difficult to explain. For example,

1. Sharp ductile to brittle transition with temperature would not be predicted from changes in  $\gamma$  with temperature since no such sudden changes would be expected in  $\gamma$  versus temperature curve; and
2. Strain rate effect is prominent in these steels. Conditions such as high strain rate and triaxial state of stress can easily differentiate between an embrittled and nonembrittled state. Since  $\gamma$  is independent of these while  $\gamma_p$  is sensitive to these variables, it is natural to choose  $\gamma_p$  as the main factor controlling the term  $\sigma_b$ .

Thus  $\gamma_p$ , the plastic strain energy term, might appear to be the controlling factor in causing embrittlement in steels. This conclusion is based upon the assumption that  $\gamma$  and  $\gamma_p$  are two completely independent variables. However, it appears that  $\gamma$  will have a profound influence on  $\gamma_p$ . If  $\gamma$  can be reduced considerably along a chosen internal surface without affecting the solid solution strengthening in the nearby atomic layers, the consequences would be interesting. The energy required to fracture along the surface (to break up the atomic bonds) will be low; the plastic work done will also be correspondingly low. Thus, in the case of a highly surface active impurity the  $\gamma$  term is reduced quickly so that little plastic deformation occurs during the fracture. We are of the opinion that in extreme cases, such as grain boundary embrittlement by penetration of liquid metals, for example, liquid gallium in aluminum and mercury or lead in copper alloys, the  $\gamma$  term and hence the  $\gamma_p$  term are reduced to near 0 and hence the fracture stress approaches 0. The same conclusion can also be deduced from the Griffith equation (Eq 3) by replacing  $\gamma_p$  by  $\alpha\sigma_b^2$  ( $\alpha$  being a constant) to represent the plastic work [47] and rearranging the terms, giving

$$\sigma_b = [2E\gamma/\beta\pi c]^{1/2} \quad (4)$$

where

$$\beta = 1 - (2E\alpha/\pi c)$$

Since the presence of impurities or alloying elements in minor quantities would not appreciably alter the elastic modulus  $E$ , the term  $\gamma$  should be of major importance. For cleavage fracture  $\gamma$  is equal to  $2\gamma_s$ , where  $\gamma_s$  is the energy per unit area of the cleavage surface. For intergranular fracture,

$$\gamma = (2\gamma_s - \gamma_b) \quad (5)$$

where  $\gamma_b$  is the grain boundary energy per unit area since the energy of the

two new surfaces is partly reduced by the energy of the grain boundary along which fracture is taking place. When an impurity segregates to the boundary, due to Gibb's adsorption, it reduces  $\gamma_b$ , thus contributing to an increase in  $\gamma$  and hence to  $\sigma_b$ . Since most grain boundary active impurities are surface active they also decrease  $\gamma_s$ . The degree of this influence determines the embrittling influence of an impurity.

Extremely large reductions in  $(2\gamma_s - \gamma_b)$  are possible. For Cu,  $\gamma$  is about 3000 erg/cm<sup>2</sup> [47]. The grain boundary activity of Bi in Cu is about 4000 erg/cm<sup>2</sup> [35,48] while the surface activity is about 120,000 erg/cm<sup>2</sup>. Therefore, it would be expected that Bi would be an effective embrittler of Cu. Experiments on the Cu-Bi system [49] indicate that the estimates of the decrease in strength by the surface energy criterion (Eq 4) are reasonably close to the experimental values. This suggests that the model has some validity.

### *Discussion of Other Results*

*Influence of Cr and C.* It is of interest to note the role of C on temper embrittlement. C is known [5] to cause a large increase in  $\Delta TT$  upon embrittling and it was suggested that this may be at least partly due to its presence in the grain boundaries in the form of carbides. The tenacity of the ferrite-cementite interface is low when segregation of Sb occurs [2,10]. In the present experiments it was observed that there is an increased C concentration in the grain boundaries after an embrittling treatment in some steels. This is a result of C segregation in the form of atoms or carbides or both. In steels containing Cr two results are noticeable: 1. C content on the fresh fracture surface is observed to be less in steel containing Cr than in steel without Cr (both steels in the embrittled state); and 2. Cr also segregates to the grain boundaries.

These results can be put together to explain the increased embrittlement. Cr forms carbides at the grain boundaries at the expense of some segregated C and cementite. Reduction in atomic C from the grain boundaries may have deleterious consequences in Fe and steels containing impurities such as Sb and P. This position is supported by experiments made on Fe-P alloys [50]. Fe containing P is highly susceptible to intergranular embrittlement, but only in the absence of C. Similar behavior is expected to be followed in case of Fe containing Sb. The combination of the two effects (reduction in segregated C and added Cr segregation) can cause the observed enhancement of embrittlement due to Cr.

Examination may be made of what happens when a stronger carbide forming element such as Mo is present in the steel. The tendency would be to form a smaller volume of carbides at the expense of segregated C and cementite. However, this can happen only if Mo also segregates to the boundary where enough C is available to form such precipitates. In the examination of some embrittled steels containing Mo [51], no evidence of Mo segregation to grain boundaries was noticed. Hence it is possible that, while carbides containing

Mo are present within the matrix of the grain, segregation of C in the grain boundary continues to occur thus causing no increase in  $\Delta T_T$  due to Mo. The decreased volume of total carbide in the boundary (due to smaller volume of Mo-carbide instead of other carbides) may be giving rise to the actually reported improvement in properties.

*Prior austenite boundaries.* Temper embrittlement is characterized by fracture along prior austenite grain boundaries. McMahon [2] has proposed that some of the embrittling elements segregate to austenite boundaries during austenitization and are retained there upon quenching. This is expected since the impurity elements such as Sn, Sb, and P have lower solid solubility in  $\gamma$ Fe than in  $\alpha$ Fe. When the steel is tempered at 600 C the embrittlers are progressively dispersed away from these boundaries. Since they are always in the general vicinity, the prior austenite boundaries receive large doses of these impurities during the embrittling treatment, and thus become preferred paths for fracture. Longer embrittling times would cause considerable segregation even to the subboundaries. This is in agreement with the findings of Katsumata et al [52] who observed a finer network of etching grooves upon increasing the embrittling time.

Intergranular fractures could occur in steels containing embrittling impurities and after being rapidly quenched from the  $\gamma$  region. This result gives partial support to McMahon's hypothesis. A 31-100 heat steel so treated was fractured and analyzed under vacuum using Auger spectroscopy. The preliminary results obtained did not indicate any segregation of Ni, Cr, or Sb to the grain boundaries. However, it is suspected that Sb is segregated to boundaries in amounts smaller than those detectable by Auger spectroscopy (0.6 atom percent) and this is probably enough to cause embrittlement in  $\alpha$  Fe. Further experiments are planned to evaluate this model in detail.

## Conclusions

1. The alloying elements Ni and Cr and the impurities Sb, Sn, and P segregate to grain boundaries during step cooling in a low alloy steel. No segregation of As is revealed by Auger spectroscopy.

2. Segregation and embrittlement are closely related. Little or no segregation is observed in all cases where embrittlement is slight.

3. No segregation is revealed in nonembrittled steels. Thus, the model based upon two dimensional phase transformations and the double segregation model are inadequate to explain the temper embrittlement phenomenon.

4. The extent of segregation (distance from grain boundary) determined by sputtering is large for Ni (and possibly for Cr) as compared to that of Sb or Sn.

5. The observed segregation appears to be inconsistent with only an equilibrium (or Gibbsian) model of segregation. The hump in the Ni concentration profile and the overall segregation are explained using a model that employs both equilibrium and nonequilibrium segregation models.

6. Sputtering experiments indicate cluster formation at a distance of a few angstroms from the grain boundary. This effect and the solution hardening resulting from segregation induce embrittlement in the near grain boundary atomic layers. This appears to be the major influence on embrittlement in low alloy steels. The plastic strain energy criterion and its dependence upon the true surface energy are related for a general case of grain boundary embrittlement.

### *Acknowledgments*

We are grateful for the many helpful suggestions made by G. K. Wehner, Dept. of Electrical Engineering, University of Minnesota. This work was performed in the Physical Electronic Laboratories of the University of Minnesota and was sponsored by the Atomic Energy Commission under Contract AT(11-1)-1778. An equipment grant from the Graduate School of the University of Minnesota is gratefully acknowledged.

## APPENDIX

### **Ion Sputtering**

In understanding the segregation at surfaces and interfaces, the ion sputtering technique is widely used in conjunction with Auger spectroscopy for elemental chemical analysis. Although the technique has been used for some time as a process for removing or depositing metal atoms, little is understood about it. This is true particularly with respect to sputter removal of atoms from alloys. The constituent elements of the alloy may have different yield rates in their pure states, in which case selective sputter removal may occur resulting in the enrichment of one of the constituents on the alloy surface. When estimating the surface segregation as a function of distance from the surface, a knowledge of the alloy sputtering characteristics will be helpful. Such data are rarely available and hence several assumptions have to be made. These are

1. Sputtering removes the atoms from the surface without selection;
2. Yield at the surface (of different composition) is the same as that of the base metal (iron in case of steels); and
3. Yield behavior is not altered with the progression of sputtering.

Sputtering experiments on steels that suffer transgranular fractures give some conclusive results on sputtering Ni in Fe. The Ni concentration as indicated by Auger peak height in the fracture surface did not alter with the progression of sputtering. This indicates that no selective sputtering occurs between Fe and Ni in these steels. This result is important in the interpretation of results obtained from Ni concentration profiles. The Auger peak height of Ni exhibited a dip and a hump (Fig. 14) as atoms were removed layer by layer from the fracture surface of embrittled steels. This profile is apparently related to the actual concentration profile of Ni. The recent experiments of Tarny and Wehner [39] shed light on this from a different direction. They deposited an estimated 20 atomic monolayers of Mo on several substrates. Mo deposited on Au was probably in the form of islands while Mo on W formed a nearly uniform layer. The substrates were used as targets for a

sputter removal study. The Mo concentration, as estimated from Auger peak heights, varied as the sputtering progressed (see Fig. 18). Mo on a W substrate disappeared within 25 monoatomic layers as expected, whereas on a Au substrate it indicated a hump in the concentration profile at approximately 5 atomic monolayers. This is thought to be a result of sputtering of the Mo present in the form of islands, with subsequent redistribution on the Au surface.

In the case of steels, a hump in Ni profile may be expected if some of it is present in the form of clusters just beneath the exposed fracture surface. Such a situation was discussed earlier with reference to Fig. 17.

Careful interpretation of the sputtering concentration profiles is required, even if all the above-mentioned assumptions are justified. This need arises from the likelihood that the sputter-removal process does not occur layer by layer. Palmberg and Marcus [27] approached the problem on a statistical basis and concluded that the apparent P and Sb profiles [26, 27] in embrittled steels correspond to their actual presence in 1 or 2 atomic layers near the fracture surface. The assumptions made in their analysis are 1) all sputtered atoms originate from the surface layer and 2) all atoms are removed with equal probability. Thus, the sputtering variables or material and physical variables are not involved in the analysis. To check this analysis experimentally, they deposited an estimated 0.5 monolayer of Ag on the fracture surface of an Fe-P alloy. However, they assumed all the deposited Ag to be in the first atomic layer of the fracture surface, which need not be the case. The sputtering results indicated that the Ag Auger attenuation rate is only slightly more rapid than that of a P peak. Since it is not known if the Ag is actually present in the first monolayer or in more than one, not much can be said about the actual distribution of P or Sb near the grain boundary fracture surface. Experiments [39] on the sputter deposition and removal of Mo on a W substrate (Fig. 18) indicate that, if a statistical model holds good for deposition, the concentration profile obtained from Auger peak heights probably represent the true distribution near the surface.

Thus, in view of the lack of sufficient information concerning the sputter removal characteristics, the sputtering profiles obtained have been used as true representations of the actual concentration levels. Any error involved in this will be passed on to the calculations on Sb segregation. The overall conclusions will not be affected, however, in spite of any error, since the Sb segregation is only a minor fraction of the overall segregation observed in the study.

## References

- [1] Capus, J. M. in *Temper Embrittlement in Steel, ASTM STP 407*, American Society for Testing and Materials, Aug. 1968, pp. 3-19.
- [2] McMahan, C. J., Jr., in *Temper Embrittlement in Steel, ASTM STP 407*, American Society for Testing and Materials, Aug. 1968, pp. 127-167.
- [3] Steven, W. and Balajiva, K., *Journal of the Iron and Steel Institute, JISIA*, Vol. 193, 1959, pp. 141-147.
- [4] Balajiva, K., Cook, R. M., and Worn, D. K., *Nature, NATUA*, Vol. 178, 1956, p. 433.
- [5] Low, J. R., Jr., Stein, D. F., Turkalo, A. M., and Laforce, R. P., *Transactions of the Metallurgical Society of AIME, MTGTB*, Vol. 242, 1968, pp. 14-24.
- [6] Powers, A. E., *Transactions, American Society for Metals, TASEA*, Vol. 48, 1956, p. 149.
- [7] Mikus, E. B. and Siebert, C. A., *Transactions, American Society for Metals, TASEA*, Vol. 50, 1958, p. 682.
- [8] Stein, D. F., *Transactions of the Metallurgical Society of AIME, MTGTB*, Vol. 239, 1967, pp. 1721-1726.
- [9] Powers, A. E., *Journal of the Iron and Steel Institute, JISIA*, Vol. 186, 1957, pp. 323-328.
- [10] Restiano, P. A. and McMahan, C. J., Jr., *Transactions, American Society for Metals, TASEA*, Vol. 60, 1967, p. 699.

- [11] Plateau, J., Henry, G., and Crussard, C. in *Precipitation Processes in Steels*, Special Report No. 64, Iron and Steel Institute, 1959, p. 157.
- [12] Arkharov, V. I. et al, *Fizika Metallov i Metallovedenie*, FMMTA, Vol. 2, 1956, p. 57.
- [13] Inman, M. C. and Tipler, H. R., *Acta Metallurgica*, AMETA, Vol. 6, 1958, p. 73.
- [14] Harris, L. A., *Journal of Applied Physics*, JAPIA, Vol. 39, 1968, pp. 1419-27.
- [15] Harris, L. A., *Journal of Applied Physics*, JAPIA, Vol. 39, 1968, pp. 1428-31.
- [16] Weber, R. E. and Peria, W. T., *Journal of Applied Physics*, JAPIA, Vol. 38, 1967, pp. 4355-58.
- [17] Weber, R. E. and Johnson, A. L., *Journal of Applied Physics*, JAPIA, Vol. 40, 1969, pp. 314-318.
- [18] Palmberg, P. W. and Rhodin, T. N., *Journal of Applied Physics*, JAPIA, Vol. 39, 1968, pp. 2425-32.
- [19] Oswald, R. C. "Auger Spectroscopy for the Chemical Analysis of Surfaces", M.S. thesis, University of Minnesota, 1969; also, Oswald, R. C. and Weber, R. E., Technical Report AFAL-TR-70-12 Electrical Engineering Dept., University of Minnesota, 1970.
- [20] Hill, R. G. C. and Martin, J. W., *Metal Treatment and Drop Forging*, METMA, 1962, pp. 922-927.
- [21] Palmberg, P. W., *Journal of Applied Physics*, JAPIA, Vol. 38, 1967, pp. 2137-48.
- [22] Palmberg, P. W., *Applied Physics Letters*, APPLA, Vol. 13, 1968, pp. 183-185.
- [23] Wehner, G. K., "Sputtering Yield Data in the 100-600 ev Energy Range," General Mills Report 2309, 15 July 1962.
- [24] Haas, T. W., Grant, J. T., and Dooley, G. J., *Physical Review B 1*, PLRBA, 1970, pp. 1449-59.
- [25] Stein, D. F., Joshi, A., and Laforce, R. P., *Transactions*, American Society for Metals, TASEA, Vol. 62, 1969, pp. 776-783.
- [26] Marcus, H. L. and Palmberg, P. W., *Transactions of the Metallurgical Society of AIME*, MTGTB, Vol. 245, 1966, pp. 1664-66.
- [27] Palmberg, P. W. and Marcus, H. L., *Transactions*, American Society for Metals, TASEA, Vol. 62, 1969, p. 1016.
- [28] Viswanathan, R., *Metallurgical Transactions*, MTGTB, Vol. 2, 1971, pp. 809-815.
- [29] R. Viswanathan and T. P. Sherlock, private communication, Westinghouse Research Laboratory, Pittsburgh, Pa.
- [30] Hart, E. W., *Scripta Metallurgica*, SCRMB, Vol. 2, 1968, pp. 179-182.
- [31] Cahn, J. W. and Hilliard, J. E., *Acta Metallurgica*, AMETA, Vol. 7, 1958, pp. 219-221.
- [32] Schulz, B. J. and McMahon, C. J., Jr., in *Temper Embrittlement of Alloy Steels*, ASTM STP 499, American Society for Testing and Materials, 1972, pp. 104-135.
- [33] VanVlack, J. H., *Transactions of the Metallurgical Society of AIME*, MTGTB, Vol. 191, 1951, pp. 251-95.
- [34] "Handbook of Binary Metallic Systems, Structure and Properties" Vol. I, translated from Russian, Israel Program for Scientific Translations Ltd., Jerusalem, 1967. The values are lower limits deduced from the available data.
- [35] Low, J. R., Jr., *Transactions of the Metallurgical Society of AIME*, MTGTB, Vol. 245, 1969, pp. 2481-94.
- [36] Hondros, E. D., *Journal*, Australian Institute of Metals, JAMTA, 1970, pp. 77-100.
- [37] Aust, K. T., Hanneman, R. E., Niessen, P., and Westbrook, J. H., *Acta Metallurgica*, AMETA, Vol. 16, 1968, pp. 291.
- [38] Hultgren, R., Orr, R. L., Anderson, P. D., and Kelly, K. K., *Selected Values of Thermodynamic Properties of Metals and Alloys*, Wiley, New York-London, 1963.
- [39] Tarng, M. L. and Wehner, G. K., to be submitted to *Journal of Applied Physics*.
- [40] Howard, R. E. and Lidiard, A. B., *Philosophical Magazine*, PHMAA, Vol. 11, 1965, pp. 1179-87.
- [41] Anthony, T. R., *Acta Metallurgica*, AMETA, Vol. 17, 1969, pp. 603-609.
- [42] Hollomon, J. H., *Transactions*, American Society for Metals, AMETA, Vol. 36, 1946, pp. 473-540.
- [43] Greaves, R. H. and Jones, J. A., *Journal of Iron and Steel Institute*, JISIA, Vol. 102, 1920, p. 171.
- [44] Jaffe, L. D. and Buffman, D. C., *Transactions*, American Society for Metals, AMETA, Vol. 42, 1950, pp. 604-618.

- [45] Westbrook, J. H., "Solute Segregation at Interfaces," Report No. 69-C-374, G. E. Research and Development Center, Schenectady, N.Y.
- [46] Aust, K. T., "Some Mechanical Effects of Grain Boundaries," presented at the 14th Sagamore Materials Research Conference, Aug. 1967; also, Aust, K. T. in *Surfaces and Interfaces*, Vol. II, Syracuse University Press, Syracuse, N.Y., pp. 235-276.
- [47] McLean, D., *Mechanical Properties of Metals*, Wiley, New York-London, 1962, p. 259.
- [48] Hondros, E. D. and McLean, D., Monograph No. 28, Society of the Chemical Industry, London, 1968, p. 39.
- [49] Joshi, A. and Stein, D. F., "An Auger Spectroscopic Analysis of Bismuth Segregated to Grain Boundaries in Copper," *Journal*, Institute of Metals, JIMEA, London, Vol. 99, 1971, pp. 178-181.
- [50] Ramasubramanian, P. V. and Stein, D. F., Dept. of Mechanical Engineering, University of Minnesota, Minneapolis, Minn., work to be published.
- [51] Coldren, A. P., Joshi, A., and Stein, D. F., "Auger Analysis of Boron Adsorption at Grain Boundaries in 0.5Mo-B Steels," presented at the AIME Fall meeting, Oct. 1971, Detroit, Mich.
- [52] M. Katsumata, S. Kinoshita, and A. Suzuki, private communication, Central Research Laboratory, Kobe Steel Ltd., Kobe, Japan.

## Effect of Solute Elements on Temper Embrittlement of Low Alloy Steels

---

**REFERENCE:** Marcus, H. L., Hackett, L. H., Jr., and Palmberg, P. W., "Effect of Solute Elements on Temper Embrittlement of Low Alloy Steels," *Temper Embrittlement of Alloy Steels*, ASTM STP 499, American Society for Testing and Materials, 1972, pp. 90-103.

**ABSTRACT:** Extensive studies on alloy steels have correlated temper embrittlement with the presence of electronegative elements such as Sb, P, Sn, and As. This paper studies the relationship of impurity grain boundary segregation to several of the steps involved in the embrittling process through Auger electron spectroscopic analysis of the fracture surfaces of several steels that are distinguished by a ductile-brittle transition.

**KEY WORDS:** spectroscopy, Auger electrons, electron microscopy, embrittlement, separation, fracturing, sputtering, austenitizing, isothermal treatment, grain boundaries, alloy steels, antimony, phosphorus, tin, molybdenum

This study concerns the following elements in the temper embrittlement of alloy steels: (1) the influence of an austenitic heat treatment, (2) the presence of trace alloying elements, (3) the role of secondary alloying elements such as Mo, and (4) the diffusional nature of the embrittling process. The paper relates impurity grain boundary segregation to several of the steps involved in the embrittling process through Auger electron spectroscopic [1-5] analysis of the fracture surfaces of several steels that are distinguished by a ductile-brittle transition.

Extensive studies on alloy steels have correlated temper embrittlement [6-10] with the presence of electronegative elements such as Sb, P, Sn, and As. Aging of these alloys between 400 and 600 C for varying periods of time has been found to raise the ductile to brittle transition temperature. Auger electron spectroscopy (AES) was used by Marcus and Palmberg [11,12] and Stein et al [13] to chemically analyze the fracture surfaces of several low alloy steels containing trace alloying elements. Their studies indicated extensive

<sup>1</sup> Group leader, Fracture and Metal Physics Group, North American Rockwell Science Center, Thousand Oaks, Calif. 91360.

<sup>2</sup> Research associate, North American Rockwell Science Center, Thousand Oaks, Calif. 91360.

<sup>3</sup> Formerly, North American Rockwell Science Center, Thousand Oaks, Calif.; now, research director, Physical Electronics Industries, Inc., Edina, Minn.

segregation, up to three orders of magnitude higher than bulk concentration, of Sb and P. Sputtering experiments [11,12], using a controlled argon ion beam for nearly uniform removal of material, showed that the segregation was highly localized at the grain boundary to a depth on the order of 5 to 10 Å. Similar results have been found for other steels by Stein et al [14] and Viswanathan [15].

### Experimental Procedures

Compositions of the low alloy steels used for the studies are tabulated in Table 1; their mechanical behavior is discussed in this volume by Schulz and McMahon [10]. All of the specimens were given the step cooling treatment described by Low et al [16] in hot salt baths. In addition, the Mo-bearing steel was isothermally aged for 3000 h at 480 C. The 0.140 by 0.100 by 1.000 in.-long specimens were prenotched to localize fracture. They were then inserted into an ultrahigh vacuum ( $10^{-9}$  torr) Auger spectrometer (Fig. 1), and the system was baked at 200 C for 8 h. They were cooled in vacuum to  $-100$  C by flowing liquid nitrogen through the specimen holder and fractured.

TABLE 1—Composition of low alloy steels.

Iron Alloys, weight percent						
C	Ni	Cr	P	Sb	Sn	Mo
0.4	3.5	1.7		0.065		
0.4	3.5			0.065		
0.4		1.7		0.065		
0.3	3.5	1.7	0.06	0.065		
0.4	3.5		0.06			
0.4		1.7	0.06			
0.4	3.5	1.7			0.05	
0.4	3.5				0.05	
0.4		1.7			0.05	
<i>AISI 3340 × Sb</i>						
0.4	3.5	1.7		0.06		
<i>AISI 3340 × Sb × Mo</i>						
0.4	3.5	1.7	0.003	0.066		0.61

The resulting fracture surface was then chemically analyzed using the cylindrical mirror AES analyzer [17]. After the fresh fracture surface had been analyzed, the chamber was backfilled with argon to about  $5 \times 10^{-5}$  torr. Chemical profiles were obtained by sequentially sputtering the surface with 400-eV argon atoms, removing the argon, and performing Auger analysis. The fractured specimens were then removed from the Auger spectrometer and the surface was examined by scanning electron microscopy (SEM). The light sputtering used for obtaining chemical profiles of the fracture surfaces produced no observable effects on the fracture surface topography.

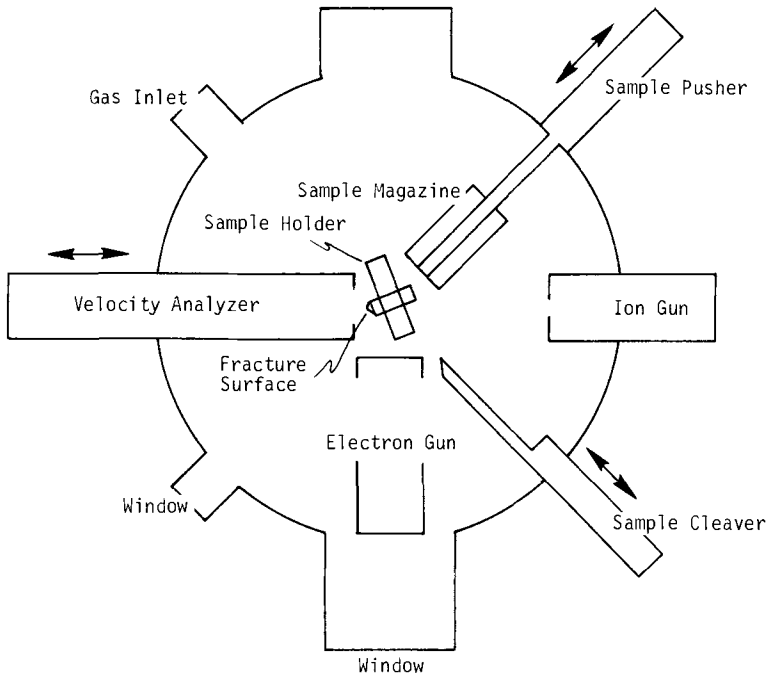


FIG. 1—Schematic of Auger spectrometer in  $10^{-10}$  torr all-metal vacuum system.

In addition to the fracture work in the AES, a limited number of specimens were fractured in the high vacuum ( $10^{-8}$  torr) SEM and the spatial homogeneity of their fracture surface was examined.

### Results and Discussion

AES analyzes the chemistry of the first few atomic layers of a material; thus, when intergranular fracture occurs, it can define the chemistry of the grain boundary *in situ*. Auger spectra are plots of the derivative of the secondary electron distribution,  $N(E)$ , as a function of the energy of the secondary electrons, that is,  $dN(E)/dE$  versus  $E$ . Because the beam was approximately 0.020 in. in diameter, the chemical analysis represents an average over several grains. The Auger spectra obtained in this study reveal clear differences in the fracture surface chemistry of alloys containing Ni, Cr, and both Ni and Cr. P, Sn, or Sb was present in each. The addition of Mo to a Sb-containing AISI 3340 steel dramatically influences the thermal treatment required for temper embrittlement. The topography of the fracture surfaces, evaluated at both low and high magnification in the SEM, correlates with impurity grain boundary segregation.

### *Effects of Ni and Cr*

Figure 2 shows the results for alloys containing 600 ppm P. All specimens were step cooled. The top Auger spectrum and corresponding SEM fractograph were obtained from a steel containing Cr, the middle spectrum from a steel containing Ni, and the bottom spectrum from a steel containing Cr and Ni. The element's peak-to-peak height relative to the Fe peak-to-peak height gives a measure of the amount of that element present at the surface. Although intergranular failure along prior austenite grain boundaries is evident in each case, about 50 percent less P is present in the steel containing Ni alone and 20 percent less in that containing Cr alone than when both Ni and Cr are in the alloy. The Ni concentration is also higher on the fracture surface than in the bulk.

Figures 3 and 4 show similar results for alloys containing Sn and Sb, respectively. In these two cases, the combination of Cr and Ni is clearly more effective than Ni alone in influencing segregation of Sn or Sb at the grain boundary. The grain boundary concentration of Sn or Sb is approximately 100 to 500 times the bulk concentration. The small S peak is also associated with segregation. Its presence at grain boundaries does not seem to be necessary for embrittlement, as reported previously [11,12].

The fracture has a mixed transgranular and intergranular mode only when Cr or Ni is present, for which SEM micrographs show that differences in prior austenite grain size are not responsible. In a mixed mode failure, the area of transgranular failure must be accounted for when determining grain boundary concentrations. The combined effect of Cr and Ni in inducing embrittlement is not immediately apparent and the lack of detectable segregation of Cr while the Ni is segregated is also not easily explained. However, it seems probable that these elements influence the cleavage strength of the parent matrix, with the combined alloying effect shifting the transgranular cleavage strength to a higher value than that for intergranular failure.

Another interesting result is evident from higher magnification SEM fractographs (Fig. 5), which reveal a large amount of deformation of the alloy, particularly when Sn or Sb are present. P seems to be the most effective embrittling element, even when Ni or Cr are present individually. This can be explained in part by the larger atomic percent to weight percent ratio for P than for Sb or Sn.

The apparent unevenness of the fracture surface and the local extent of the segregation, appear contradictory, since, even on a very rough fracture surface, impurities are concentrated within a few atomic layers of the surface. A probable explanation for this is that deformation takes place locally near the grain boundary as the crack propagates, but that actual fracture takes place in the region of enhanced solute element concentration. This could occur whenever the cracks which precede the main crack front coalesce. This variation of deformation can account for the variation of impact energy from alloy to alloy, even when they are in the embrittled condition.

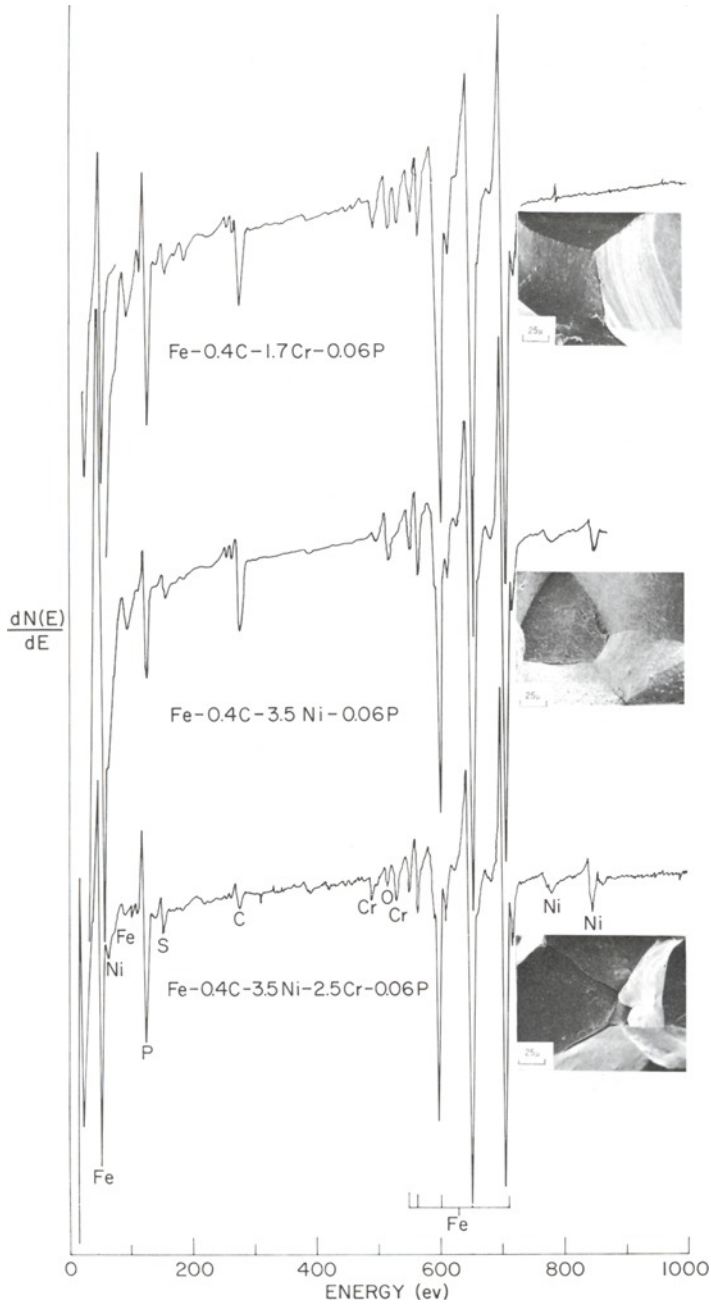


FIG. 2—Auger spectrum and scanning electron micrographs of fracture surfaces of P-bearing low alloy steels.

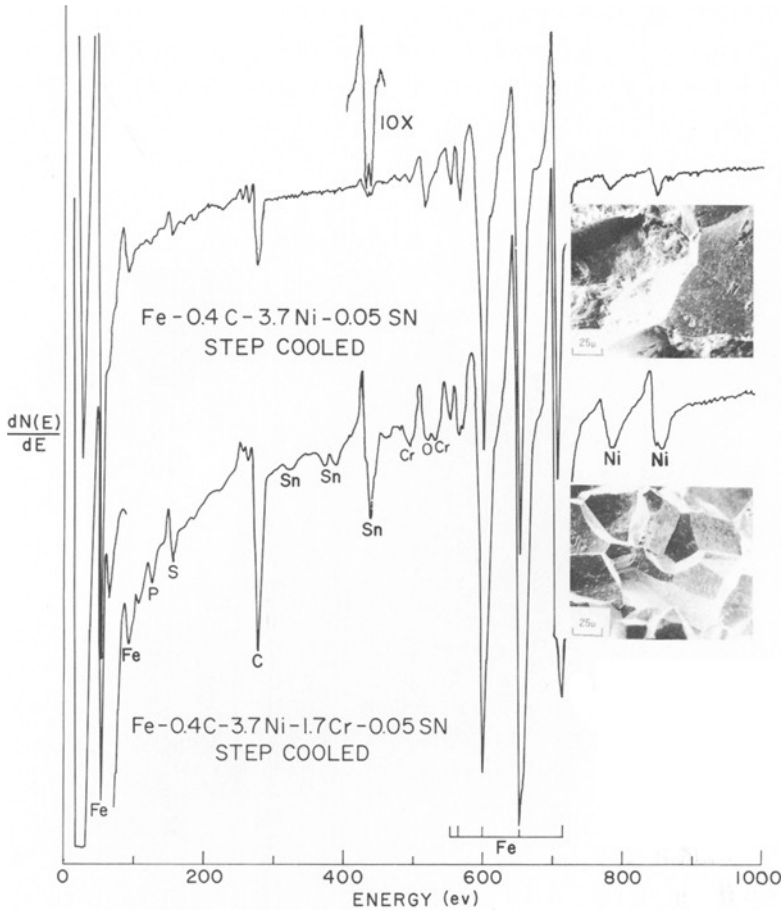


FIG. 3—Auger spectrum and scanning electron micrographs of fracture surfaces of Sn-bearing low alloy steels.

### Effect of Austenitizing

In previous work [11,13] Sb was found present on the fracture surface of AISI 3340 low alloy steel containing 600 ppm Sb. Figure 6 shows the Auger spectrum and SEM micrograph of a fracture surface of this alloy after it had received an oil quench from 960 C subsequent to slow cooling from a 1200 C austenitizing treatment. While intergranular failure is apparent, Sb is not indicated in the Auger spectrum. These results suggest that segregation does not occur during the austenitizing treatment, rather, that the segregating species diffuse to the prior austenite grain boundaries during the step cooling treatment. Thus, the main action of the austenitizing treatment is apparently the effect it has on the prior austenite grain size and its subsequent influence on the ductile-to-brittle transition temperature.

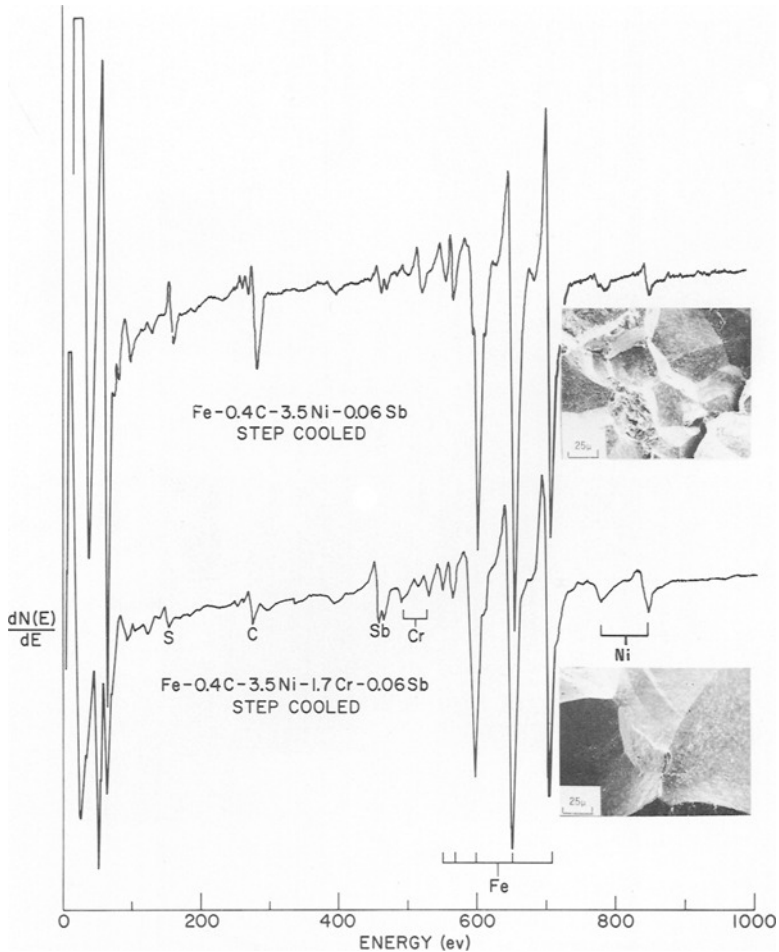
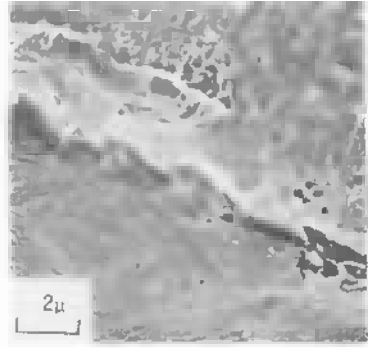
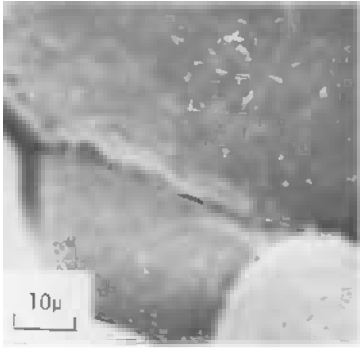


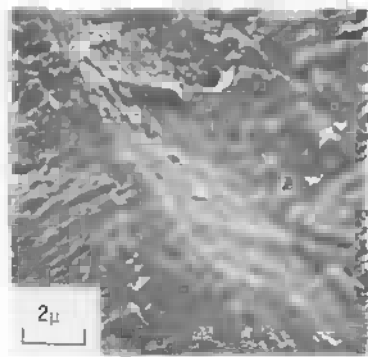
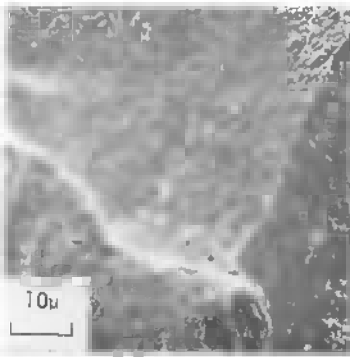
FIG. 4—Auger spectrum and scanning electron micrographs of fracture surfaces of Sb-bearing low alloy steels.

### Effect of Molybdenum

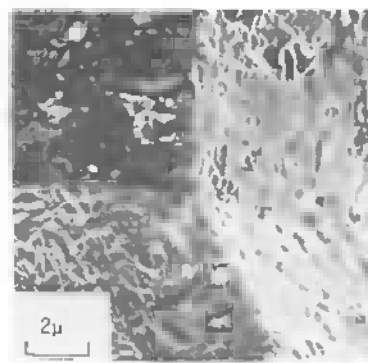
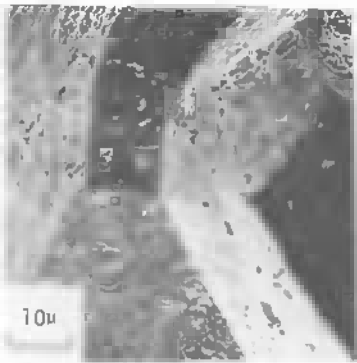
Figure 7 shows Auger spectra and SEM micrographs from fracture surfaces of a modified 3340 steel containing 660 ppm Sb and 0.61 weight percent Mo. When the specimen is fractured in the step cooled condition the failure mode is transgranular, but if it is aged isothermally for 1000, 2000, and 3000 h at 480 C the failure mode becomes mixed. The Auger spectrum clearly shows that the amount of Sb on the fracture surface increases with longer aging times. Part of this increase can be accounted for by an increase in the amount of prior austenite intergranular fracture. This result demonstrates that Mo critically influences grain boundary segregation either through changes in



Fe-0.4C-3.5Ni-2.5Cr - 0.06P



Fe-0.4C-3.5Ni-2.5Cr - 0.06Sb



Fe-0.4C-3.5Ni-2.5Cr - 0.06Sb

FIG. 5—Scanning electron micrographs of fracture surfaces of low alloy steels.

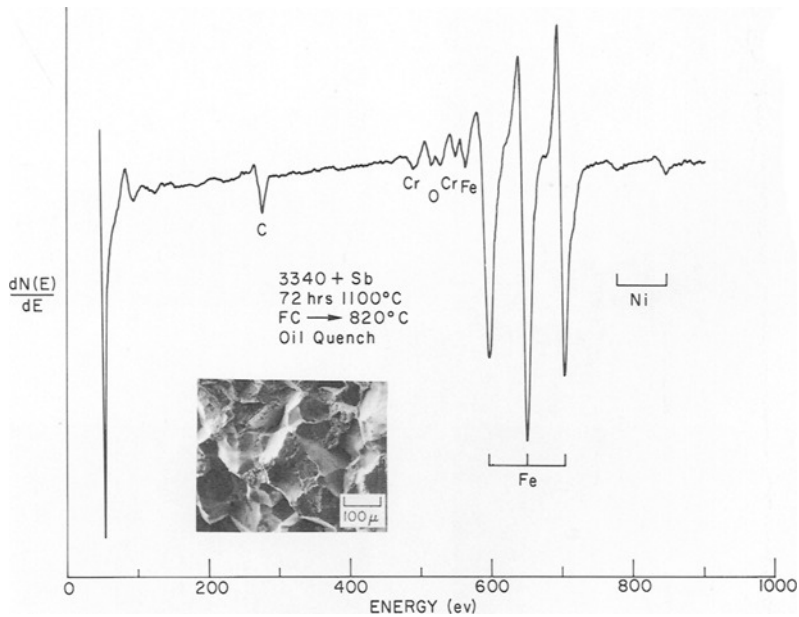


FIG. 6—Auger spectra and scanning electron micrographs of fracture surface of quenched AISI 3340 steel.

kinetics or equilibrium thermodynamics or both. Such segregation is best explained by Fig. 8, which shows how step cooling combines faster kinetics at the higher temperatures with lower kinetics, but higher chemical driving forces, at lower temperatures. If Mo shifts the  $\Gamma$  versus  $T$  curve toward lower temperatures, the first few steps of the step cooling treatment may not contribute significantly to the embrittling process, resulting in no apparent embrittlement. For this reason the accelerated process associated with step cooling is only applicable to certain steels, and the common practice of using it for screening purposes may need to be carefully evaluated.

### Sputtering Experiments

Figure 9 combines limited results from several of the sputtering experiments in this and previous [11,12] studies. All data were analyzed based on the assumption of unity sputtering efficiency [11,12]. The curve represents the profile expected for random sputtering of a uniform layer [12]. The thicknesses measured here are for only one side of the fracture surface. It seems probable that they should be doubled when describing the enriched region.

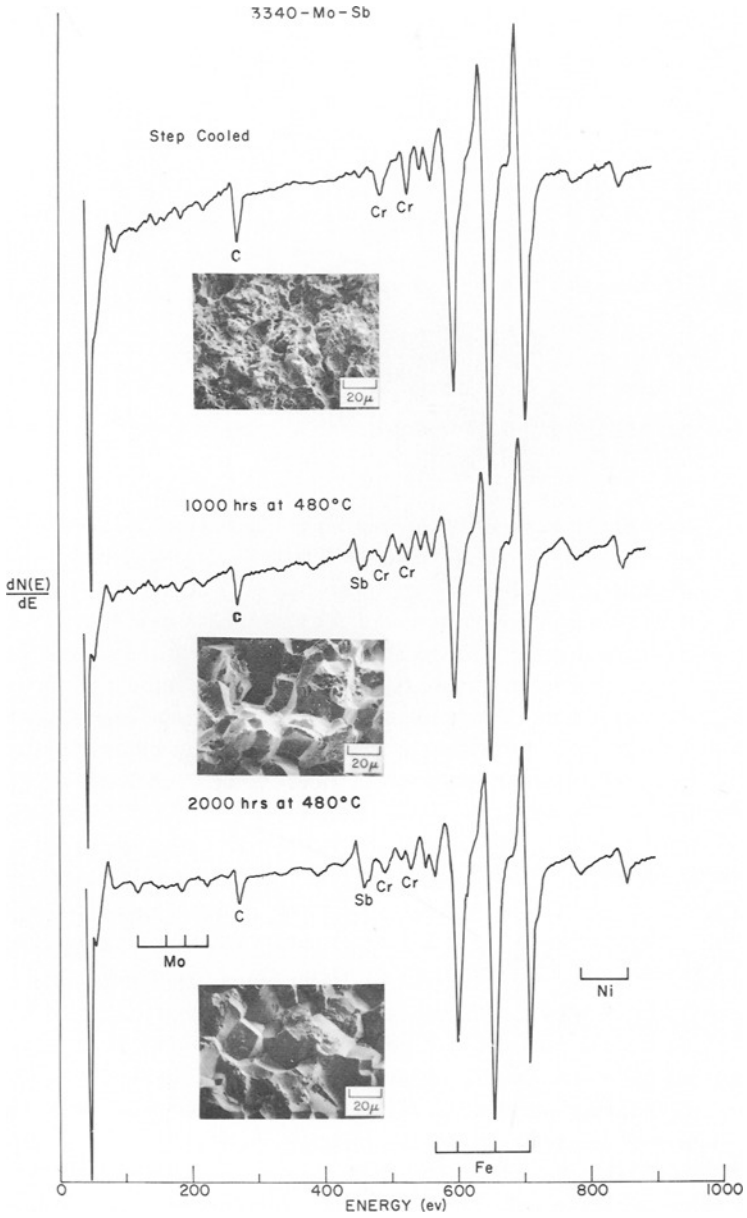


FIG. 7—Auger spectrum and scanning electron micrographs of fracture surfaces of AISI 3340 Mo steel.

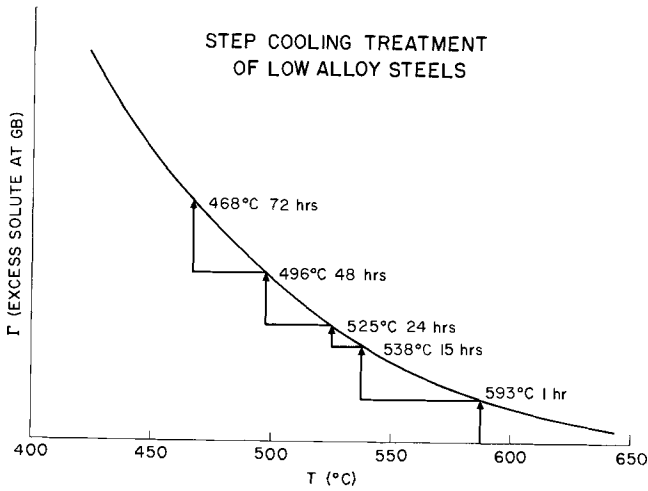


FIG. 8—Schematic of excess grain boundary concentration as a function of temperature showing step cooling heat treatment.

That the extent of segregation of the more electronegative solute remains local is demonstrated for all cases where detailed sputtering was performed. The excess seems to be confined to a region 2 or 3 atomic layers thick. Ni segregation is not highly localized and seems to be concentrated within a region 30 to 50 Å in extent. The problems associated with nonhomogeneous sputtering when excessive amounts of material are removed makes any positive interpretation of long range chemical profiles difficult. The Gibbs adsorption model may apply for the segregated electronegative elements, but the long range of the Ni segregation is more likely associated with kinetic phenomena.

#### *AES in the SEM*

In these experiments, the specimens were fractured in the SEM, and the SEM electron beam was used as the source of excitation for Auger electrons. The energy of the latter electrons was analyzed by a small cylindrical mirror analyzer. Because of excess C and O associated with the O ring sealed  $10^{-8}$  torr vacuum system, the sensitivity was not high but sufficient to investigate two-dimensional homogeneity along the fracture surface. When fracture occurred along prior austenite grain boundaries, no regions where a significantly higher concentration of the segregated species was present could be found on the fracture surface. In contrast, previous results [18,19] had reported large variations in surface chemistry along the fracture surface of a standard high concentration Fe-Sb two-phase binary alloy. The low sensitivity of the AES method prevents determination of whether the fracture path is through the enriched region.

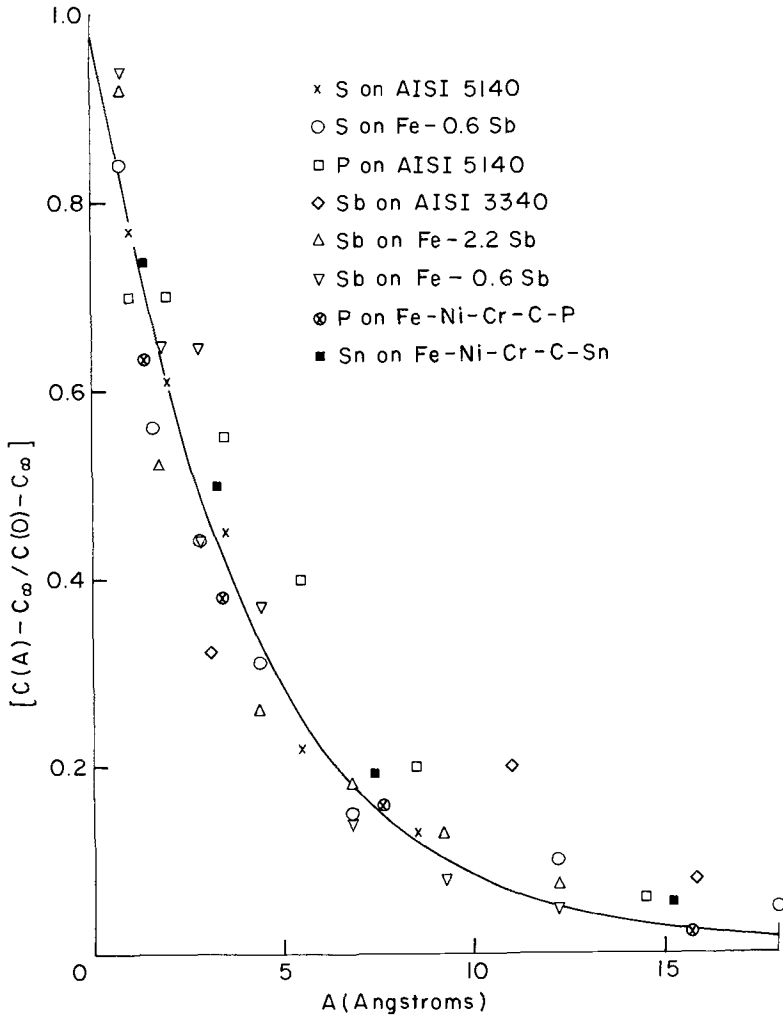


FIG. 9—Normalized concentration of segregated solute on fracture surface versus average amount removed by ion sputtering.

### Summary

1. When fracture takes place along prior austenite grain boundaries in low alloy steels, Sb, Sn, and P are found to be present in significant amounts (100 to 500 times the bulk concentration).

2. The combined presence of Ni and Cr leads to more segregation of Sb, Sn, or P to grain boundaries than when either is present alone.

3. P seems to be a more effective embrittling agent than Sn or Sb showing less plastic deformation during fracture.

4. Addition of Mo to an Sb-bearing AISI 3340 steel changes the kinetics of embrittlement; extended isothermal aging at 480 C leads to embrittlement and associated Sb segregation whereas step cooling does not.

5. The formation of large austenite grains in an AISI 3340 steel by a high temperature austenitizing treatment allows the fracture of as-quenched specimens to occur at grain boundaries. Because segregation of Sb was not detected, diffusion to the grain boundaries must take place during the embrittling heat treatment.

6. Sputtering profiles show that segregated P, Sb, and Sn atoms are localized within two or three atomic layers of the grain boundary.

7. AES in SEM shows that the concentration of a segregated species is fairly homogeneous along prior austenite grain boundaries, with no evidence for regions of excess concentration.

### *Acknowledgments*

We wish to acknowledge the work of P. J. Stocker and E. H. Wright of the North American Rockwell Science Center, in helping prepare the specimens. In addition, thanks are due to B. J. Schulz and C. J. McMahon, Jr., for providing the steels. We also wish to thank N. E. Paton, North American Rockwell Science Center, for his critical review of the manuscript.

### **References**

- [1] Harris, L. A., *Journal of Applied Physics*, JAPIA, Vol. 39, 1968, p. 1419.
- [2] Harris, L. A., *Journal of Applied Physics*, JAPIA, Vol. 39, 1968, p. 1428.
- [3] Stein, D. F., Weber, R. E., and Palmberg, P. W., *Journal of Metals*, JOMTA, Vol. 23, 1971, p. 39.
- [4] Dooley, G. J., III, and Haas, T. W., *Journal of Metals*, JOMTA, Vol. 22, 1970, p. 17.
- [5] Chang, Chuan C., *Surface Science*, SUSCA, Vol. 25, 1971, p. 53.
- [6] Low, J. R., Jr., *Transactions of the Metallurgical Society of AIME*, MTGTB, Vol. 245, 1969, p. 2481.
- [7] McMahon, C. J., Jr., in *Temper Embrittlement in Steel*, ASTM STP 407, American Society for Testing and Materials, 1968, p. 127.
- [8] Low, J. R., Jr., *Fracture of Engineering Materials*, American Society for Metals, 1964, p. 127.
- [9] Woodfine, B. C., *Journal of the Iron and Steel Institute*, JISIA, Vol. 173, 1953, p. 229.
- [10] Schulz, B. J. and McMahon, C. J., Jr., in *Temper Embrittlement of Alloy Steels*, ASTM STP 499, American Society for Testing and Materials, 1972, pp. 104-135.
- [11] Marcus, H. L. and Palmberg, P. W., *Transactions of the Metallurgical Society of AIME*, MTGTB, Vol. 245, 1969, p. 776.
- [12] Palmberg, P. W. and Marcus, H. L., *Transactions, American Society for Metals*, TASEA, Vol. 62, 1969, p. 1016.
- [13] Stein, D. F., Joshi, A., and LaForce, R. P., *Transactions, American Society for Metals*, TASEA, Vol. 62, 1969, p. 776.
- [14] Stein, D. F., Joshi, A., and Ramasubramian, P. V., *Proceedings, Second International Conference on the Strength of Metals and Alloys*, American Society for Metals, Vol. 1, 1970, p. 317.
- [15] Viswanathan, R., *Metallurgical Transactions*, American Society for Metals, MTGTB, Vol. 2, 1971, p. 809.

- [16] Low, J. R., Jr., Stein, D. F., Turkalo, A. M., and LaForce, R. P., *Transactions of the Metallurgical Society of AIME*, MTGTB, Vol. 242, 1968, p. 14.
- [17] Palmberg, P. W., Bohn, G. K., and Tracy, J. C., *Applied Physics Letters*, APPLA, Vol. 15, 1969, p. 15.
- [18] MacDonald, N. C., Proceedings of the Third Annual Scanning Electron Microscope Symposium, IIT Research Institute, Chicago, Ill., 1970, p. 481.
- [19] MacDonald, N. C., Marcus, H. L., and Palmberg, P. W., Proceedings of the Third Annual Scanning Electron Microscope Symposium, IIT Research Institute, Chicago, Ill., 1970, p. 25.

## Alloy Effects in Temper Embrittlement

---

**REFERENCE:** Schulz, B. J. and McMahon, C. J., Jr., "Alloy Effects in Temper Embrittlement," *Temper Embrittlement of Alloy Steels, ASTM STP 499*, American Society for Testing and Materials, 1972, pp. 104-135.

**ABSTRACT:** Ductile-to-brittle transition temperatures obtained from notched bar bend tests were used in conjunction with fracture surface analysis by scanning electron microscopy (SEM) to study various aspects of temper embrittlement in a series of 3.5Ni-1.7Cr-0.4C base steels. Addition of Mo was found to eliminate embrittlement due to step cooling for Sb, Sn, As, and Mn, but not for P. Mn as well as Si, Bi, Se, Ge, and Te are shown to be embrittling elements. The phenomenon of intergranular dimpled rupture was common in these steels. Steels exhibit intergranular embrittlement after quenching from austenite, to an extent determined by the quenching rate.

**KEY WORDS:** embrittlement, tempering, aging(metallurgy), cooling, heat treatment, electron microscopy, grain boundaries, fracture surfaces, transition temperature, alloy steels, molybdenum, manganese, antimony, arsenic, tin, phosphorus, silicon, tellurium, germanium, bismuth, selenium

The understanding of the problem of temper embrittlement has been enhanced in recent years by the demonstration that specific impurities (for example, Sb, As, Sn, P) are responsible for the embrittlement [1], the behavior of these impurities depends on the alloy content of the steel [2], and the embrittlement is due to reversible segregation of the impurities to prior austenite grain boundaries [3-5]. One of the major concerns at present is the effect of alloy content on the amount and rate of embrittlement in the various classes of alloy steels. This is important not only for a full understanding of the nature of the interactions but also for the optimization of alloy steel compositions.

This paper is a study of the effects of Mo and Mn in the 3.5 percent Ni, 1.7 percent Cr alloy that forms the basis of rotor steels. It is an extension of the previous work by Low et al [2] on this alloy, which dealt with the embrittling effects of Sb, As, Sn, and P in 0.4 percent C steels containing 3.5 percent Ni and 1.7 percent Cr, either singly or in combination, when the step cooling embrittlement treatment was applied. They showed that substantial

<sup>1</sup> School of Metallurgy and Materials Science and Laboratory for Research on the Structure of Matter, University of Pennsylvania, Philadelphia, Pa. 19104.

<sup>2</sup> Associate professor, School of Metallurgy and Materials Science and Laboratory for Research on the Structure of Matter, University of Pennsylvania, Philadelphia, Pa. 19104.

step cooling embrittlement by Sb, Sn, and As occurred only when Ni and Cr were present together, but Ni was not necessary for P embrittlement.

Although the present study is not yet complete, a definite picture has begun to emerge and is presented here. Results on additional embrittling elements and the interesting effects of quenching rate on as-quenched embrittlement are also included.

### Experimental Procedure

The alloys utilized in this work are based on AISI 3340 steel (3.5 Ni, 1.7 Cr, and 0.4 percent C), to which various impurity elements were added. The steels were vacuum melted at the General Electric Research and Development Center; heat numbers and chemical analyses are shown in Table 1.

TABLE 1—Chemical analysis of alloying elements in AISI 3340 steel.<sup>a</sup>

GE Heat No.	Alloying Addition	Mn %	Sb, ppm	P, ppm	Sn, ppm	As, ppm	Other
3217	Mo + Sb		640	35	25	3	
3947	Mo + Sb		190	50	<20	...	
PV-434	Mo + P		<5	630	<20	...	
PV-433	Mo + Sn		<5	20	580	...	
PV-435	Mo + As		<5	50	<20	600	
3815	Mn	0.69	<5	20	<20	...	
3892	Mo + Mn	0.69	<5	30	<20	...	
3893	Mo + Mn + Sb	0.7	225	30	<20	...	
3896	Mo + Mn + P	0.7	<5	610	<20	...	
3895	Mo + Mn + Sn	0.7	<5	20	605	...	
3897	Mo + Mn + As	0.7	<5	50	<20	600	
3812	Si		<5	30	<20	...	0.2% Si
3737	Bi		<5	40	<20	...	100 Bi ppm
3816	Se		<5	50	<20	...	100 Se
3817	Ge		<5	60	<20	...	100 Ge
3826	Te		<5	60	<20	...	100 Te

<sup>a</sup> Nominal composition of the Mo-bearing AISI 3340 steel is, in weight percent, 3.5 Ni, 1.7 Cr, 0.4 C, 0.6 Mo; a check on heat number 3217 showed 3.56 Ni, 1.66 Cr, 0.356 C, and 0.61 Mo. No check analysis was done for As, Si, Bi, Se, Ge, and Te.

The 2-lb heats were received in the form of hot swaged bars of 0.33 in. in diameter, which were cut into blanks 2 in. long for heat treatment. A typical heat treatment consisted of austenitization at 1250 C for 4 h, followed either by an immediate quench or a furnace cool to 900 C and then a quench, and finally, tempering for several hours at 650 C.<sup>3</sup> The embrittlement treatment involved heating at various temperatures in the range of 450 to 550 C, for up to 1000 h, as well as step cooling.

<sup>3</sup> In keeping with previous practice, quenched and tempered conditions will be referred to as the "unembrittled condition," even though they are not devoid of all intergranular embrittlement in many cases.

The specimen was a 2-in. long bar with a diameter of 0.25 in. and a 0.043-in. deep notch with a 60 degree included angle and a 0.005-in. root radius. Four tests were performed on each specimen, either at different temperatures or after several consecutive heat treatments. The specimens were tested with a slow bending device, employing the principle developed by R. P. Laforce [6]. This device is shown in Fig. 1.

The specimen holder was immersed in a constant temperature bath which was in turn mounted on the compression load cell of an Instron testing machine. The load versus displacement curve was recorded and the area under this curve, proportional to the fracture energy absorbed by the specimen, was plotted versus the testing temperature. In this way the ductile-to-brittle transition temperature could be determined. The fracture surface was viewed in a scanning electron microscope (SEM) at several magnifications. The amount of embrittlement was characterized by the shift in transition temperature and the mode of brittle fracture.

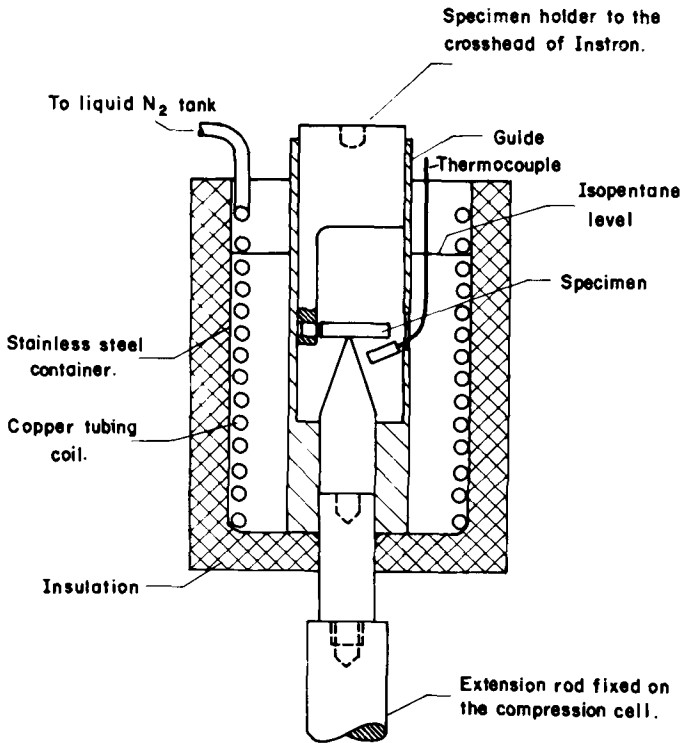


FIG. 1—Apparatus for notched bar bend tests over temperature range  $-196$  to  $250$  C.

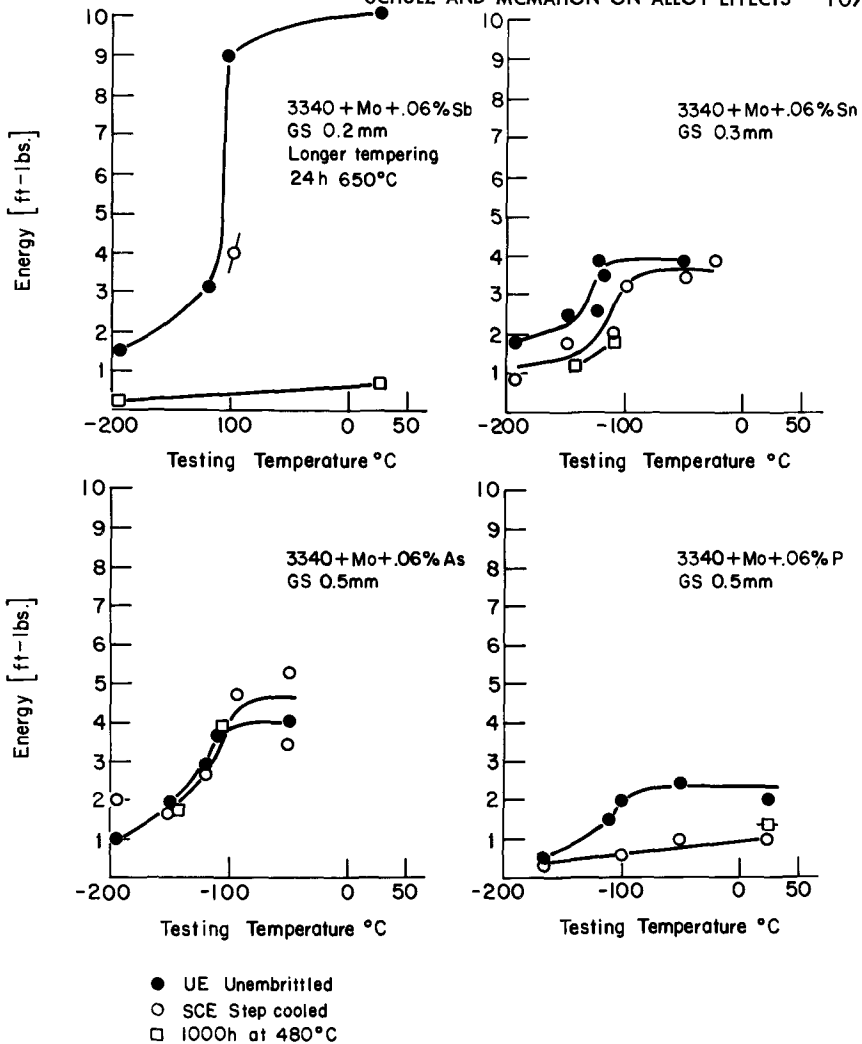


FIG. 2—Transition temperature curves obtained from bend tests for unembrittled and embrittled conditions.

**Results**

*Molybdenum in AISI 3340 Steel*

The curves of energy absorbed versus test temperature for the round notched bar cantilever bend tests on Sb, P, Sn, and As are given in Fig. 2 in the following conditions: unembrittled (UE), step cool embrittled (SCE), and isothermally embrittled 1000 h at 480 C.<sup>4</sup>

<sup>4</sup> The transition temperatures for a high purity AISI 3340 steel, containing 45 ppm P from the electrolytic Fe used in the charge, were shown by Low et al [2] to be -130 C in the quenched and tempered conditions and -103 C after step cooling.

*Antimony.* In the 3340 steel containing 0.6 percent Mo and 600 ppm Sb, the Mo addition had virtually eliminated the embrittlement due to step cooling (Fig. 2). In a similar heat, free of Mo, Low et al [2] found a transition temperature shift of  $>695$  C, while in the present case the shift was 15 C. However, isothermal aging at 480 C for 1000 h was shown to result in appreciable embrittlement ( $>130$  C).

The SEM fractographs in Fig. 3 show modes of fracture in the notched bars in the 3 conditions of heat treatment at both cryogenic and ambient temperatures. The 6 fractographs (b, c, f, g, j, k) show almost the entire fracture surface, while the other 6 (a, d, e, h, i, l), show details, usually of grain boundary fractures at higher magnification. In the unembrittled condition the fracture is transgranular cleavage at  $-196$  C and dimpled rupture at 25 C. In the latter case there is a tendency for the ductile fracture to occur roughly along prior austenite grain boundaries. The surface of these areas is shown in Fig. 3d. This is a fairly common effect. The step cooled specimen showed essentially the same behavior as the unembrittled. The fractographic appearances are somewhat dissimilar because the grain size in the step cooled specimens, which came from an earlier batch of material, was smaller (0.1 mm versus 0.2 mm). A later check with a coarse grained specimen showed that the lack of embrittlement during step cooling was not a grain size effect. In the specimens embrittled for 1000 h at 480 C the fractures at both temperatures were totally intergranular and the fracture facets were quite smooth.

*Tin.* In the 3340 steel containing 0.6 percent Mo and 600 ppm Sn, Mo greatly reduced the step cooled embrittlement from the 255 C transition temperature shift found by Low et al [2] in Mo-free heat, to a shift of about 25 C. As shown by Fig. 4, in the unembrittled condition the brittle-to-ductile transition involves a shift from entirely transgranular (cleavage) fracture (b) to a fracture which is apparently 50 to 60 percent intergranular (c). In the step cooled condition there is about 10 to 15 percent smooth intergranular fracture (remainder cleavage) in the brittle (low temperature) fracture (f) and 60 to 70 percent apparent intergranular fracture in the ductile (higher temperature) fracture (g). As shown by the fractographs at higher magnification (d) and (h), the apparent intergranular fracture is again a ductile rupture by microvoid coalescence which has occurred along the prior austenite grain boundaries. Isothermal aging for 1000 h at 480 C produced a larger shift in transition temperature than the step cooling.

*Arsenic.* Essentially no embrittlement resulted when 600 ppm As was added to the Mo-bearing 3340 steel from either step cooling or isothermal aging at 480 C for 1000 h. The SEM fractographs in Fig. 5 again show the intergranular dimpled rupture at the higher temperatures due to microvoid coalescence along prior austenite grain boundaries. (Results for longer aging at 480 C are not yet available.)

*Phosphorus.* In contrast with the behavior of Sb, As, and Sn in the Mo-bearing 3340 steels, the Mo addition had no apparent effect on the embrittle-

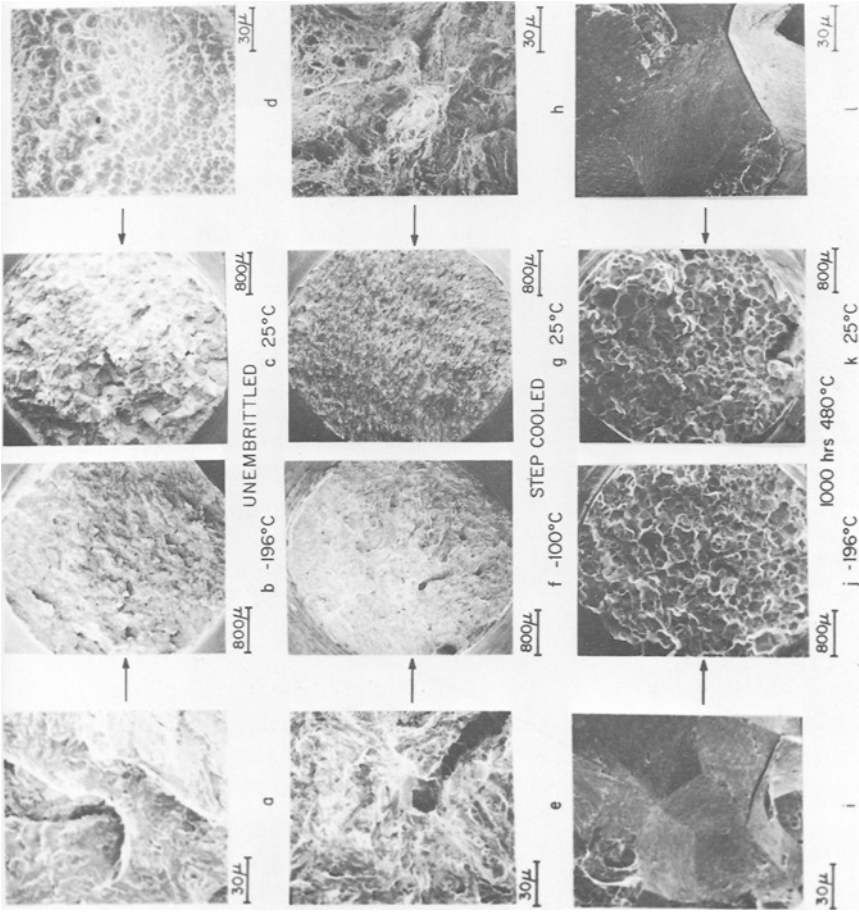


FIG. 3—Scanning electron fractographs of unembrittled, step cooled, and isothermally embrittled 3340 + 0.6%Mo + 600 ppm Sb.

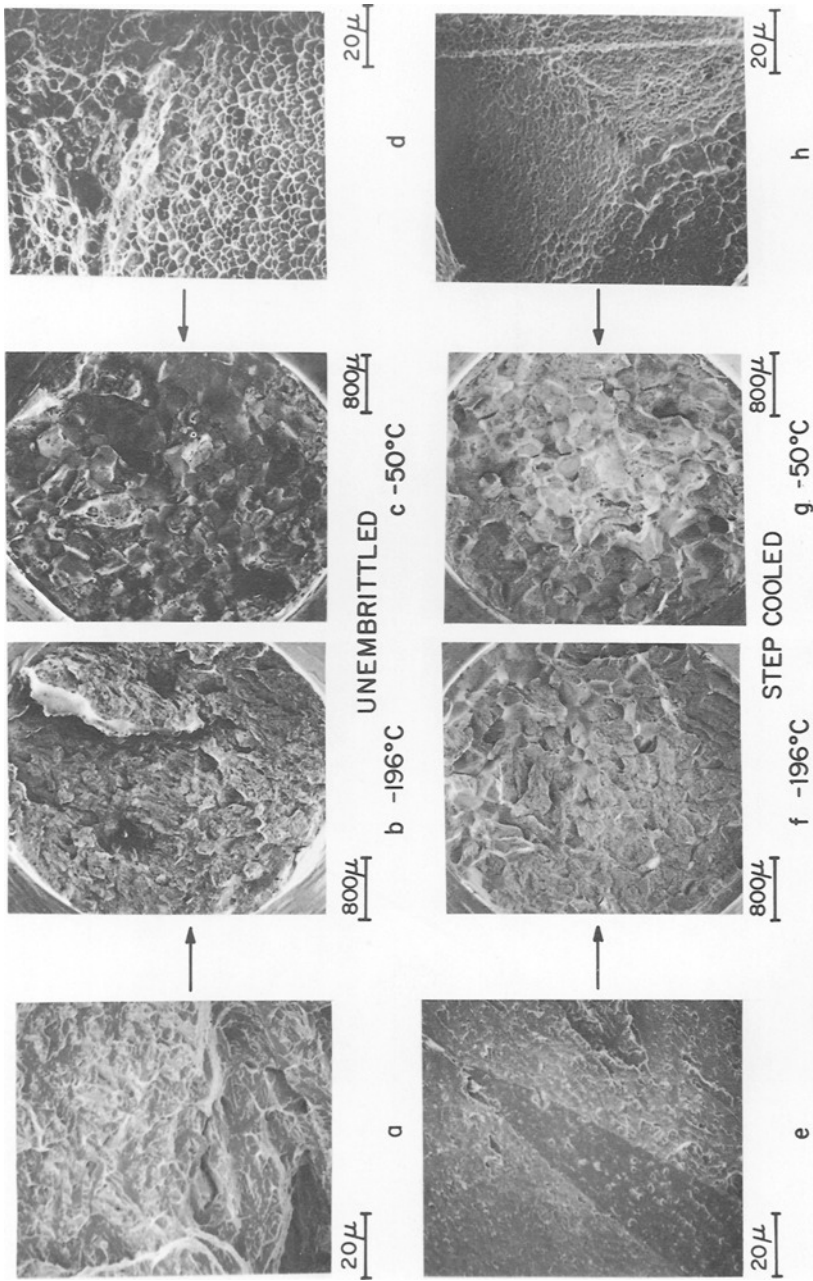


FIG. 4—Scanning electron fractographs of unembrittled and step cooled 3340 + 0.6%Mo + 600 ppm Sn.

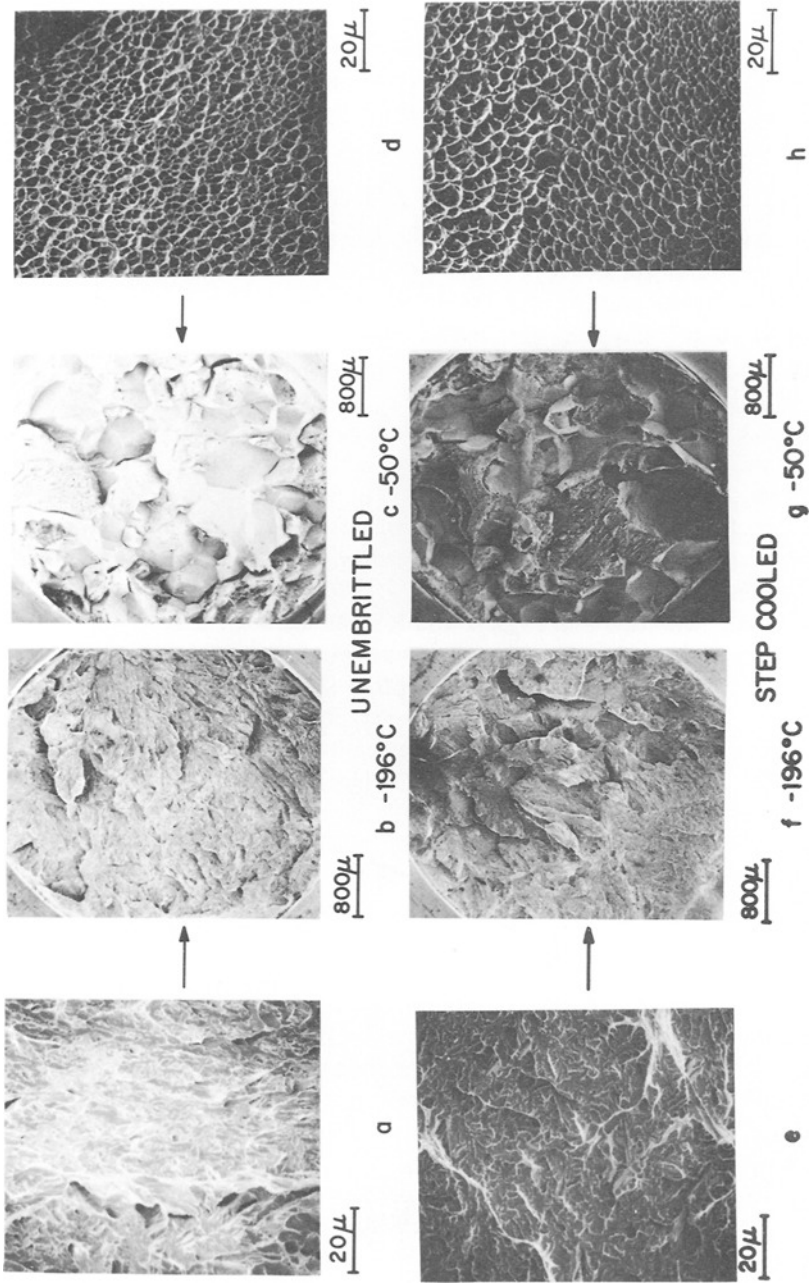


FIG. 5—Scanning electron fractographs of unembrittled and step cooled 3340 + 0.6%Mo + 600 ppm As.

ment due to 600 ppm P. The notched bar data in Fig. 2 show that the transition temperatures of the embrittled steels lie above our range of testing. The SEM fractographs in Fig. 6 show that in the "unembrittled" condition the low temperature fracture is 50 to 60 percent smooth intergranular and more than 80 percent intergranular dimpled rupture at room temperature. In the embrittled condition the fractures are essentially 100 percent smooth intergranular at all temperatures up to 25 C.

#### *Manganese in Molybdenum-bearing AISI 3340 Steel*

Since commercial steels contain at least a few tenths percent Mn, primarily for steel making purposes, it is of interest to know what the effects are of a Mn addition to the Mo-bearing 3340 steels. This is particularly interesting because Mn, itself, has been cited as an embrittling element [1,5], and past work has suggested that Mn may act like Cr in enhancing the embrittling effects of P [7].

The effect of Mn alone is shown in Figs. 7, 8, and 9. The notched bar data in Fig. 7 show that a 0.7 weight percent Mn addition results in extensive embrittlement of a 3340 steel in 300 h at 480 C and that addition of 0.6 percent Mo almost eliminates this embrittlement, even after 1000 h at 480 C. Thus, Mn appears similar to As and Sn, both in its behavior as an embrittling element and in its response to Mo additions.

The SEM fractographs in Figs. 8 and 9 show behavior similar to the As and Sn steels, except that the ductile intergranular dimpled rupture, where it appears, is not as well defined as in the other steels.

Table 2 gives the notched bar transition temperature data available at this time for the Mn steels. In addition to the points already made, one can see that the Mn additions do nothing to alter the behaviors of Sb, Sn, As, and P in 3340 steels containing Mo. In the case of Sb, we have used steels containing only 200 ppm Sb to investigate the Mn effect and have included data on a Mn-free, 200 ppm Sb, Mo-bearing 3340 steel for comparison. Notice that 200 ppm Sb in the steel does not result in embrittlement after 300 h at 480 C.

#### *Other Elements in AISI 3340 Steel*

It has been reported by Steven and Balajiva [1] that Si acted as an embrittling element, although this has never been independently verified. In addition, it is natural to ask about the possibilities of embrittlement of steels by Bi, Se, Ge, and Te, due to their proximity to the known embrittling elements in groups IVB, VB, and VIB in the periodic table. Hence, these elements have been added individually to a 3340 steel and transition temperatures and fracture behaviors have been determined.

The notched bar data are shown in Table 2 and the transition temperature curves are plotted in Fig. 10 for all except the Te alloy. It is apparent that slight (10 to 25 C) embrittlement occurs in 300 h at 480 C in the cases of Si, Se, and Ge. The embrittlement by Bi is more substantial (40 C). (Data for longer

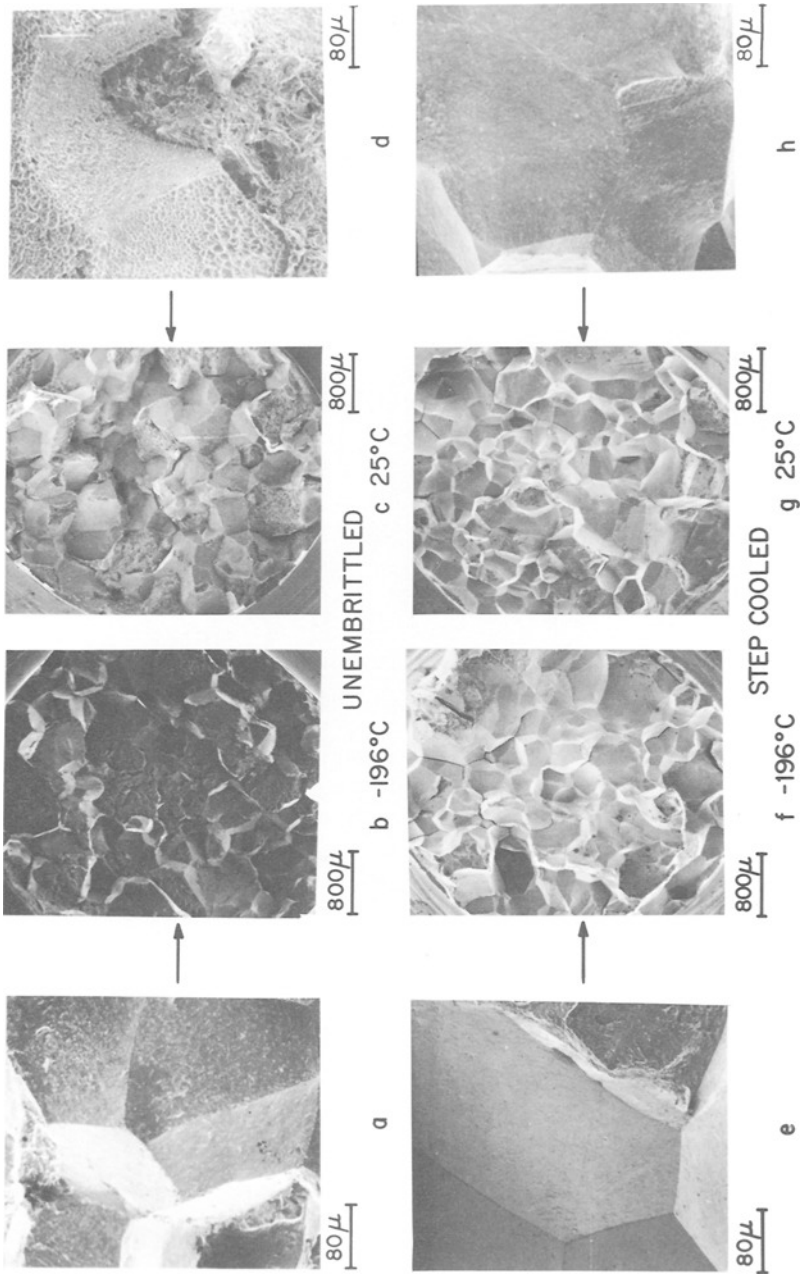


FIG. 6—Scanning electron fractographs of unembrittled and step cooled 3340 + 0.6% Mo + 600 ppm P.

TABLE 2—Effects of various embrittling elements on AISI 3340 steel.

Embrittling Element	Embrittling treatment	Molybdenum Bearing										Heat treatment
		Transition Temperature, deg C		Shift T.T., deg C	Grain Size, mm	Hardness, HRC		Brittle Mode of fracture <sup>a</sup>		E		
		U	E			U	E	U	E	U	E	
.06%Sb	Step cooled	-115	-100	15	0.10	32	33	Tx	Tx	1200 C 4h OQ		
	1000 h 480 C	-105	>25	>130	0.2	25	25	Tx	Ix	625 C 2h WQ		
	Step cooled	-115	>25	>140	0.5	31	32	0.5Ix	Ix	1250 C 4h F.C. 900 CHWQ <sup>b</sup>		
	1000 h 480 C	-115	>25	>140	0.5	31	30	0.5Ix	Ix	650 C 24h WQ		
.06%Sn	Step cooled	-135	-110	25	0.3	29	29	Tx	0.8Tx	650 C 4h F.C. 900 C OQ		
	1000 h 480 C	-135	-90	45	0.3	29	30	Tx	0.8Tx	650 C 2h WQ		
.06%As	Step cooled	-115	-110	5	0.5	31	30	Tx	Tx	1250 C 4h F.C. 900 C OQ		
	1000 h 480 C	-115	-115	0	0.5	31	30	Tx	Tx	650 C 2h WQ		
Mo	<i>Manganese Bearing</i>											
	300 h 480 C	-75	>25	>105	0.4	27	28	0.9Ix	Ix	1300 C 4h F.C. 900 C OQ		
	1000 h 480 C	-135	-115	20	0.15	32	32	Tx	Tx	650 C 2h WQ		

Mo + .02%Sb	1000 h 480 C	-140	-130	10	0.3	31	29	Tx	Tx	1250 C 4h F.C. 900 C OQ 650 C 2h WQ
Mo + .02%Sb	300 h 480 C	-135	-125	10	0.5	31	30	Tx	Tx	
Mo + .06%P	1000 h 480 C	-80	>25	>105	0.4	32	31	0.9Ix	Ix	
Mo + .06%Sn	1000 h 480 C	-130	-125	5	0.2	33	32	Tx	Tx	1300 C 4h F.C. 900 C OQ 650 C 2h WQ
Mo + .06%As	1000 h 480 C	-130	-125	5	0.1	31	32	Tx	Tx	
<i>Other Embrittling Elements</i>										
.2%Si	300 h 480 C	-125	-100	25	0.3	26	29	Tx	0.8Ix	1100 C 4h F.C. 900 C OQ 650 C 2h WQ
.7%Mn	300 h 480 C	-75	>25	>105	0.4	27	28	0.9Ix	Ix	1300 C 8h F.C. 900 C OQ 625 C 2h WQ
.01%Bi	300 h 480 C	-125	-85	40	0.2	31	30	0.9Tx	0.9Ix	1300 C 4h F.C. 900 C OQ 625 C 2h WQ
.01%Se	300 h 480 C	-115	-100	15	0.4	28	29	0.8Tx	0.7Ix	1300 C 8h F.C. 900 C OQ 625 C 2h WQ
.01%Ge	300 h 480 C	-125	-115	10	0.1	29	27	Tx	0.8Ix	1300 C 4h F.C. 900 C OQ 625 C 2h WQ
.01%Te	300 h 480 C	>25	>25	...	1.0	29	28	Ix	Ix	1300 C 8h F.C. 900 C OQ 625 C 2h WQ

<sup>a</sup> Tx = transgranular, Ix = intergranular.

<sup>b</sup> Furnace cooled to 900 C, held 24h followed by hot water quench (HWQ) at 80 C; room temperature oil quench (OQ).

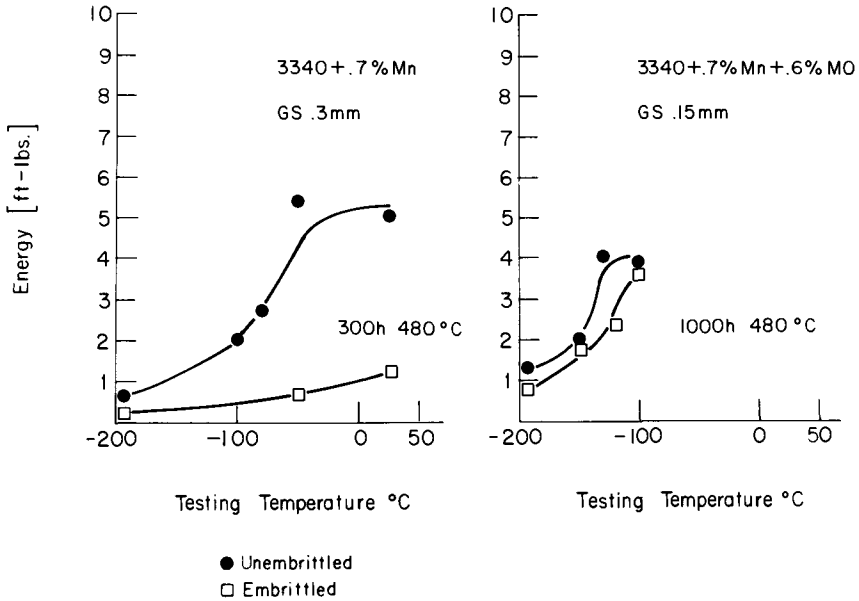


FIG. 7—Transition temperature curves obtained from bend tests in unembrittled and embrittled conditions.

times are not yet available.) In the case of the 3340 + Te, the prior austenite grain size was 1 mm, and the fracture energy was low for both the embrittled and unembrittled conditions at all temperatures up to room temperature. However, the fracture mode changed from smooth intergranular to intergranular dimpled rupture below room temperature in both cases. Fine grain specimens would be necessary to measure a transition temperature shift.

A better physical appreciation of the effects of these elements can be gained from the SEM fractographs of these samples in Figs. 11 through 15 which show the fracture mode in the unembrittled and embrittled conditions both above and below the transition temperatures. From the smooth intergranular facets at low temperatures in the embrittled steels and from the shift in transition temperatures one can see that these impurities give true temper embrittlement. It is also worth noting that all of these elements give the intergranular dimpled rupture at higher temperatures.

It should be pointed out that all of our high purity vacuum-melted heats contained a residual amount of P between 20 and 60 ppm; this possibly came from the electrolytic Fe used in the charge. The alloys discussed failed intergranularly at low temperatures in the embrittled condition, whereas the high purity steel (heat 465) of Low et al [2], which contained 45 ppm P, was reported to have failed transgranularly in the embrittled condition. On this basis, it appears that Si, Bi, Se, and Ge contribute their own embrittling effects.

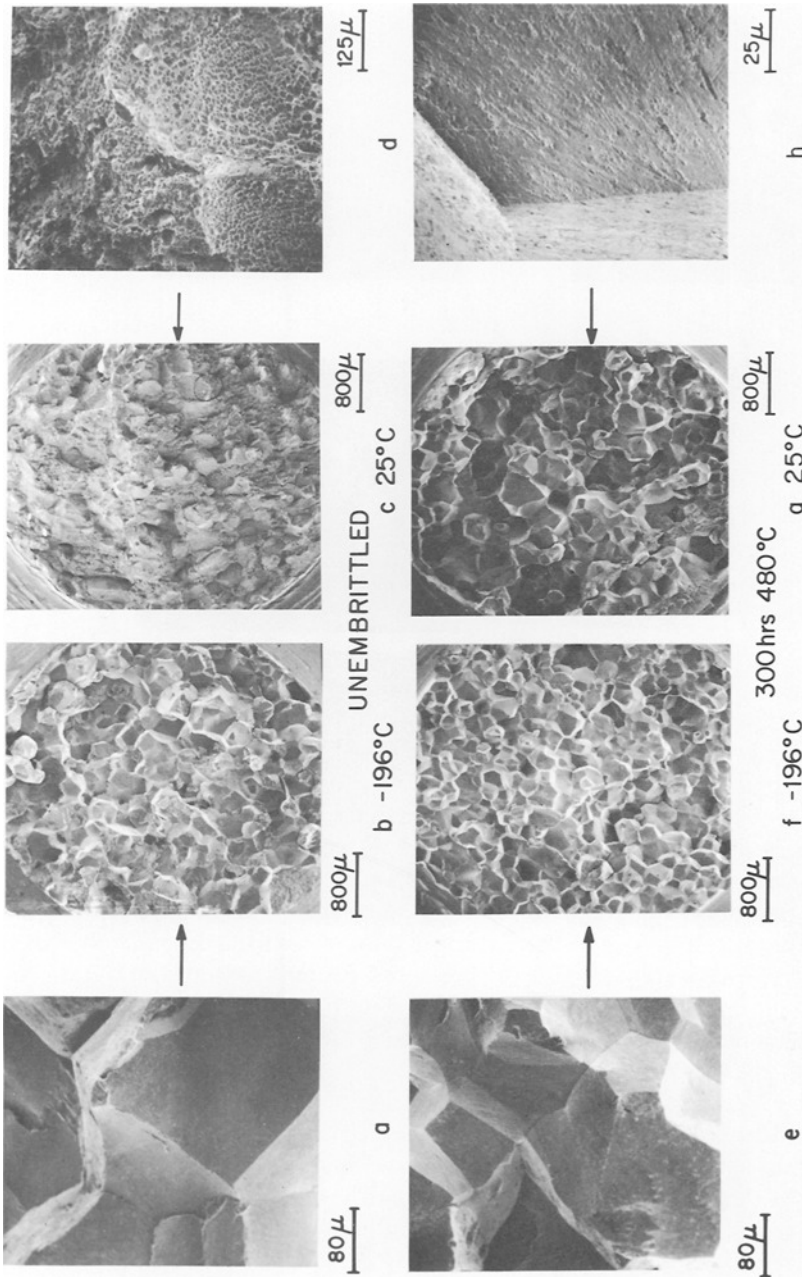


FIG. 8—Scanning electron fractographs of unembrittled and embrittled 3340 + 0.7% Mn.

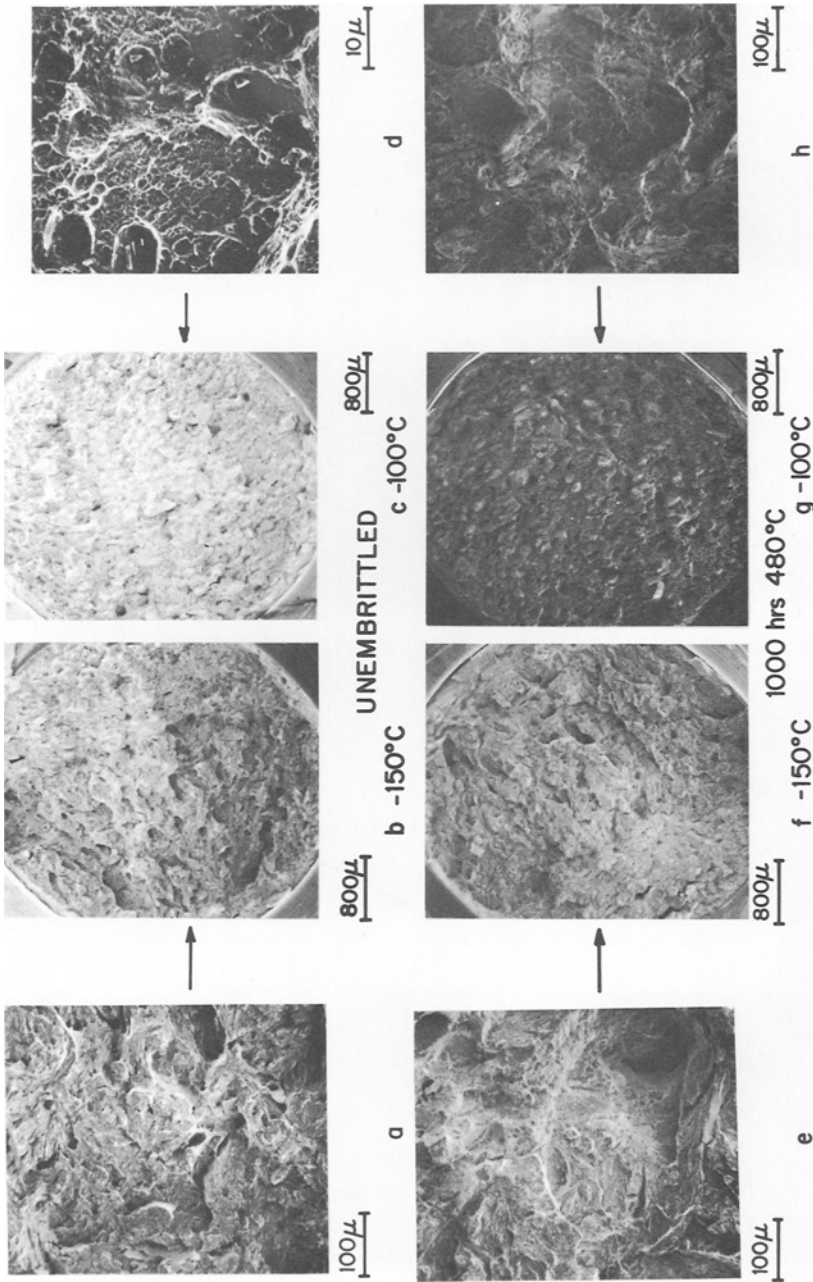


FIG. 9—Scanning electron fractographs of unembrittled and embrittled 3340 + 0.6% Mo + 0.7% Mn.

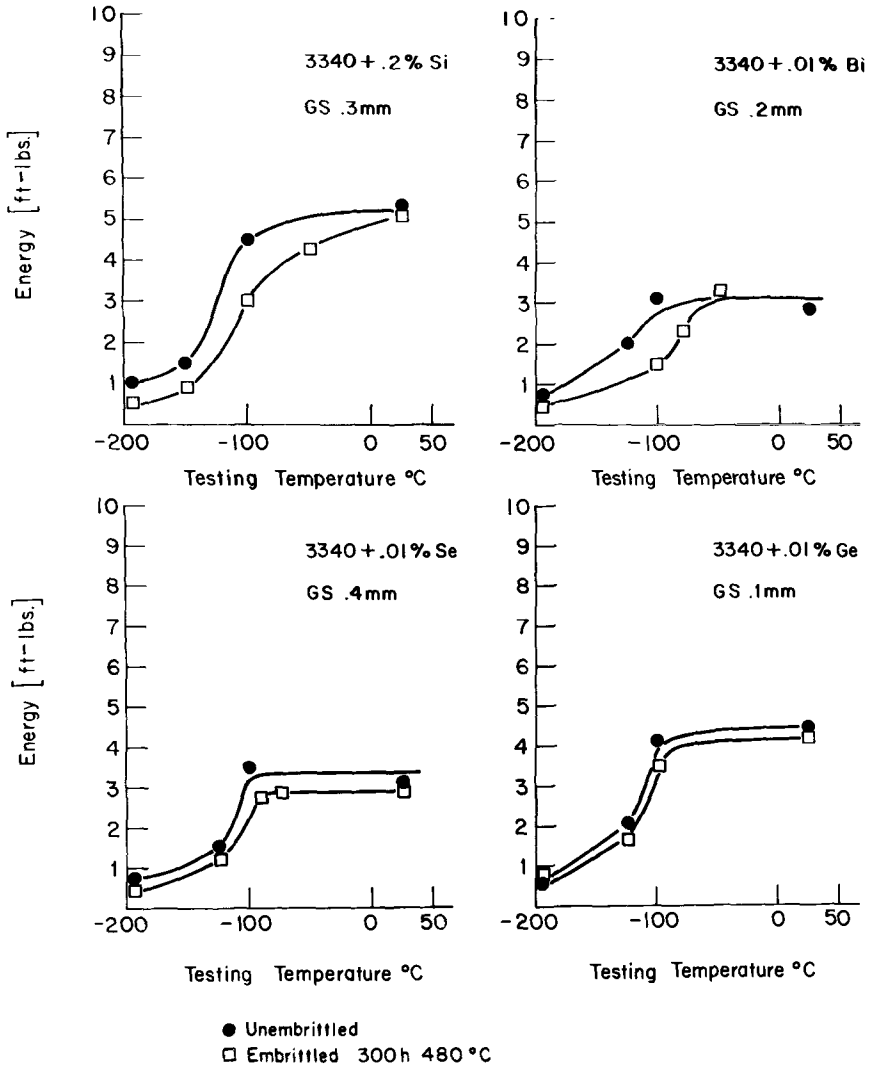


FIG. 10—Transition temperature curves obtained from bend tests for 3340 + 0.2% Si, 100 ppm Bi, 100 ppm Se, and 100 ppm Ge.

### Intergranular Brittleness in As-Quenched Steels

Fracture along prior austenite grain boundaries has been noted before in as-quenched (martensitic) alloy steels, and we have been studying this phenomenon along with its close relative, quench cracking [8]. We have found that all specimens of commercial and laboratory made plain carbon and low alloy steels with C content around 0.4 weight percent which we have tested exhibit quench cracking along prior austenite grain boundaries and can be fractured

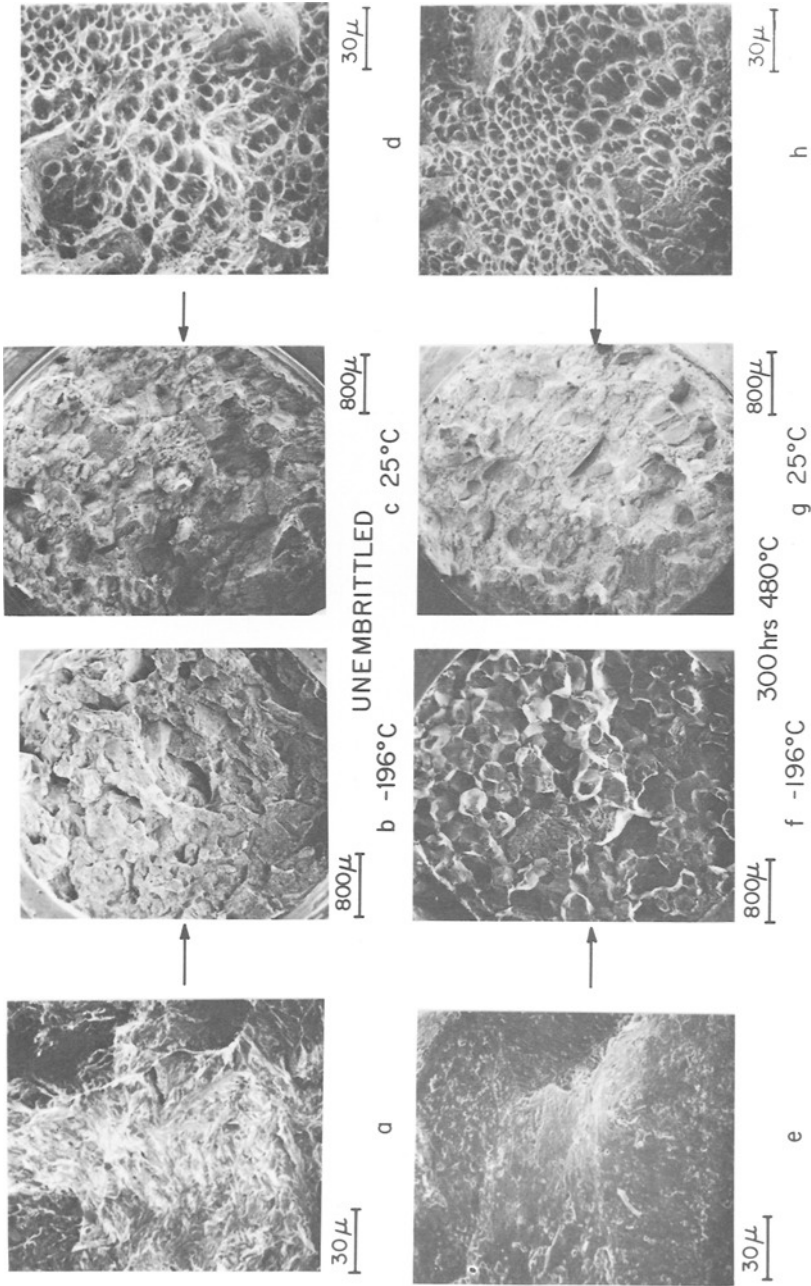


FIG. 11—Scanning electron fractographs of 3340 + 0.2%Si in the unembrittled and embrittled conditions.

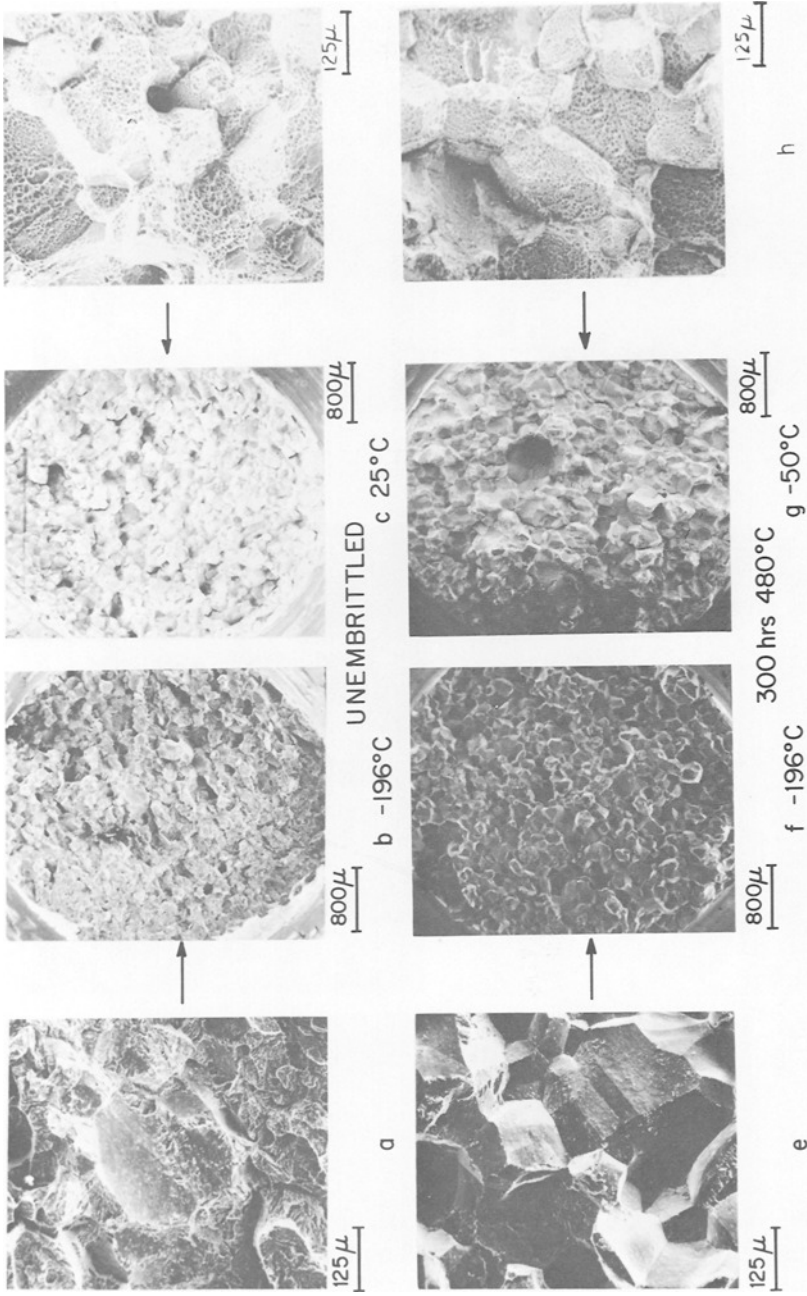


FIG. 12—Scanning electron fractographs of 3340 + 100 ppm Bi in the unembrittled and embrittled conditions.

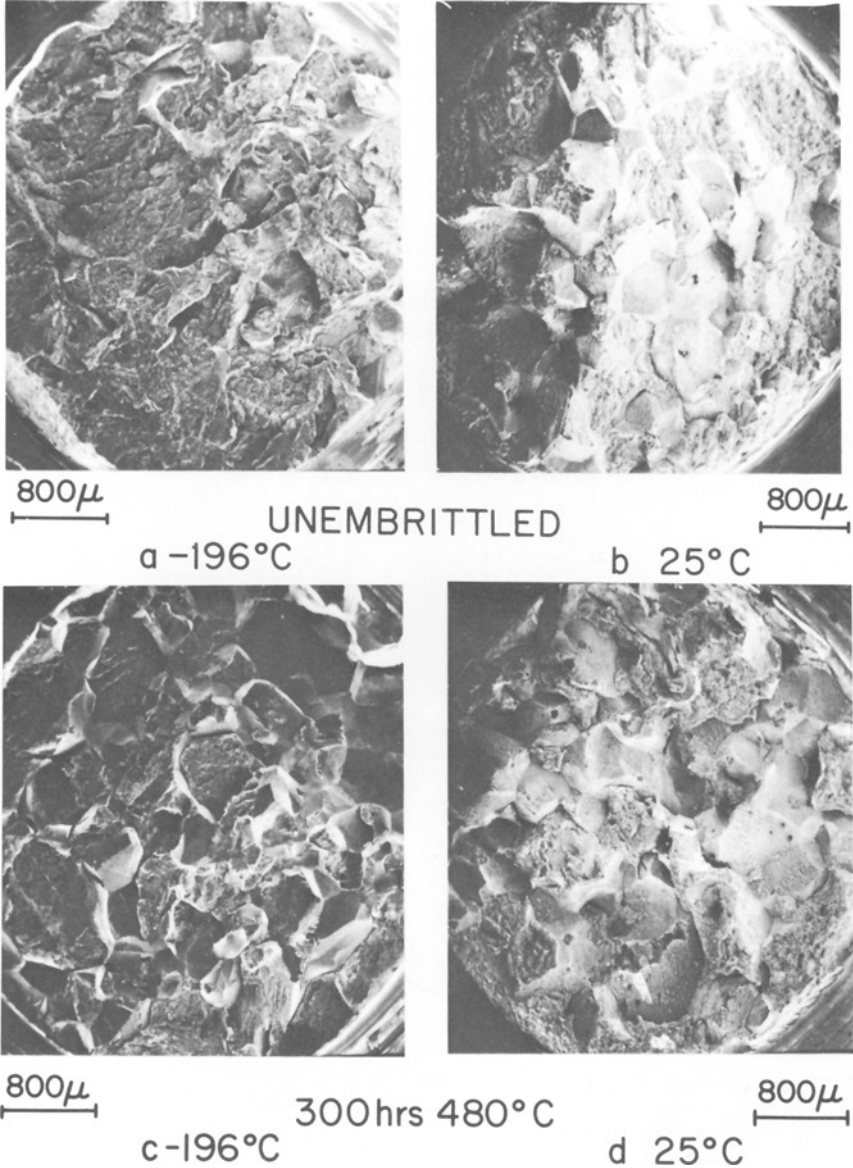


FIG. 13—Scanning electron fractographs of 3340 + 100 ppm Se in the unembrittled and embrittled conditions.

completely along these boundaries if they are rapidly quenched. We have been interested in this particularly because we wish to learn what kind of impurity segregation during austenitization is responsible for this cracking, since this may shed some light on the precursor processes in the problem of temper embrittlement.

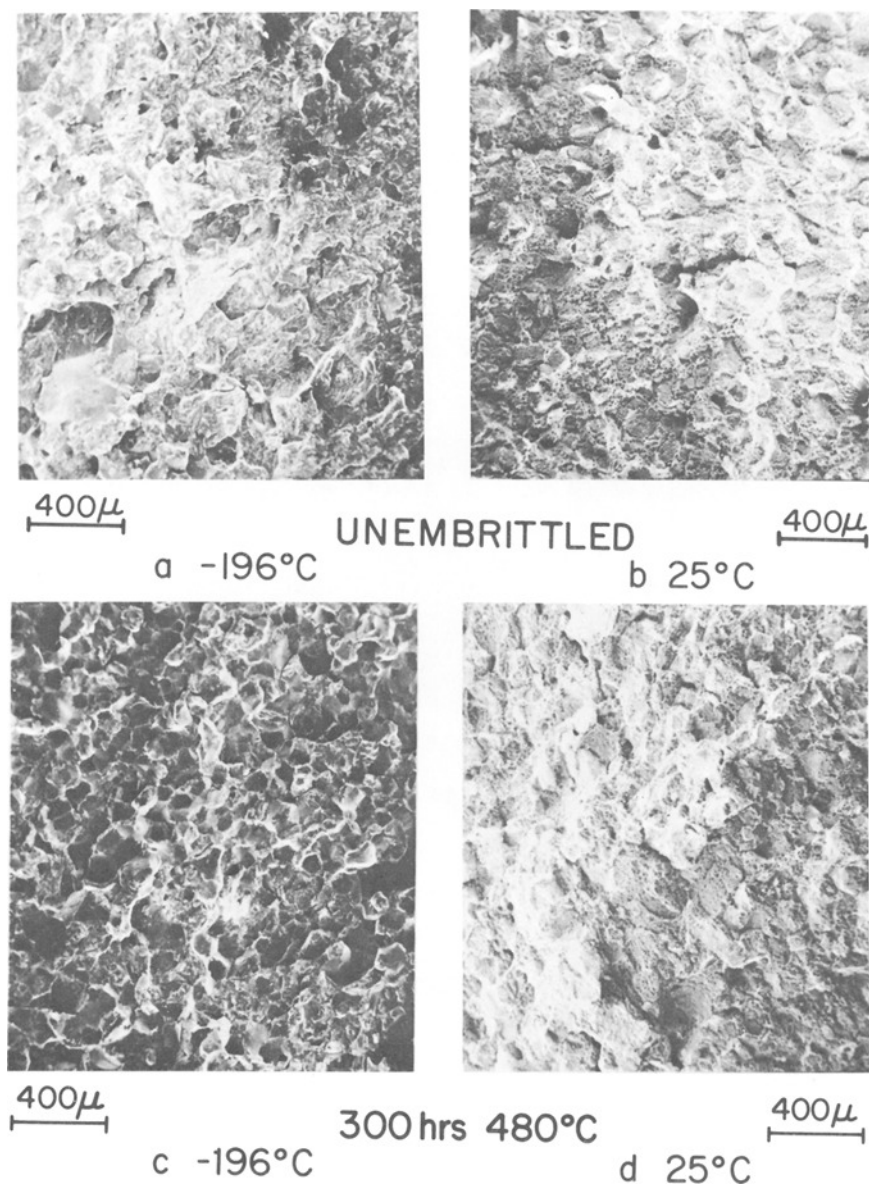


FIG. 14—Scanning electron fractographs of 3340 + 100 ppm Ge in the unembrittled and embrittled conditions.

Recently we have discovered an effect of quenching rate which we feel has the possibility of giving information about transformations in steels and their relation to grain boundary embrittlement. The effect can be illustrated by Fig. 16 which shows the difference in fracture behavior of as-quenched martensite in 3340 steel containing 600 ppm Sb depending on whether it has

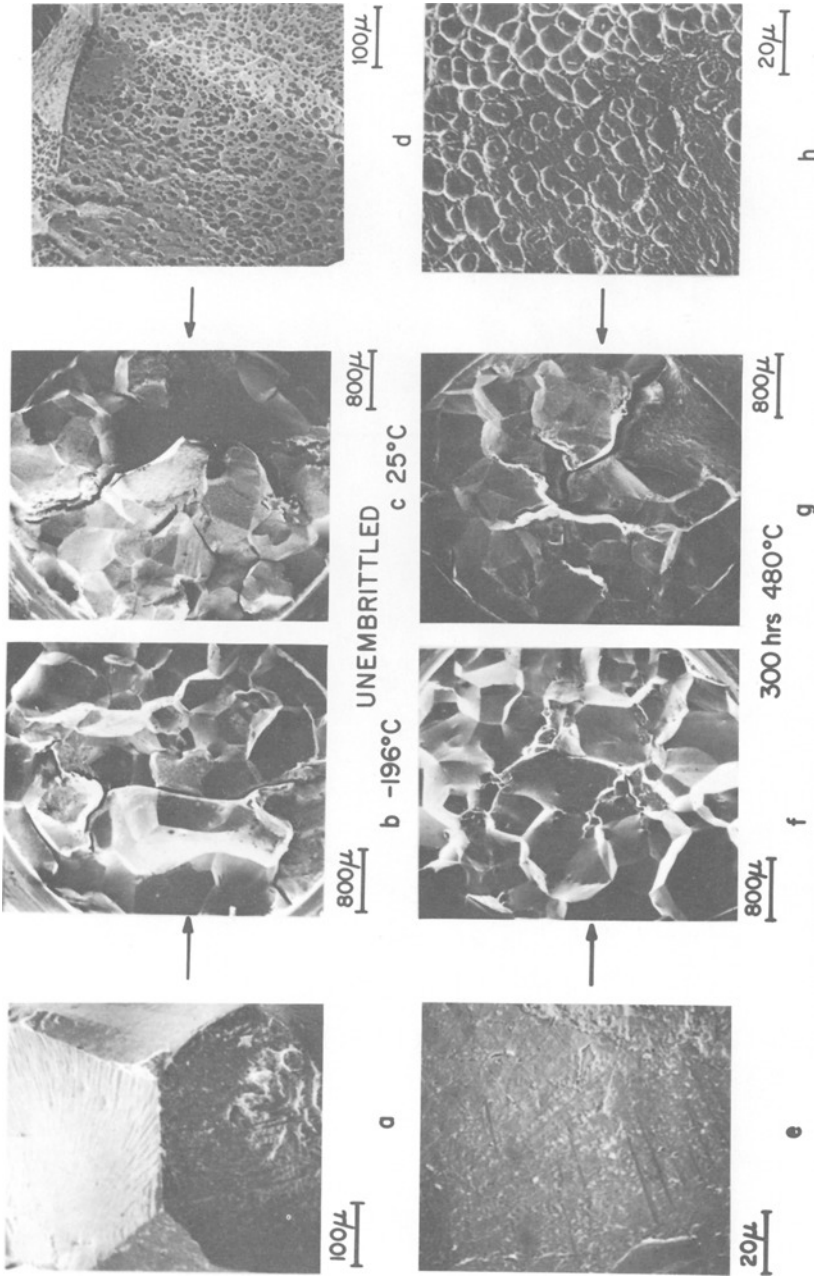


FIG. 15—Scanning electron fractographs of 3340 + 100 ppm Te in the unembrittled and embrittled conditions.

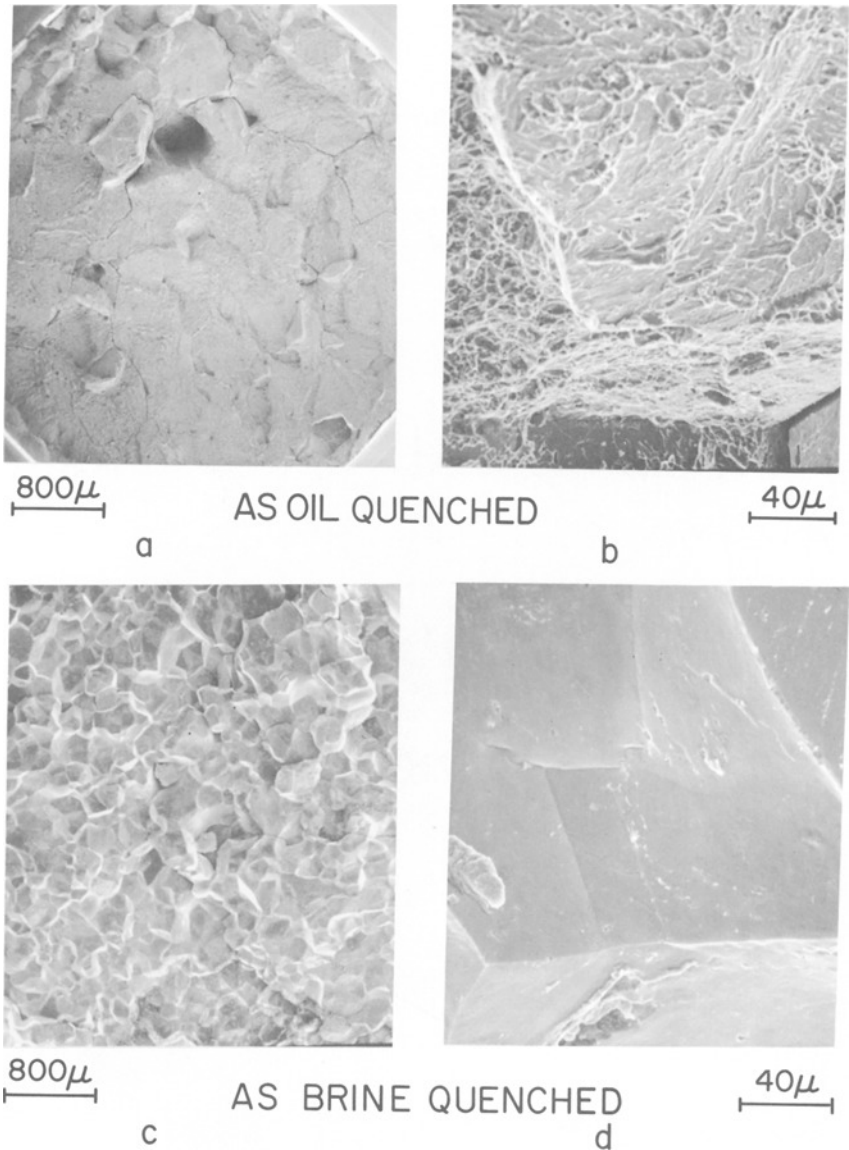


FIG. 16—Scanning electron fractographs of 3340 + 600 ppm Sb fractured at room temperature.

been quenched (after 4 h at 1250 C) into iced brine or room temperature oil. The rapidly quenched steel fractured while the notch was being machined and the prior austenite grain boundaries are almost perfectly smooth in most places (Fig. 16c and d), indicating that the fracture proceeded exactly along the prior austenite boundaries with almost no plastic deformation. In the oil quenched condition the specimens were tougher and the fracture was inter-

granular only along part of the periphery (Fig. 16a and b). There was obviously a certain amount of tearing involved.

In order to get some idea of what impurities are responsible for the smooth intergranular fracture, an as-quenched sample was fractured in a vacuum of  $<10^{-9}$  torr and Auger electron spectroscopy was performed. The spectra from the as-fractured surface and after sputtering away  $\sim 6$  atomic layers are shown in Fig. 17. Interestingly enough, no Sb was found. This casts doubt

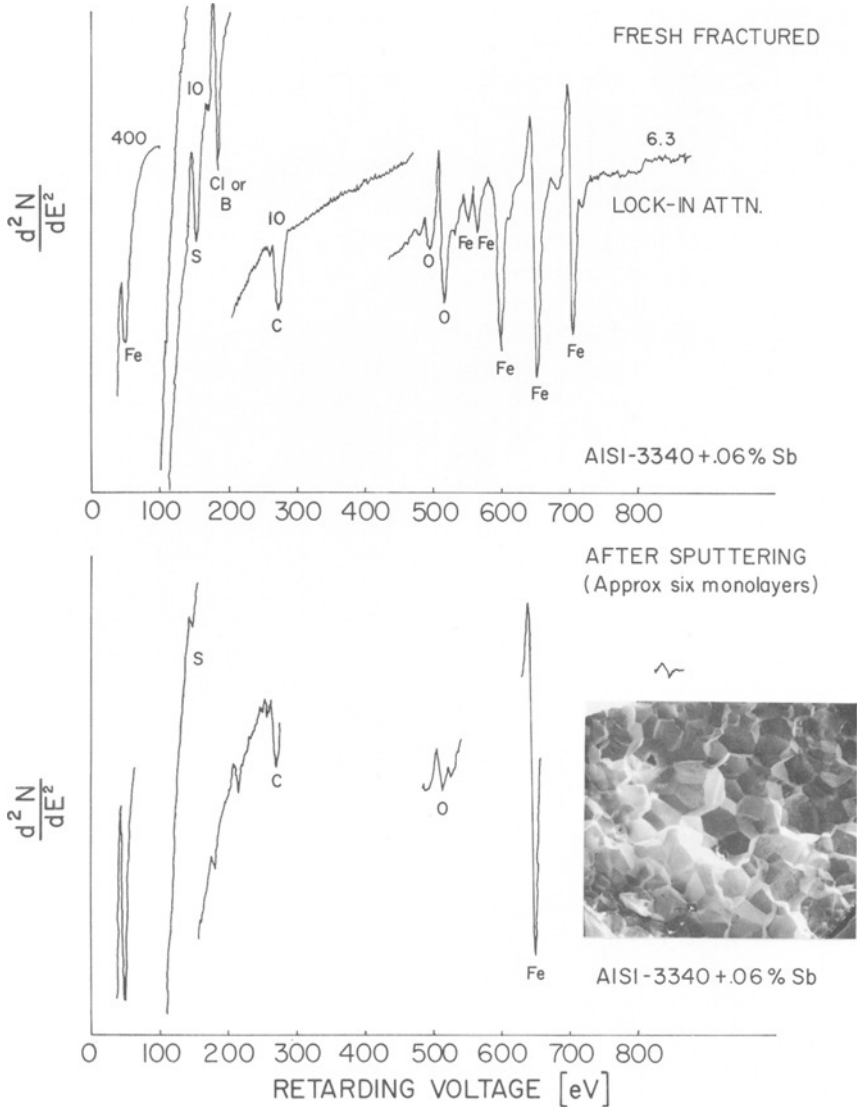


FIG. 17—Auger electron spectra from fracture surface of 3340 + 600 ppm Sb in brine quenched condition.

on a hypothesis made previously [9] that the embrittling elements may segregate in austenite prior to quenching. The elements to be considered are apparently S, O, and Cl or B. (The latter two cannot be differentiated by this equipment.) Our tentative thoughts at this time are that Cl and O are present because they contaminated the quench cracks which connected with the specimen surface and the embrittling impurity may be the S. Of course, there is also the possibility that some other element was responsible for the embrittlement but was present at levels below the limit of detectability of this Auger electron spectroscopy apparatus.

The origin of the quench rate effect is yet unknown. Two possibilities have been considered:

1. There may be some kind of austenite decomposition, hitherto unsuspected in this hardenable steel, which originates at the austenite grain boundaries and sufficiently disrupts the atomic arrangements in the boundaries so that the embrittling elements are dislodged from their original positions enough to preclude smooth intergranular fracture. This would seem to imply that the quantity segregated is not large.

2. Some kind of diffusive process may occur which allows the embrittling element to escape from the boundaries during a slow quench. This seems unlikely, since one would expect from the thermodynamics of surfaces that diffusion of segregating elements would occur toward the boundaries in a slow quench, rather than vice versa.

We find the same effect in a "high purity" 3340 steel (heat 465 of Low et al [2]) as shown in Fig. 18 and in a 1040 steel (actually vacuum melted Fe plus 0.4 weight percent C) to which 800 ppm Sb were added.

The 3340 steel with 600 ppm P behaves differently than non-P-bearing steels in that complete intergranular fracture can be achieved even in oil quenched specimens (Fig. 19). The Auger spectra from a fracture (in vacuum) in a brine quenched specimen are shown in Fig. 20. This time P is found in addition to the S, O, and Cl and it sputters off within the first 6 atomic layers. Thus it appears that P does segregate in the austenite, even though Sb apparently does not. This is in keeping with the nature of the element P, which tends to behave in the opposite sense to Sb, Sn, and As in many aspects of the interface embrittlement problem.

The interesting features on the prior austenite grain boundaries in Fig. 19 should be noted. There seems to be a definite indication of some kind of austenite decomposition (bainite or widmanstätten ferrite?) during the oil quench. This was unexpected in a  $\frac{1}{4}$ -in. bar quenched from 1250 C into oil, since the nose of the TTT curve for this alloy is reported to be at 430 C and 20 s [10]. Apparently, transformations in steels are not as well understood as we would like to believe, especially along grain boundaries where diffusion is much faster.

Finally, the smooth intergranular fracture in the oil quenched 3340 steel with 600 ppm P persisted even after tempering when the specimens were

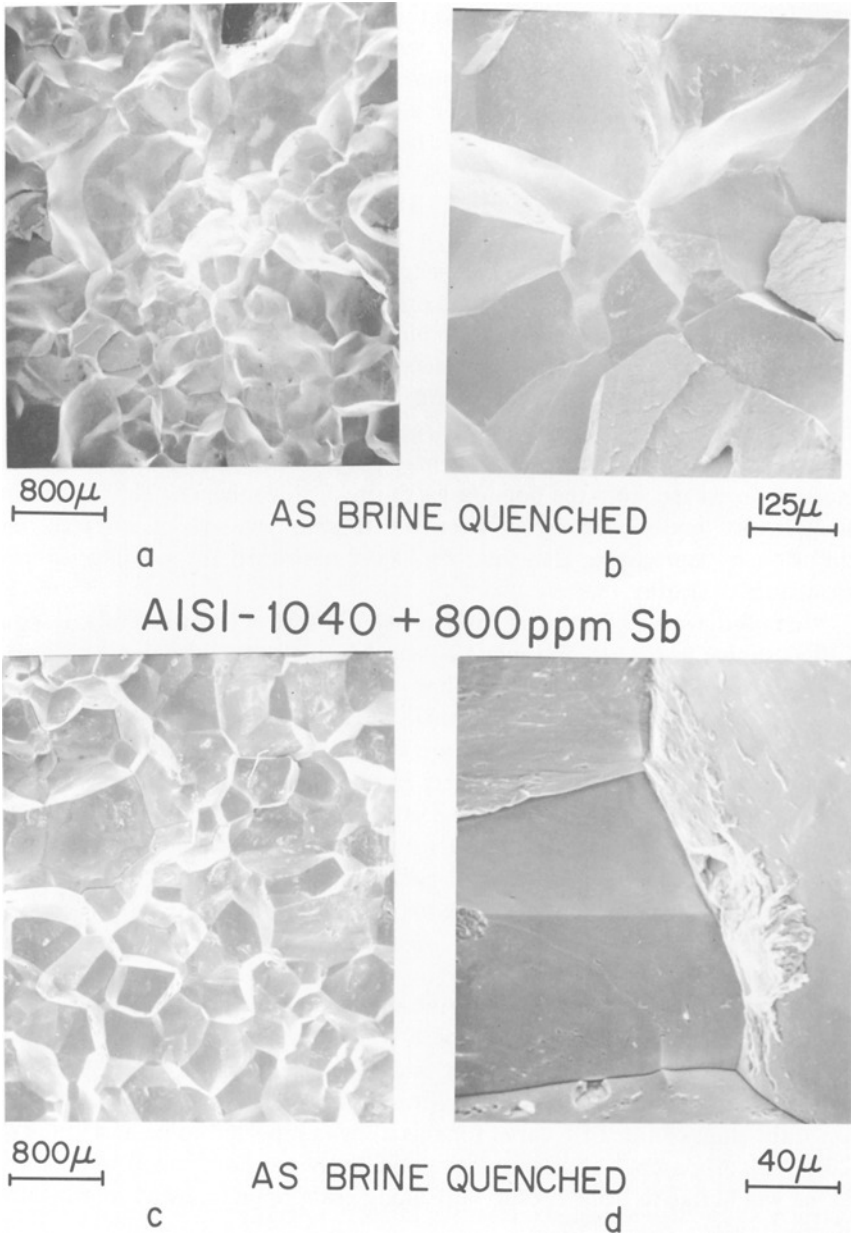


FIG. 18—Scanning electron fractographs of 1040 + 800 ppm Sb and high purity 3340 fractured at room temperature.

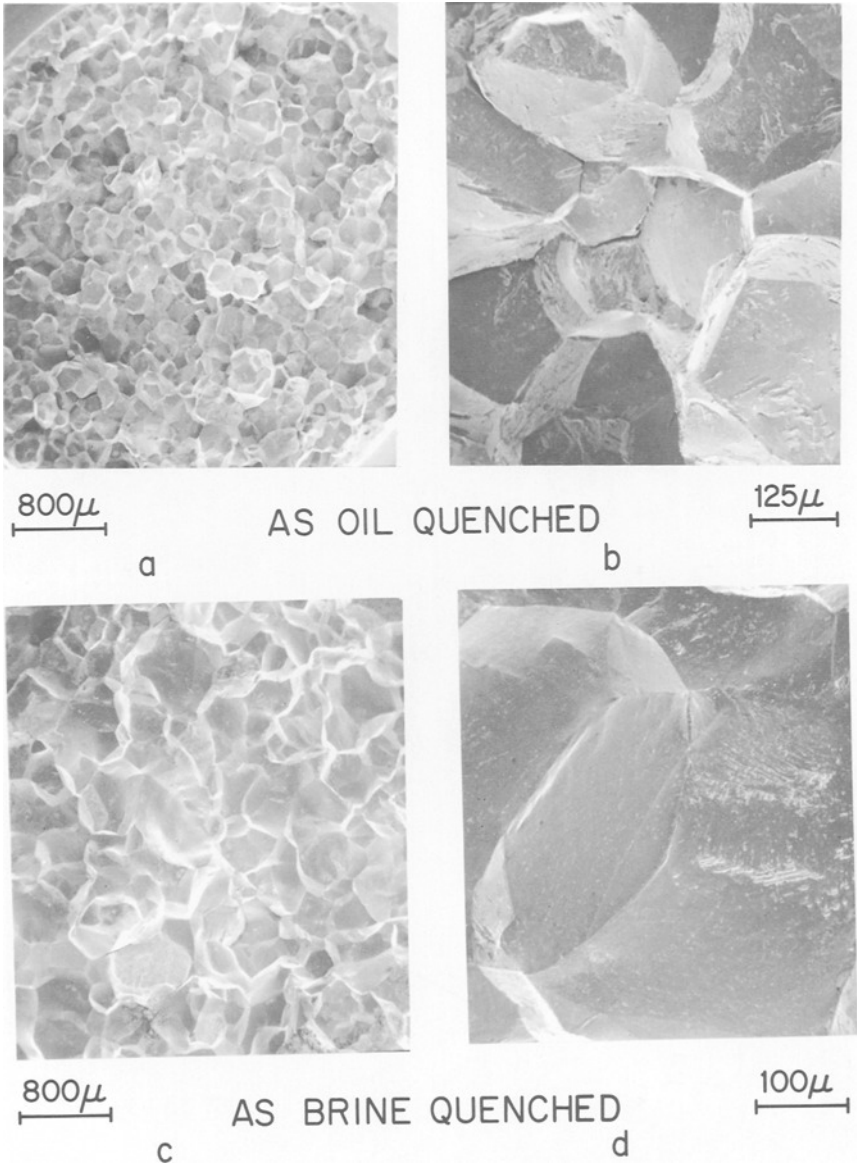


FIG. 19—Scanning electron fractographs of 3340 + 600 ppm P fractured at room temperature.

broken at  $-196$  C. Specimens were tempered for 1 h at temperatures up to 700 C (re-austenitization begins around 725 C), and the smooth intergranular fracture persisted. A specimen tempered for 20 h at 670 C was found to fracture in a transgranular manner at  $-196$  C. This behavior is consistent with the results of Low et al [2], who found that this steel fractured in an inter-

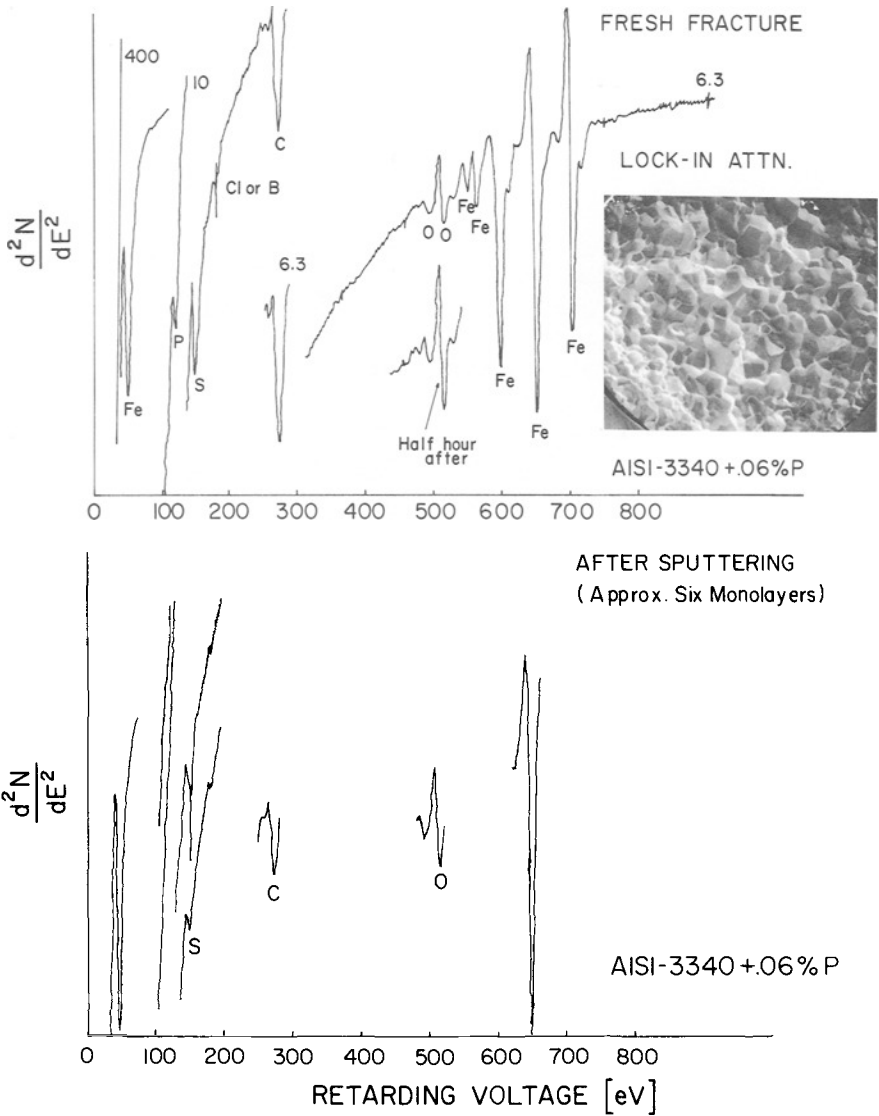


FIG. 20—Auger electron spectra from fracture surface of 3340 + 600 ppm P in brine quenched condition.

granular mode in the "de-embrittled" condition (1 h at 650 C). The reason for the persistence of what is presumably P segregation is not yet understood.

## Discussion

### *Effect of Molybdenum*

Of the four best known embrittling elements, three of them, Sb, Sn, and As, appear to respond to additions of Mo in a similar way. The transition temperature shift due to step cooling is either greatly reduced or eliminated. However, the tendency for embrittlement still remains, as shown by the presence of the intergranular dimpled rupture. The results for isothermal aging 1000 h at 480 C show that Sb embrittlement has returned in full force by this time, and it would not be surprising if similar results are found for As and Sn if steels containing them were aged a sufficient length of time. At this point it would appear that Mo may not change the ultimate amount of embrittlement so much as the rate of embrittlement. The details of the Mo effect may be quite complicated. For example, after only a small amount of tempering the 0.6 weight percent Mo may still be largely in solution in the ferrite where it presumably interacts with Sb, Sn, or As in some way. However, as the tempering or aging continues the Mo precipitates as a carbide, thereby lowering its activity in the ferrite and removing the interaction with embrittling elements.

In the case of P, the work to date does not appear to show any interaction with Mo, contrary to the long held belief that the beneficial effect of Mo was to form some kind of phosphide and thereby remove P embrittlement.

### *Manganese as an Embrittling Element*

Although Mn was reported by Steven and Balajiva [1] to be an embrittling element, we have been reluctant to accept this result because this group VII A element should behave like a metal, not a metalloid as all the others, and being an austenite stabilizer, Mn has effects on phase equilibria in Fe different than any other embrittling element. (The rest are all ferrite stabilizers.) However, current results, as well as previous results of Joshi, Stein, and Laforce [6], along with the fact that Mn seems to respond to Mo just like Sb, Sn, and As, all point to the conclusion that Mn is indeed an embrittling element, and not just an enhancer of some other embrittling element.

### *Other Embrittling Elements*

Further work on the behavior of Si, Bi, Se, and Ge is needed. Si, Bi, and Te have been shown to be strong embrittlors, and long time aging may show that the others exert greater effects than found to date.

*Intergranular Dimpled Rupture*

This phenomenon seems to be characteristic of weak embrittlement. It is suspected that the particles which give rise to the microvoids on the prior austenite grain boundaries may be carbides. From past work [8,9], we are led to believe that the void formation results from decreased cohesion along carbide-ferrite interfaces due to the presence of an embrittling element. We postulate this because of the observations that carbide-ferrite interfaces in steels do not tend to split open unless they are contaminated by some embrittling element.

In the case of intergranular dimpled rupture it appears that the ferrite-ferrite interfaces, which make up the rest of the prior austenite grain boundaries, do not split open easily. The splitting of embrittled carbide-ferrite interfaces should be easy, due to the rigid nature of the carbides which inhibits plastic relaxation of stress concentrations (for example, blocked slip bands). If the ferrite-ferrite interfaces were also embrittled, a lowering of the test temperature (which would make the ferrite less plastic) would result in a transition to smooth intergranular fracture. This happens in the case of strong embrittlement by P and Te (Figs. 6 and 15). However, in the case of Sn and As (Figs. 4 and 5), we see a transition to cleavage at low temperatures in the unembrittled condition, indicating that here the ferrite-ferrite interfaces are not embrittled. Note, also, the obvious differences in the size and depth of the voids on the dimpled rupture surfaces in Figs. 4 and 5 as opposed to Figs. 6 and 15. This also suggests a tendency for ferrite-ferrite boundary embrittlement in the latter.

The incidence of intergranular dimpled rupture in steel might be taken as an indication that a tendency toward intergranular embrittlement exists and may develop further with continued aging or tempering treatments. A full understanding of the details of the development of intergranular dimpled rupture and of the shift to smooth intergranular fracture is beyond the reach of current instrumental techniques for chemical analysis on the scale of atomic dimensions. We say this because we expect complex local compositional changes during aging or tempering, but at the same time these changes are important in regulating the amount of embrittlement. To illustrate this we give the following hypothetical series of events which might occur during thermal treatment of steel. The steps are schematically presented in Fig. 21.

In step 1, austenitization, and step 2, after quench, we assume for simplicity no concentration gradients near the interface. After a small amount of tempering, step 3, we have a carbide which is mainly  $\text{Fe}_3\text{C}$ , but which also contains the Mo and Cr atoms which were entrained in the growing carbide. The Ni atoms on the other hand have been rejected by the carbide and have piled-up ahead of the carbide. (There has not yet been time enough for them to diffuse away.) The embrittling atoms ( $E$ ) have undergone a similar process, and this excess of  $E$  in the interface causes low cohesion and easy splitting of

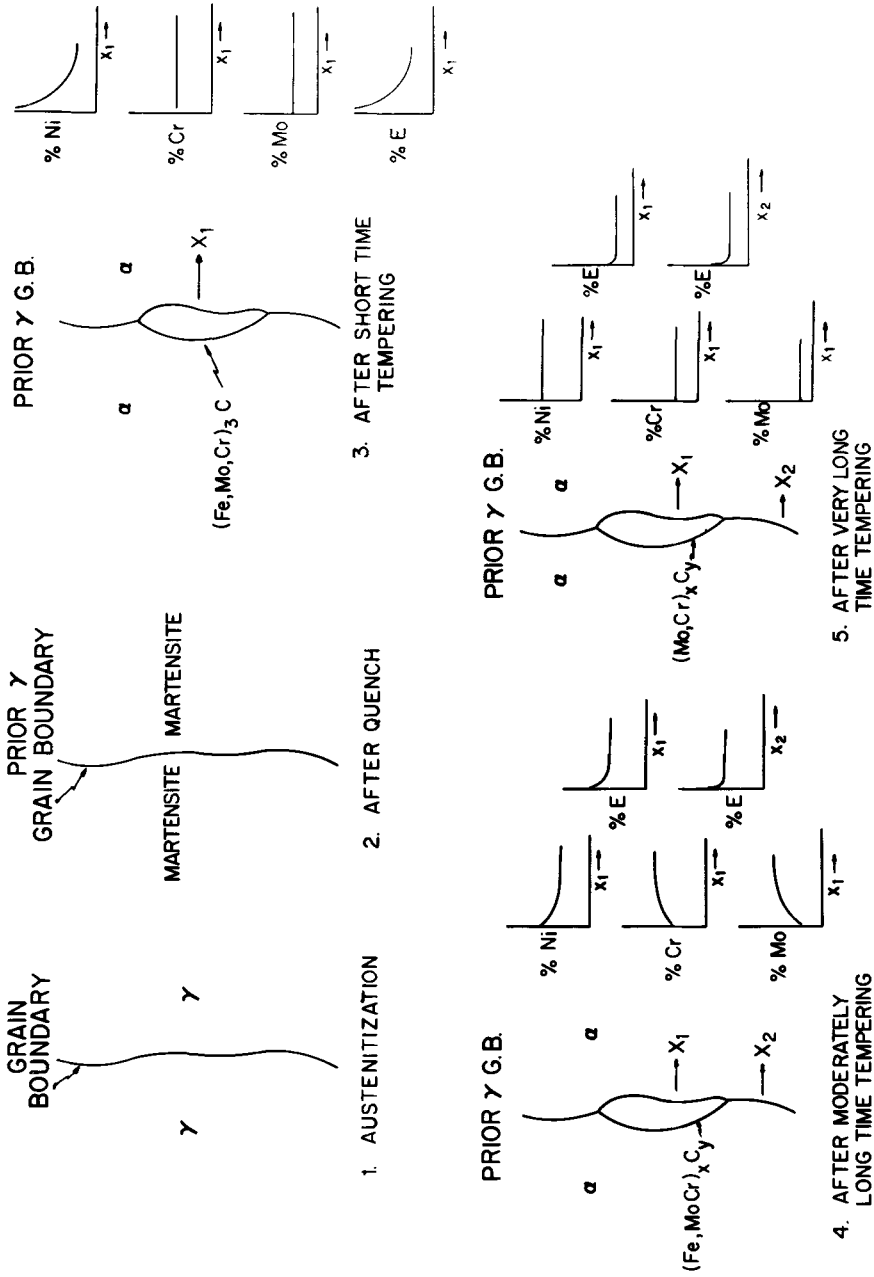


FIG. 21—Model for hypothetical local composition changes during thermal treatment of steel; E = embrittling element.

the interface. No segregation has occurred in the ferrite. This model of embrittling element pile-up has been used previously to rationalize the phenomenon of 500 F embrittlement [7,10] and interface embrittlement of carbide-ferrite interfaces in Fe-C-E alloys.

After long embrittlement, step 4, the carbide has begun to take up additional Cr and Mo and the region adjacent to the carbide has become depleted in these elements. The gradients in Ni and E have begun to diminish due to outward diffusion. Some segregation of E to ferrite-ferrite interfaces has occurred.

In step 5 after long tempering in the embrittling range we find no gradients in Ni-Cr or Mo, a stable alloy carbide having formed, and only Gibbsian segregation of E at all interfaces.

Various aspects of this hypothetical model may change in any specific case, depending on composition and thermal history. However, the model contains the essence of what may happen in these steels. Presumably, the transition from intergranular dimpled rupture to smooth intergranular fracture occurs somewhere between steps 3 and 5. A recent report by Smith and Low [11] indicates that the ferrite along prior austenite grain boundaries is depleted in Cr and enriched in Ni, and use has been made of their etching results in constructing this hypothetical model. It should be noted that Auger spectroscopy of a fracture surface cannot show these details, because it would not differentiate between the compositions of the carbide, the ferrite around the carbide, and the ferrite away from the carbide.

The point to be noted here is that one cannot predict what might happen around carbides. The alloy content changes in an unknown way with time and therefore must affect the action of embrittling elements.

### *Acknowledgments*

This work has been supported by the American Iron and Steel Institute and the Advanced Research Projects Agency of the Department of Defense. It is part of a research program which will form the basis of a thesis to be submitted by B. J. Schulz in partial fulfillment of requirements for the Ph.D. degree at the University of Pennsylvania. We would also like to acknowledge the contributions of our colleague, J. R. Rellick in the course of many fruitful discussions. The Auger spectroscopy was carried out by D. F. Stein and A. Joshi at the University of Minnesota.

### **References**

- [1] Steven, W. and Balajiva, K., *Journal of the Iron and Steel Institute*, JISIA, Vol. 193, 1959, pp. 141-147.
- [2] Low, J. R., Jr., et al., *Transactions of the Metallurgical Society of AIME*, MTGTB, Vol. 242, 1968, p. 14.
- [3] Marcus, H. L. and Palmberg, P. W., *Transactions of the Metallurgical Society of AIME*, MTGTB, Vol. 245, 1969, pp. 1664-1666.
- [4] Palmberg, P. W. and Marcus, H. L., *Transactions, American Society for Metals*, TASEA, Vol. 62, 1969, pp. 1016-1018.

- [5] Stein, D. F., Joshi, A., and Laforce, R. P., *Transactions, American Society for Metals*, TASEA, Vol. 62, 1969, pp. 776-783.
- [6] Laforce, R. P., "A Small Specimen Test Method for Determining Ductile-Brittle Transition Temperatures," Report 66-C-057, G. E. Res. and Dev. Center, Feb. 1966.
- [7] McMahon, C. J., Jr., in *Temper Embrittlement in Steel, ASTM STP 407*, American Society for Testing and Materials, 1968, pp. 127-167.
- [8] McMahon, C. J., Jr., Rellick, J. R., and Schulz, B. J. in *Fracture 1969*, Chapman and Hall, Ltd., London, 1969, pp. 278-287.
- [9] Restaino, P. A. and McMahon, C. J., Jr., *Transactions, American Society for Metals*, TASEA, Vol. 60, 1967, p. 699.
- [10] Kula, E. B. and Anctil, A. A., "Tempered Martensite Embrittlement and Fracture Toughness in 4340 Steel," U.S. Army Materials Research Agency Technical Report 67-06 (AD 651066), Jan. 1967.
- [11] Low, J. R., Jr., and Smith, C. L., "Grain Boundary Segregation of Impurities in Metals and Intergranular Brittle Fracture," Carnegie-Mellon University Report 031-727-3, May 1971.

